2011

Development of a Muscle Force Optimization Algorithm to Improve Center of Pressure During Simulated Walking

Lawrence Dean Noble
Cleveland State University

DEVELOPMENT OF A MUSCLE FORCE OPTIMIZATION ALGORITHM TO IMPROVE CENTER OF PRESSURE DURING SIMULATED WALKING

LAWRENCE DEAN NOBLE, JR.

Bachelor of Science in Chemical Engineering
Cleveland State University
May, 1984

Masters of Science in Chemical Engineering
Cleveland State University
May, 2005

Submitted in partial fulfillment of requirements for the degree
DOCTOR OF ENGINEERING, APPLIED BIOMEDICAL ENGINEERING
at the
CLEVELAND STATE UNIVERSITY

January, 2011

This dissertation has been approved for the Department of Chemical and Biomedical Engineering and the College of Graduate Studies by

_____

Brian L. Davis, Ph.D.
Medical Device Development Center
Austen BioInnovation Institution in Akron

_____
Date

_____

Sridhar Ungarala, Ph.D.
Department of Chemical Engineering
Cleveland State University

_____
Date

_____

Antonie J. van den Bogert, Ph.D.
Orchard Kinetics

_____
Date

_____

Dan J. Simon, Ph.D.

Department of Electrical and Computer Engineering

Cleveland State University

_____

Date

_____

Jeffrey Dean, Ph.D.

Department of Biological, Geological, and Environmental Sciences

Cleveland State University

_____

Date

Dedicated to loving parents

Lawrence Dean Noble Sr. and Joyce Ann (Johnson) Noble

whose sacrifices and encouragement have enabled this accomplishment.

ACKNOWLEDGEMENTS

First and foremost, I would like to thank Dr. Brian Davis (formerly at the Cleveland Clinic) and Dr. George Chatzimavroudis (Cleveland State University) who jointly encouraged me to enter this doctoral program. Without their support, I would never have attempted this undertaking.

I am very grateful for my advisory panel who kept me focused in the proper areas during my research and who contributed significantly to the quality of the final product.

I also thank my loving wife, Cynthia, whose personal sacrifices during these years have enabled me to pursue this lofty goal.

Warmest thanks to Becky Laird and Darlene Montgomery, both of the Cleveland State University, who so kindly helped me navigate the many administrative hurtles.

Many thanks to Robb Colbrunn (Cleveland Clinic) for general robotics lab support and integration of the optimization algorithm into the LabVIEW® application software.

A special thanks to Laura Bailey, Sarah Borsuk and Tara Bonner (Cleveland Clinic) for their assistance with cadaver feet preparation and robotic simulations/testing.

Thanks to Dr. Tammy Owings (Biomedical Engineering, Cleveland Clinic), Dr. Richard Drake (Lerner College of Medicine, Cleveland Clinic) and Mary Intorcio (Hand & Upper Extremity Center, Lutheran Hospital) for cadaver foot specimens.

Lastly, without the generous support provided by Puget Sound Veterans Association (Prime Sponsor Award Number: VA260-P-0738), NASA (Grant NNJ05HF55G) and from the Cleveland Clinic Musculoskeletal Core Center (NIAMS Core Center Grant 1P30 AR-050953) this research could not have been possible, for which I am very thankful.

DEVELOPMENT OF A MUSCLE FORCE OPTIMIZATION ALGORITHM TO IMPROVE CENTER OF PRESSURE DURING SIMULATED WALKING

LAWRENCE DEAN NOBLE, JR.

ABSTRACT

The Universal Musculoskeletal Simulator (UMS) was developed at the Cleveland Clinic to facilitate general purpose orthopaedic research that allows investigators to study the *in vitro* forces applied to bones, tendons and ligaments during simulated exercise of cadaver joint systems. In its original state, the UMS hardware consisted of a rotopod (a specialized hexapod robot), a single rotary tendon actuator and custom LabVIEW software for coordinated control and operation of the system. The focus of this work was to 1) enhance the UMS with a multi-tendon actuator system, 2) develop a muscle force optimization algorithm and evaluate it with a static model of the foot/ankle, 3) integrate the algorithm with the UMS software and evaluate it with cadaver specimens, and 4) utilize the enhanced UMS to investigate the individual muscle contributions to center of pressure using cadaver specimens.

Completion of the multi-tendon actuator system has enabled researchers to simulate exercise on cadaver joints by using up to five motorized actuators to simulate muscle forces that would occur during exercise while simultaneously contacting the joint with an external load generated by the rotopod. Although the multi-tendon actuator system was first conceived as a necessary enhancement to simulate the key extrinsic muscles of the ankle/foot, required to conduct simulated walking with cadaver feet, it was soon

recognized that this system could be utilized to simulate muscles forces of other joints (i.e., shoulder, wrist, spine, etc.) and as such now provides a general purpose test bed for conducting orthopaedic research.

Initial cadaver studies of the foot/ankle using the UMS revealed that normal physiological center of pressure patterns were difficult to achieve during simulated walking. Therefore, the primary goal of this effort was to develop an algorithm that would optimize the muscle forces to better achieve the desired medial-lateral and anterior-posterior center of pressure profiles expected during physiologically accurate simulated walking. This algorithm was integrated with the existing arsenal of UMS optimization tools.

Optimization of muscle forces during simulated walking utilized the method of minimizing the cube of muscle stress and was solved through the use of sequential quadratic programming. Initially, for rapid debugging purposes, the muscle optimization technique was evaluated with a static model of the ankle/foot and then characterized using the UMS with cadaver feet. Simulated gait with three cadaver feet demonstrated that improvement to center of pressure (COP) is greatest in the mid stance portion of gate especially in the range of 41-50% stance (reduction in the mean error in the range of 83.0% to 93.4% for anterior COP and from 81.6% to 98.6% for medial COP after three iterations). Additionally, individual muscle contributions to the COP were investigated experimentally at estimated full-physiological levels. The significant finding of this test was that the triceps surae muscle groups acts as an everter (medial COP shift) at times before 65-70% stance and acts like an inverter (lateral shift in COP) at stance times above this range.

TABLE OF CONTENTS

TABLE OF CONTENTS (CONTINUED)

TABLE OF CONTENTS (CONTINUED)

LIST OF TABLES

LIST OF FIGURES

LIST OF FIGURES (CONTINUED)

LIST OF FIGURES (CONTINUED)

LIST OF FIGURES (CONTINUED)

CHAPTER I

INTRODUCTION AND LITERATURE REVIEW

1.1 The Need for the Universal Musculoskeletal Simulator

Fundamental understanding of bone and soft tissue injuries requires quantification of mechanical strains that precede the injury. Unfortunately, human *in vivo* studies of exercise-induced bone strains are difficult to conduct due to the nature of the invasive surgery required to implant strain gauges and the failure of bonding techniques between the bone strain gauges and the bone during exercise. Lanyon *et al.* [1] successfully demonstrated the feasibility of bonding bone strain gauges to the human tibial shaft, but the procedure was highly invasive and it was difficult to determine if the bond was loosening during the experiment. Burr *et al.* [2] using a similar bone strain implanting technique, experienced a hard failure of the strain gauge bond in one of two subjects tested under vigorous activity.

Trauma, such as experienced with a ruptured anterior cruciate ligament (ACL), has been shown to cause early onset osteoarthritis. *In vivo* testing has been attempted to better understand the relationships between knee positions and muscles forces on ligament biomechanics. Devices such as the Differential Variable Reluctance Transducer

DVRT) have been implanted into the anterior bundle of the ACL to measure displacement during exercise. Disadvantages of this technique include the highly invasive surgical attachment of the device to soft tissue and the sensitivity to mechanical impingement that prevents hyper-extension of the knee [3]. Even if it were possible to successfully instrument a person there are certain experiments, such as cutting a ligament to see how it affects bone strain, which would not possible with living subjects. As an alternative method, *in vitro* testing of cadaver knees using robotics has been attempted. Unfortunately, in one such investigation the robot was not capable of applying physiologically realistic loads to the knee [4].

Computational models to predict internal tissue loads based on external motion and force measurements during exercise require accurate data on tissue geometry and material properties. Reliability of these models is still problematic for mechanically complex systems such as the knee or foot where soft tissue plays an important role [5,6]. Cadaver simulation is therefore very much needed as an alternative to computational models, or to produce data for validation of computational models.

The importance of obtaining tissue strain data during activities of daily living can be illustrated by considering a progressive disease such as Charcot foot arthropathy. This is a disabling condition that is associated with dislocations or fractures in the midfoot region. The immediate cause of Charcot foot arthropathy is not well understood. The initial steps of this disease are not recognized by clinicians and as a result the initiation of treatment is often too late to avoid long healing times and even permanent deformities [7]. *In vivo* studies, if designed to measure tissue breakdown using strain gauges, would provide significant insight to the progression of this disease in diabetic subjects.

However, for ethical and scientific reasons this is not practical. Furthermore, from a scientific standpoint, obtaining repeatable and accurate *in vivo* results during long-term exercise sessions would be difficult to obtain due to intra-subject variability from one trial to another. One solution to this problem would be to perform *in vitro* testing of a diabetic cadaver foot with a device that could accurately and repeatable apply loads to the foot. It would involve simulating muscle loading to the foot structures during an exercise, such as walking, while simultaneously contacting the bottom of the foot with a surface to simulate the ground interaction. Such a device is the goal of the UMS currently under development. This proposal represents a significant portion of the UMS development effort.

Previous dynamic simulators have been developed to study the foot. Table I identifies some of these research groups and summarizes the focus of their research.

While previous systems have yielded new insight into the biomechanics of foot and ankle pathologies, each of these simulators have some combination of the limitations listed below [8-12]:

- Not capable of simulated exercises on other joints (i.e., knee, hip, wrist, shoulder)
- Not capable of simulating different exercises (running, jumping, etc.)
- Scaled velocities that do not simulate real-time dynamics
- Not obtaining full-physiological loading of the joint

In contrast, the UMS can be used to:

- Simulate most exercise modes for a given joint
- Achieve full-physiological loading in most exercise modes
- Apply these loads in a real-time (or near real-time) manner

Table I Summary of Musculoskeletal Research on Ankle/Foot using Robotics/Dynamic Simulators

Authors	Research Description	Ref.
C. Milgrom - Department of Orthopaedics, Hadassah University Hospital and Hebrew University Medical School (Jerusalem, Israel) Finestone - Department of Orthopaedics, Rabin Medical Center, Beilinson Campus (Petah Tikvah, Israel) Hamel, V. Mandes and N. Sharkey - Center for Locomotion Studies, Pennsylvania State University, (PA, USA) D. Burr - Department of Anatomy and Orthopaedics, University of Indiana School of Medicine (Indianapolis, IN)	Studied seven human cadaver lower extremities (age range of 23–81 years old) and a dynamic gait simulator to examine and compare axial strains in the tibia and second metatarsal.	[8]
C. Hurchler and J. Emmerich – Department of Orthopaedic Surgery, Medical School of Hannover (Hannover Germany) N. Wülker, Orthopaedic Clinics and Polyclinics, University of Tubingen (Tubingen, Germany)	*In vitro* simulator developed to reproduce the kinematics and kinetics of stance phase of gait on cadaver feet. Measured 3-D hindfoot and forefoot motion. Force applied to nine tendons of the foot (flexor and extensor muscle groups).	[9]
K-J Kim - Department of Mechanical Engineering at University of Wisconsin-Milwaukee (Milwaukee, WI) H.B. Kitaoka, Z-P Luo, L. J. Berglund, K. R Kaufman and K-N An, Orthopedic Biomechanics Laboratory at Mayo Clinic, Mayo Foundation (Rochester, MN) S. Ozeki - Department of Orthopedic Surgery at Dokkyo University Koshigaya Hospital (Koshigaya, Japan)	A four-bar mechanism provided the progressive motion of a tibia while the external loadings were simultaneously applied. Muscle loadings were estimated based on the physiological cross-sectional area and normal electromyography (EMG) data assuming linear EMG–force relationship. Ad hoc tuning of the unknown muscle gains was performed until a reasonable match with the normal vertical ground reaction force profile, COP advancement, and characteristic foot motion events (i.e., heel strike, foot flat, heel rise and toe-off) could be made. Three cadaver feet and an artificial foot were tested with five repeated trials.	[10]
K-J Kim - Department of Mechanical Engineering at University of Wisconsin-Milwaukee (Milwaukee, WI) E. Uchiyama, H.B.Kitaoka and K-N An - Orthopedic Biomechanics Laboratory at Mayo Clinic/Mayo Foundation (Rochester, MN)	Correlated the effects of muscle force on the movement of the COP for increased clinical utility of the COP measurement using five cadaveric specimens. A sinusoidal muscle force of 49 N was applied to isolated or grouped extrinsic ankle muscles, and a constant ankle joint reaction force at different tibial positions. Differential COP movement is interpreted as a moment arm for the vertical GRF.	[11]
E.D. Ward - Central Iowa Foot Clinic (Perry, IA) K.M. Smith - Department of Podiatric Medicine, College of Podiatric Medicine at Des Moines University (Des Moines, IA) J.R. Cocheba – Broadlawns Medical Center (Des Moines, IA) P. E. Patterson - Department of Industrial and Biomedical Engineering, Black Engineering at Iowa State University (Ames, IA) R. D. Phillips - Podiatry Section, Veterans Affairs Medical Center (Coatesville, PA)	Determined whether the amount of fascia released, from medial to lateral, causes a significant increase in force in the remaining fascia. Developed a dynamic loading system that allowed a cadaveric specimen to replicate the stance phase of gait and capable of applying appropriate muscle forces to the extrinsic tendons on the foot. Also replicated the *in vivo* timing of the muscle activity while applying force to the tibia and fibula from heel strike to toe-off.	[12]

1.2 Muscle Force Optimization Approaches Used in Biomechanics

Determination of physiologically correct muscle forces to apply during cadaver experiments with robotic simulators can be a serious limitation to this research approach. It is difficult to extrapolate muscle force magnitudes from electromyogram (EMG) data obtained from the muscles of the lower limb during exercises like walking. The primary difficulty arises from the fact that EMG provides only temporal information regarding muscle activity. In order to estimate muscle force from EMG input signals, it is necessary to apply certain assumptions, such as a linear scaling of EMG signal to muscle force magnitude. A secondary difficulty relates to the similarity of EMG patterns for related muscles, such as muscles in the anterior compartment of the leg responsible for dorsiflexion, making it extremely difficult to discern how the individual muscles contribute to the total force generation of the muscle group.

Optimization techniques are typically necessary to predict muscle forces in biomechanics studies of human joint since the equations used to model the system normally result in indeterminate systems. This occurs because there are normally more unknowns (individual muscle forces) than equilibrium equations (sum of moments) available for the joint under investigation. Optimization implies some type of objective function (cost function) that is minimized and additional constraints, such as non-negativity and maximum force generated based on the cross-sectional area of the tendon that is transferring the muscle loads to the skeletal element. A comprehensive review has recently been completed [13] that summarizes the model-based biomechanics research performed from 1975 to the present that estimated the muscle forces exerted during

movements of various joints under various exercises. Table II summarizes the objective function basis for foot/ankle studies evaluating muscles during walking to illustrate the variety of approaches for objective functions. This review also reports objective function basis for spine, neck, finger, wrist, elbow, arm and shoulder. This review shows that the most frequent objective function is the sum of nth power of muscle stresses.

For this reason the minimization of the sum of muscle stresses to the nth power was selected as the basis for this work. A value of n=3 was selected as it was the recommended value from the author [14] of this objective function methodology. In addition, it should be noted that the derivation of this objective function is based on the principle of maximizing muscle endurance.

1.3 Sequential Quadratic Programming Method

Sequential quadratic programming (SQP) techniques are used to solve non-linear optimization problems by approximating the objective (cost) function as a quadratic function and the constraints as linear approximations. The SQP method is essentially Newton's method applied to the solution of the Karusch-Kuhn Tucker (KKT) conditions. The advantages of this approach [15] are:

- This method has superior rate of convergence making it ideal for an application that desires real-time or near real-time capability
- The starting point (guess) can be infeasible
- Only the gradients of active constraints are required
- Convergence can be proven under certain conditions

Table II Objective Function Basis for Foot/Ankle Biomechanics Research [13]

Ref. No.	Muscle Groups	Objective Function Basis	Authors (Date)
1	31 (7 Segments)	Minimize sum of muscle forces + 4 * (sum of joint moments) and also original + weighted hip joint	Seireg and Arvikar (1975)
2	27 (4 Segments)	Minimize sum of muscle stresses	Crowninshield et al. (1978)
3	31 (7 DOF)	Minimize sum of muscle forces and also mechanico-chemical power output of muscles (a function of muscle rest length, endpoint velocity and zero force velocity)	Patriarco et al. (1981)
4	47 (3 Joints)	Minimize sum of nth power of muscle stresses (n = 1, 2, 3, 4 and 100)	Crowninshield and Brand (1981)
5	42 (6 DOF)	Minimize sum of muscle forces	Rohrle et al. (1984)
6	47 (3 Joints)	Maximize endurance by minimizing sum of muscle stresses cubed	Brand et al. (1986)
7	9 (3 DOF)	Minimize tracking error and metabolic energy consumption (Swing phase only), continuous controls	Davy and Audu (1987)
9	10 (8 DOF)	Minimize tracking error and sum of cubed muscle stresses (~muscle fatigue)	Yamaguchi and Zajac (1990)
10	7 (3 Joints)	Minimize sum of muscle forces/muscle forces squared/muscle stresses/ligament forces/contact forces/instantaneous muscle power	Collins (1995)
11	47 (3 Joints)	Minimize sum of muscle stresses cubed (maximize endurance)	Pedersen et al. (1997)
12	9 (9 DOF)	Minimize kinematics and kinetics tracking error	Neptune et al. (2001)

DOF – Degrees of Freedom

The use of SQP in the area of biomechanics is not uncommon. For instance, a 3D math model of the temporomandibular joint utilized a quadratic programming model to determine the compressive forces acting on the joint based on experimentally-determined forces [16]. The widespread acceptance of this method is seen as it is common to see the SQP method being used as a benchmark to evaluate new optimization techniques. For instance, simulated annealing (SA) algorithm was evaluated against SQP as part of a study of forward dynamic optimization of bicycle pedaling utilizing 27 design variables [17]. Similarly a particle swarm optimization (PSO) algorithm was evaluated against a SQP, a genetic algorithm (GA) and a quasi-Newton Broydon-Fletcher-Goldfarb-Shanno (BFGS) algorithms for biomechanical optimization test problems [18].

Since this SQP technique appears to have wide acceptance in biomechanical optimization of muscle forces, it is being proposed as the solution methodology, in conjunction with the objective function (minimizing summation of cubed muscle stresses) to form a novel combination of solving the non-linear muscle force optimization problem.

CHAPTER II

RESEARCH AIMS

2.1 Develop a Multi-tendon Actuator System and Integrate it with the UMS (Aim 1)

The goal of this aim was to develop a multi-tendon actuator system (MTAS) to simulate forces of five independent muscles or muscle groups and integrate it within the UMS. Since the existing system was already equipped with a single rotary tendon actuator, it was necessary to develop four additional actuators. Each actuator would need to have the following components:

- Servomotor drive
- Linear actuator
- In-line load cell
- Tendon freeze clamp
- Mounting bracket to aid the placement of the linear actuators around the structure
- Wire rope cables that link the tendon freeze clamp, load cell and actuator
- Pulleys as necessary to align the cables with tendon lines of action
- Software drivers, compatible with National Instrument's LabVIEW, for control of the servomotor drives

In addition, a liquid nitrogen distribution system would be required to route liquid nitrogen to the individual tendon freeze clamps.

2.2 Develop a Muscle Forces Optimization Algorithm to Improve Center of Pressure and Evaluate with a Static Model of the Foot/Ankle (Aim 2)

A study conducted to measure tibia and calcaneus bone strain during simulated walking with cadaver feet [19] revealed that achieving a physiologically accurate COP was very difficult. Attempts to improve the COP profiles by adjusting individual muscle forces using the fuzzy logic optimization tool proved unsuccessful. As a result, the team focused on maintaining the superior, also known as the vertical ground reaction force (VGRF), within ±10% of the desired force in the absence of a technique to correct COP.

The muscle force optimization algorithm will be designed to improve the desired walking profile in the medial-lateral (ML) and anterior-posterior (AP) direction COP by adjusting the simulated muscle forces at each discrete time during the stance portion of the human gait. The inputs to the optimization algorithm at each discrete time in the exercise profile will be:

- The previous muscle forces
- The error between the desired COP and the predicted COP from the static ankle model in both ML and AP-directions
- The desired superior force/VRGF

The output of the optimization algorithm will be the new forces necessary at each discrete time in the exercise profile to reduce the error in ML and AP-direction COP.

To provide a means to debug and evaluate this algorithm, it will be necessary to also develop a static model of the ankle to simulate the resulting COP for a given set of muscle forces. The static model of the ankle will take into consideration the forces and moments about the ankle joint and the subtalar joint that result from forces acting on the tendons of the five muscle groups. This model will take into account the insertion points of the various tendons and will estimate the ML and AP-direction COP resulting from the loads applied at each muscle group as predicted by the optimization algorithm.

2.3 Validate the Optimization Algorithm within the UMS using a Cadaver Foot (Aim 3)

The model-verified optimization algorithm will be integrated into the UMS foot application software in order to characterize the performance with a cadaver foot/ankle during simulated walking. The MTAS will simulate triceps surae muscle group, either tibialis anterior or extensor digitorum longus (extensor selected will depend on whether the foot under test is a right or left side, respectively), tibialis posterior, flexor hallucis longus and peroneus longus.

2.4 Utilize the Enhanced UMS to Investigate Individual Muscle Contributions to Center of Pressure during Simulated Walking with Cadaver Feet (Aim 4)

The purpose of this study is to determine how the COP changes during the stance phase due to individual muscle force during simulated walking in order to provide further insight to the muscle force optimization process. Testing will consist of establishing baseline walking profiles with five muscles being simulated simultaneously. A subsequent test will be performed where one muscle group will be inactive. The

difference in ML and AP-direction COP between these runs would be the contribution of the muscle that was inactivated. This process will be repeated such that data is collected for all extrinsic plantar flexors of the foot/ankle.

The plantar flexors are the focus of this study since they are active during mid stance and terminal stance and therefore most relevant to the muscle force optimization process that seeks to adjustment these muscle forces to improve the COP during this portion of stance. Evaluation of the muscle force optimization algorithm in early stance (where the extensors are still active following swing phase) is avoided due to dynamics pertaining to the initial contact of the heel and loading response.

CHAPTER III

DEVELOPMENT OF A MULTI-TENDON ACTUATOR SYSTEM

3.1 Overview of UMS and Multi-Tendon Actuator System

Figure 1 provides an overview of the UMS configured to conduct a typical cadaver foot experiment. The cadaver foot is mounted into a cylindrical tube which slides into the Foot Mounting Device where it is clamped into place. The Microscribe digitizer is used to acquire positional information for the foot, ankle and tibia, force platform and robot platform. From this information it is possible to perform all of the required coordinate system transformations required for coordinate motion of the force platform relative to the foot using the six degree of freedom (6 DOF) rotopod. Four linear actuators and one rotary actuator comprise the MTAS. The rotary actuator was in place prior to this current work, and was designed and fabricated to meet the high force requirements of the triceps surae muscle group. The rotary actuator provides the advantage of essentially unlimited stroke length, but the disadvantages of this approach are safety concerns and high cost. Safety issues relate to the behavior of the actuator when a failure of the tendon or clamping mechanism occurs. It is possible that, in order to maintain the force set point for the rotary actuator, the feedback control causes a rapid winding-up of the wire rope

attachment cable onto the actuator pulley. Due to these disadvantages, the additional tendon actuators that were developed were designed as linear actuators with a fixed stroke length that prevents the concern of the rotary design.

3.2 Components of the Multi-Tendon Actuator System

Figure 2 provides additional details for the test configuration, focusing on the equipment used to attach the foot to structure and attachment of the tendons to the actuators. Wire rope cables are connected to the end of the actuator cylinders and routed through various pulleys before being attached to the load cells. Load cells function as a coupling between the wire rope cable and tendon freeze clamp and attach to both via shackles.

The Liquid Nitrogen Distribution System, shown in Figure 3, is used to supply liquid nitrogen to the freeze clamps. This system consists of a 160 liter low pressure supply tank, custom fabricated Teflon manifold and 10 mm (¼ inch) OD Teflon tubing.
The tendon freeze clamps that were used by previous researchers at the Cleveland Clinic were modified to add a ¼ inch NPT-threaded boss for attachment to the liquid nitrogen supply line. In addition, the two halves of these clamps were previously held together with four screws (see Figure 4) but it was found that slipping an adjustable hose clamp over the center of the clamp body, was a convenient and sufficient means to hold the clamp together during testing.

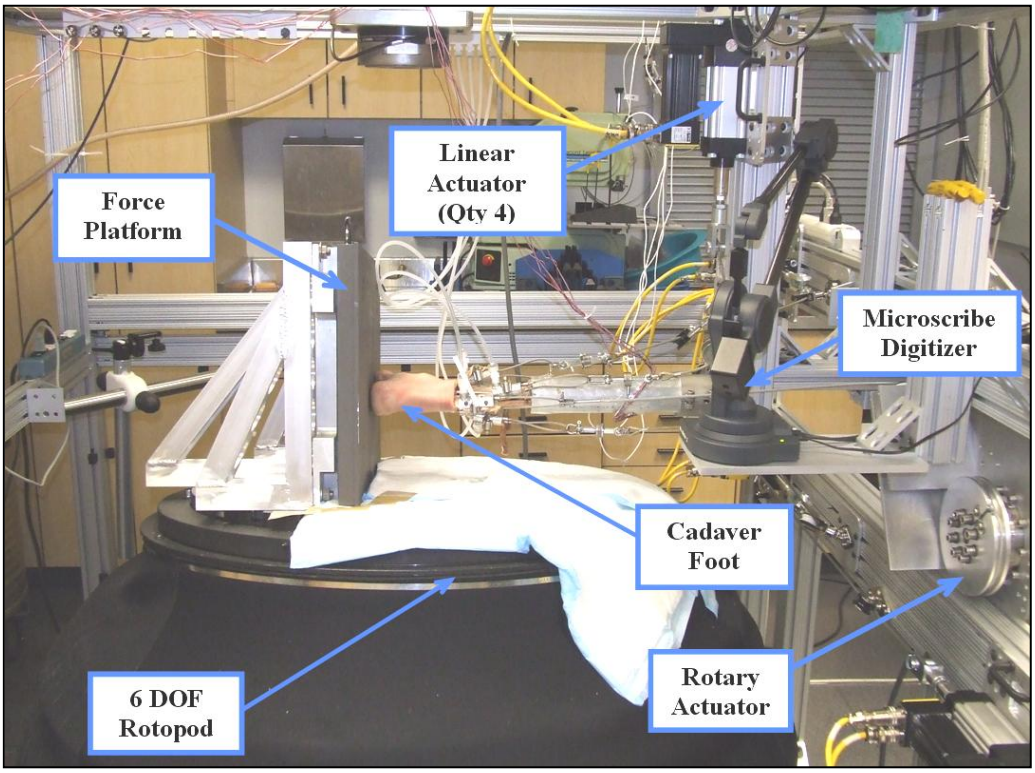

Figure 1 Universal Musculoskeletal Simulator

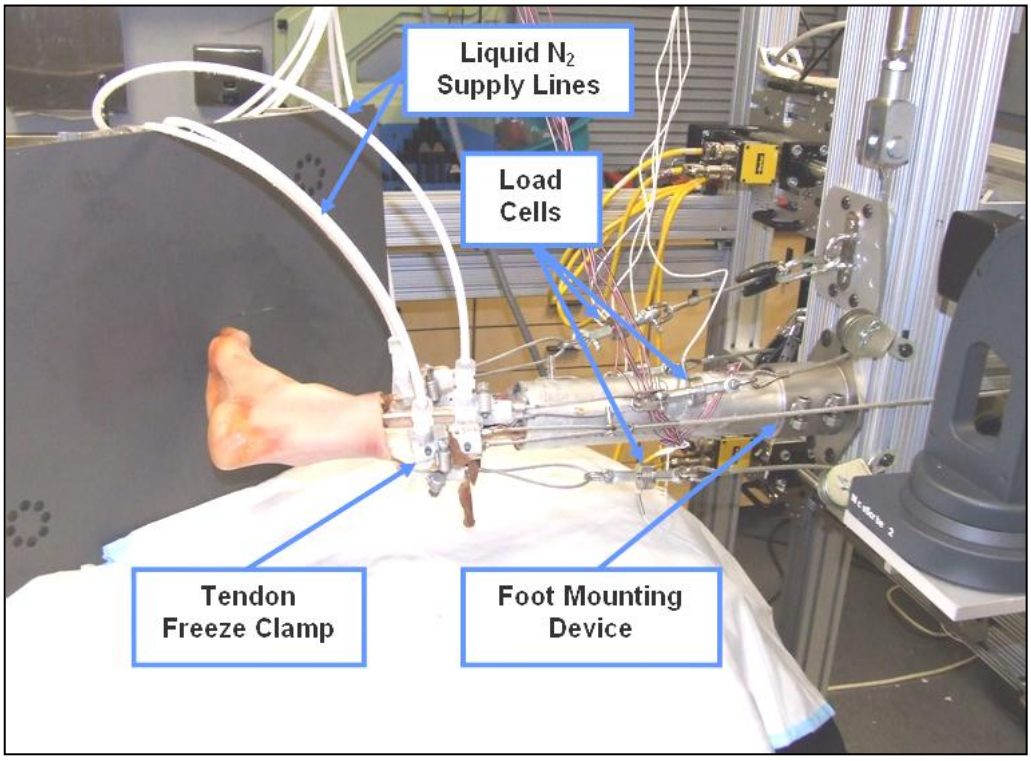

Figure 2 UMS Showing Key Components of the MTAS

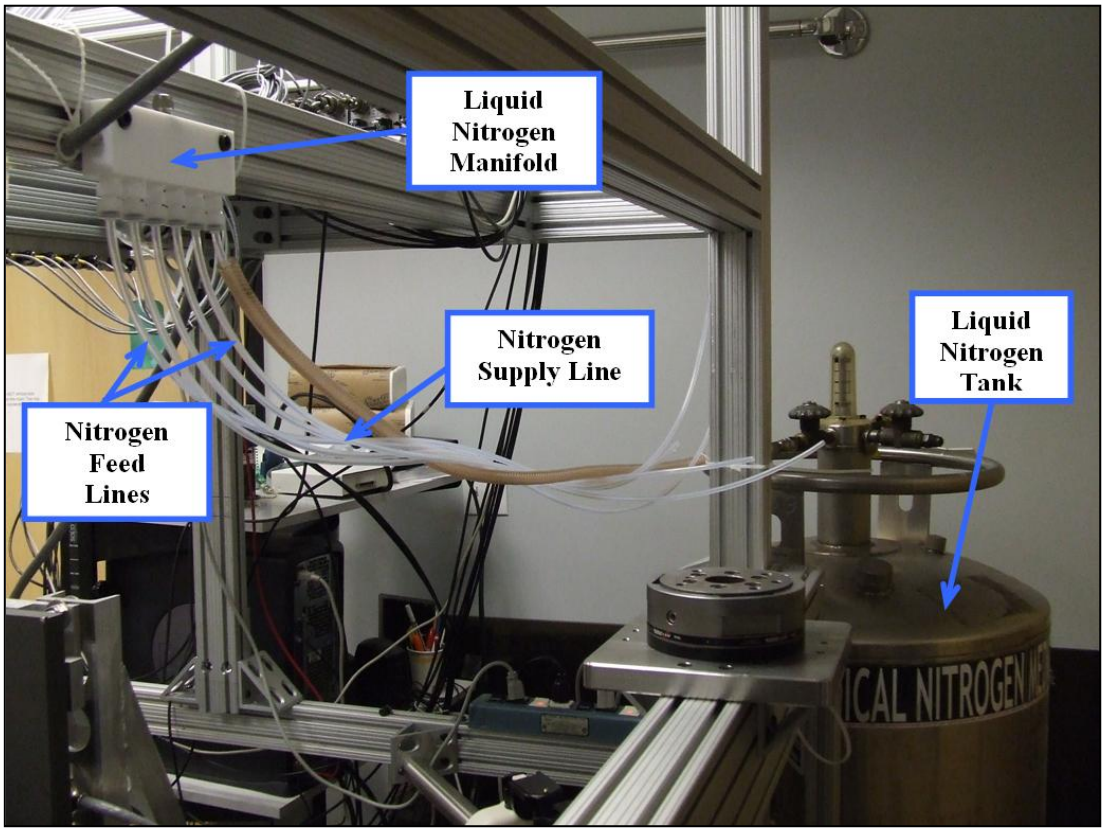

Figure 3 Liquid Nitrogen Distribution System

Figure 4 Tendon Freeze Clamp (Hose Clamp not Shown)

Specialized brackets were developed for mounting the linear actuators to allow easy attachment and positioning on the UMS frame (80/20 Inc, Columbia City, Indiana). Positioning is required to eliminate slack in the wire rope cables. The mounting bracket is shown in Figure 5 assembled and disassembled from the actuator. Figure 6 depicts how the linear actuator/mounting bracket assembly would be integrated into the UMS during testing.

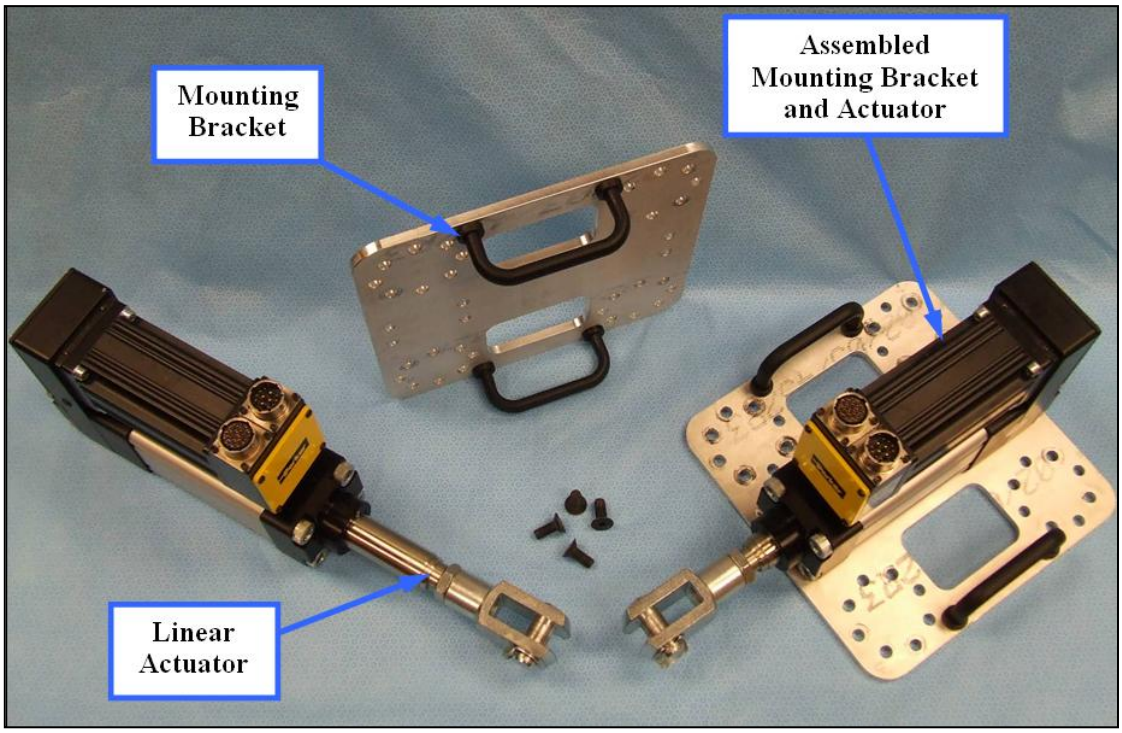

Figure 5 Linear Actuator and Mounting Bracket

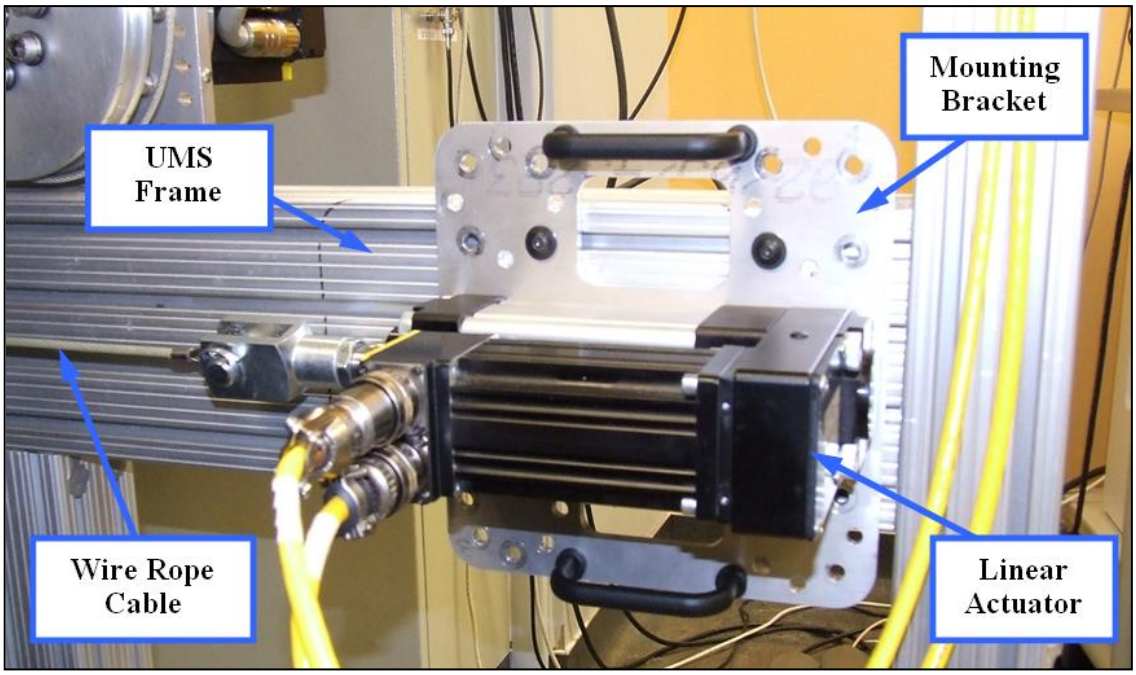

Figure 6 Actuator Integrated with Mounting Bracket Attached to the UMS

3.2 ASME Journal of Biomechanical Engineering Publication

Appendix A provides the final manuscript [19] that was accepted at the American Society of Mechanical Engineers (ASME) Journal of Biomechanical Engineering that describes the UMS, including the MTAS that has been developed as part of this effort. Also included in this journal article is an assessment of the performance of these actuators with respect to timing, accuracy and repeatability.

CHAPTER IV

DEVELOP A MUSCLE FORCE OPTIMIZATION ALGORITHM AND EVALUATE WITH A STATIC MODEL OF THE FOOT/ANKLE

4.1 Introduction

The center of pressure (COP) provides valuable insight for visualizing the force under the bottom of the foot as it contacts the ground during stance phase of the human gait. The COP represents the geometric center of the sum total of all vertical forces acting against the plantar surface of the foot due to contact with the ground at one instant of time during stance. The COP reflects the actions of muscles acting on the various joints of the foot (ankle, subtalar, metatarsophalangeal, etc.). To illustrate this principle, muscle activation of the plantar flexors should result in shifting the COP in the anterior (forward) direction. Gait analysis evaluates the progression of instantaneous COP points to assess the patient's balance and to gain insight regarding underlying pathological conditions, such as tibialis posterior dysfunction. The spatial COP progression for a normal person follows a consistent path, as depicted in Figure 7. Similarly, there is a unique temporal aspect of the COP progression. Following heel strike, the COP traverses rapidly along the bottom of the foot until it reached the metatarsal region where it dwells

for approximately half of the total stance time (30 to 55% of the entire gait cycle) before progressing toward the toe of the first metatarsal, as shown in Figure 8.

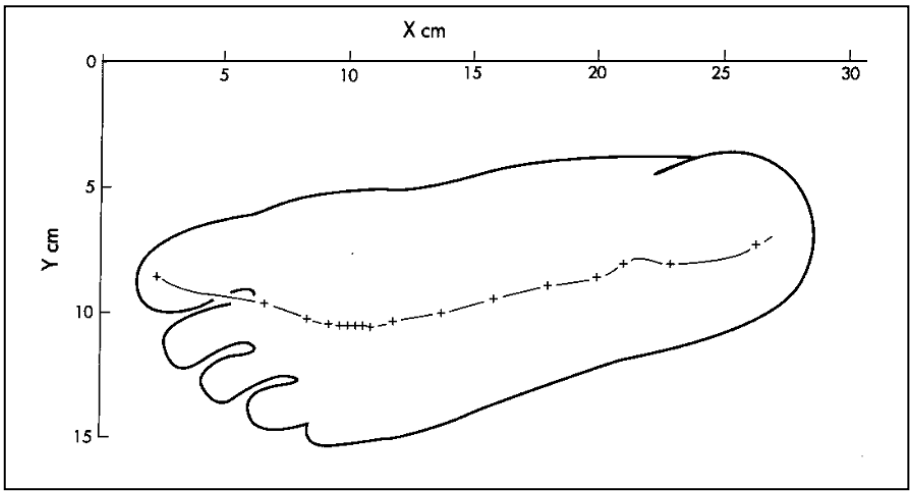

Figure 7 Spatial Progression of the COP during Stance Phase of Gait [20]

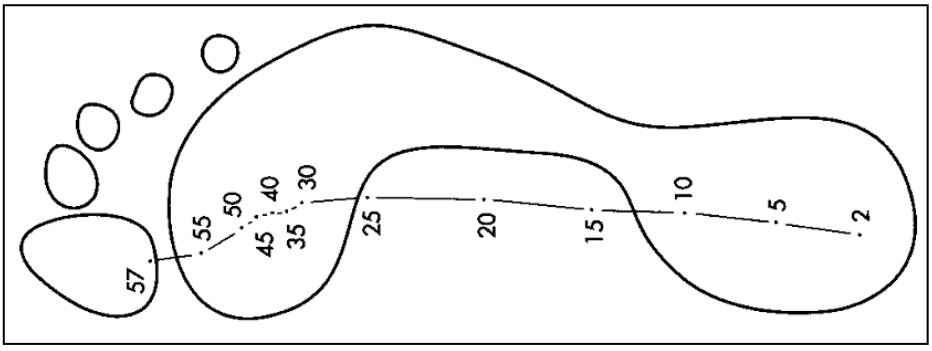

Figure 8 Temporal Progression of the COP during Stance [20]

The COP, determined from the forces and moments measured from the force plate that contacts the plantar surface of the cadaver foot, provides a useful parameter for assessing whether or not the simulation represents physiological walking. In order to evaluate the cadaveric gait simulation it is necessary to adopt a known COP standard which can serve as the desired or target COP profile in the AP and ML directions. The standard COP profiles, based on the force platform reference frame, that were utilized for

this work are shown in Figure 9. These profiles represent the mean values extracted from kinematic and kinetic data that was collected [21] from a live human subject during ten trials of normal walking within the Cleveland Clinic Biomechanics Gait Lab, shown in Figure 10. Similarly, the desired ground reaction forces used in this study, as shown in Figure 11, were also based on data from this study in the force platform reference frame. The relative motion between the foot and ground (not shown herein) was also derived from data collected from this subject and was used to compute the required force plate motion trajectory that was accomplished using the rotopod during simulated stance.

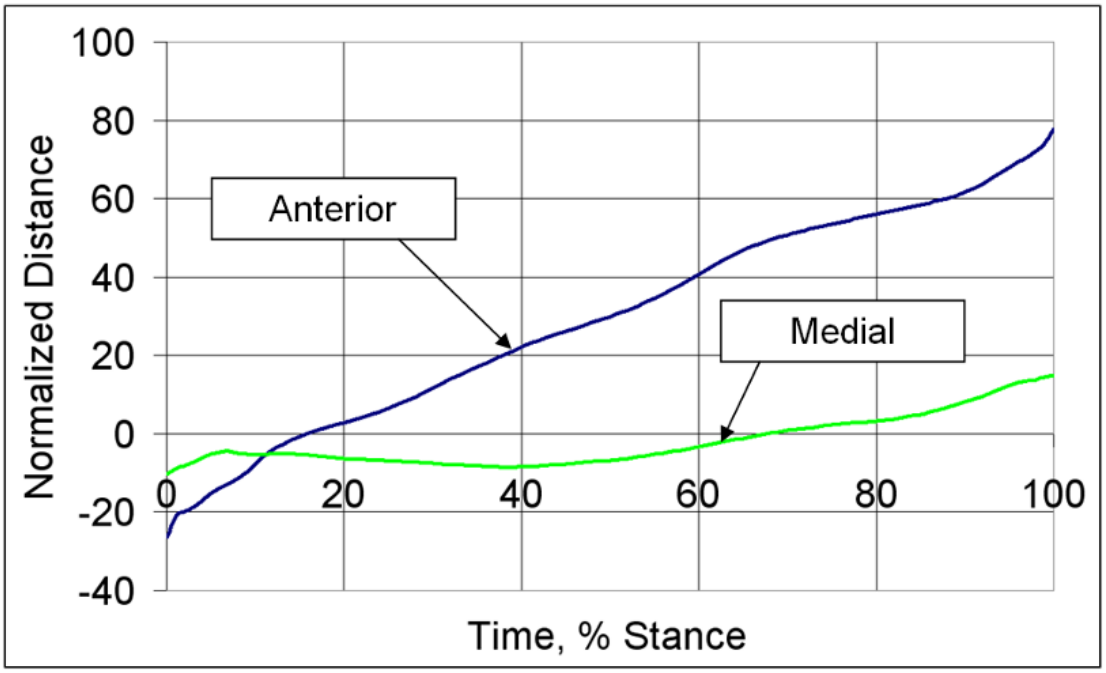

Figure 9 Desired COP during Simulated Stance Normalized to Percent Foot Width (%FW) for Medial COP and Normalized to Percent Foot Length (%FL) for Anterior COP

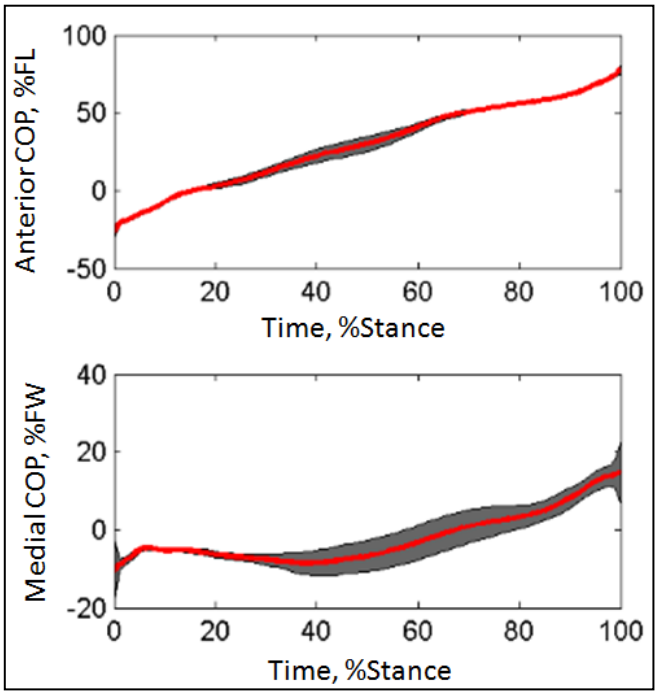

Figure 10 Anterior (Top) and Medial (Bottom) COP Measured from a Human Subject Showing Mean ±1 Standard Deviation (SD)

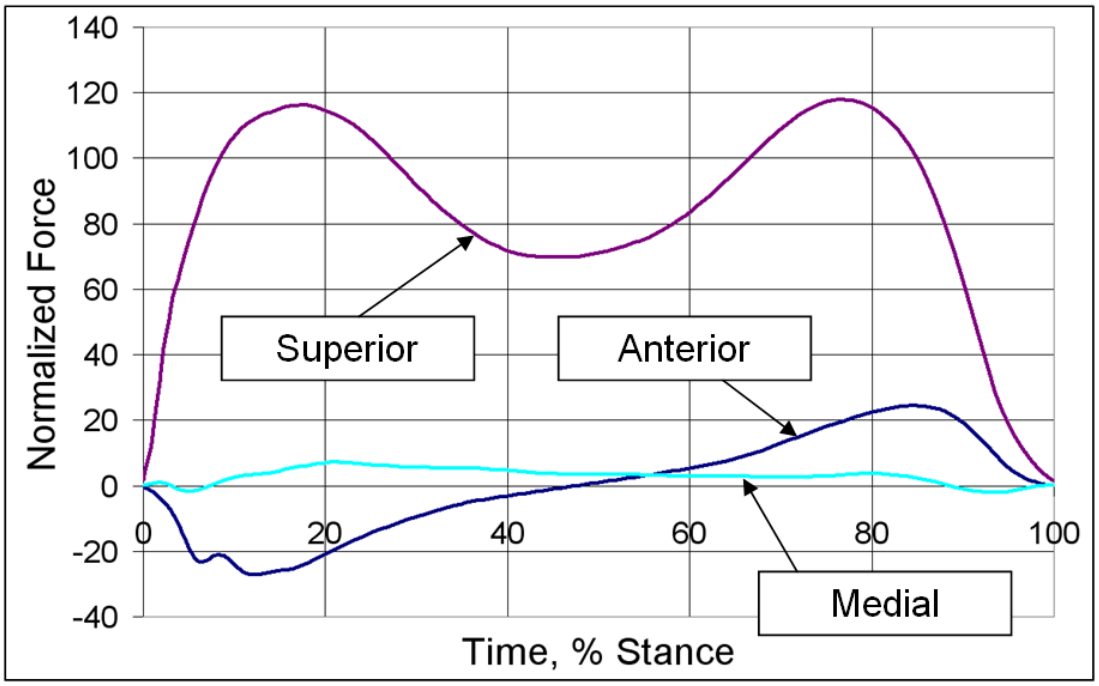

Figure 11 Desired GRFs during Simulated Stance Normalized to Percent Body Weight (%BW)

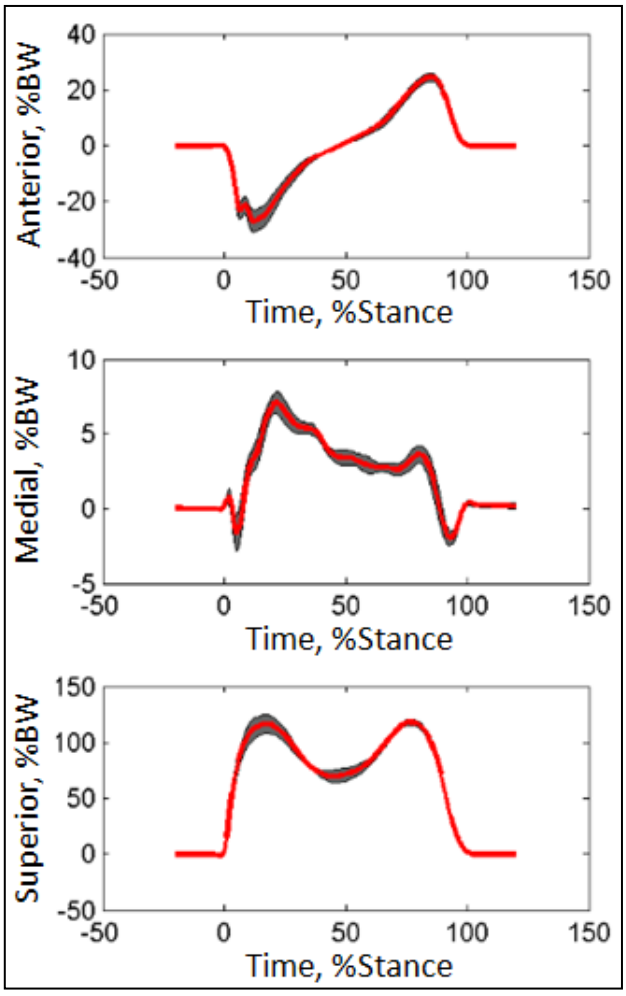

Figure 12 Anterior (Top), Medial (Center) and Superior (Bottom) GRFs Measured from a Human Subject Showing Mean ±1SD

The parameters that affect the COP during the simulated gait include the simulated muscle forces, the force platform trajectory path and the alignment of mounted cadaver foot. Adjustments are made prior to beginning the cadaver experiments to ensure that the foot is sufficiently aligned within the UMS and the force platform trajectory remains constant during experiments. Therefore, the only variable that is adjusted during the experiment is the muscle forces which are simulated by the Multi-Tendon Actuator System. Muscles under investigation for adjusting the COP during simulated walking are listed below:

- Flexors: Triceps surae, tibialis posterior, flexor hallucis longus and flexor digitorum longus
- Extensors: Tibialis anterior, extensor digitorum longus and extensor hallucis longus
- Everters: Peroneus longus and peroneus brevis

These muscles are shown pictorially in Figure 13 through Figure 15.

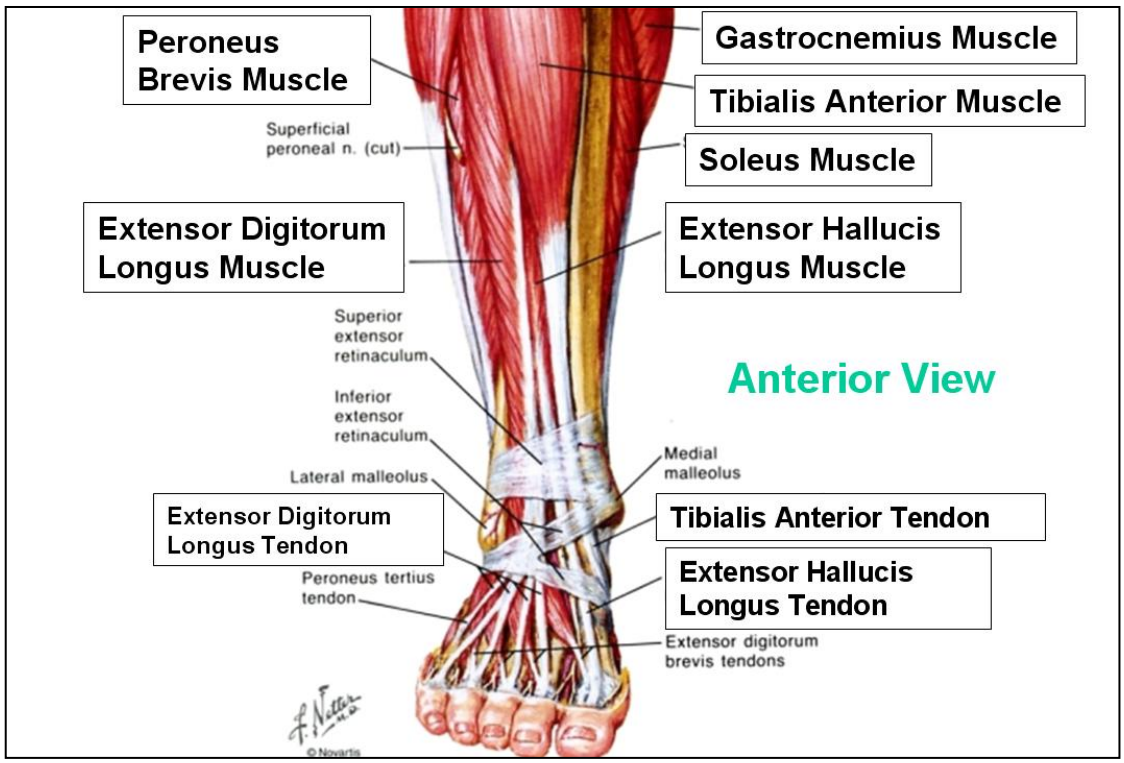

Figure 13 Anterior View of Extrinsic Muscles of the Right Ankle/Foot [22]

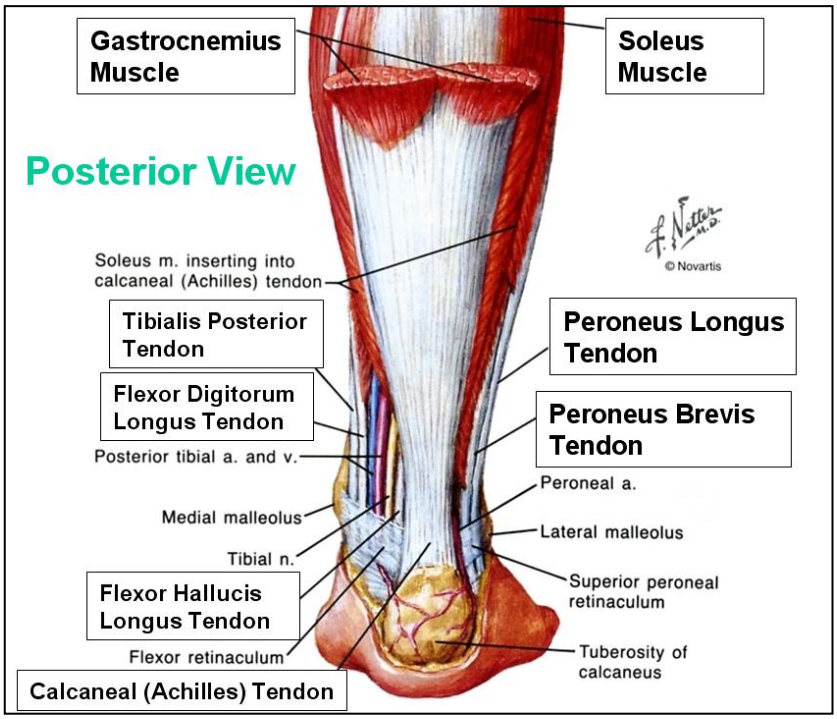

Figure 14 Lateral View of Extrinsic Muscles of the Right Ankle/Foot [22]

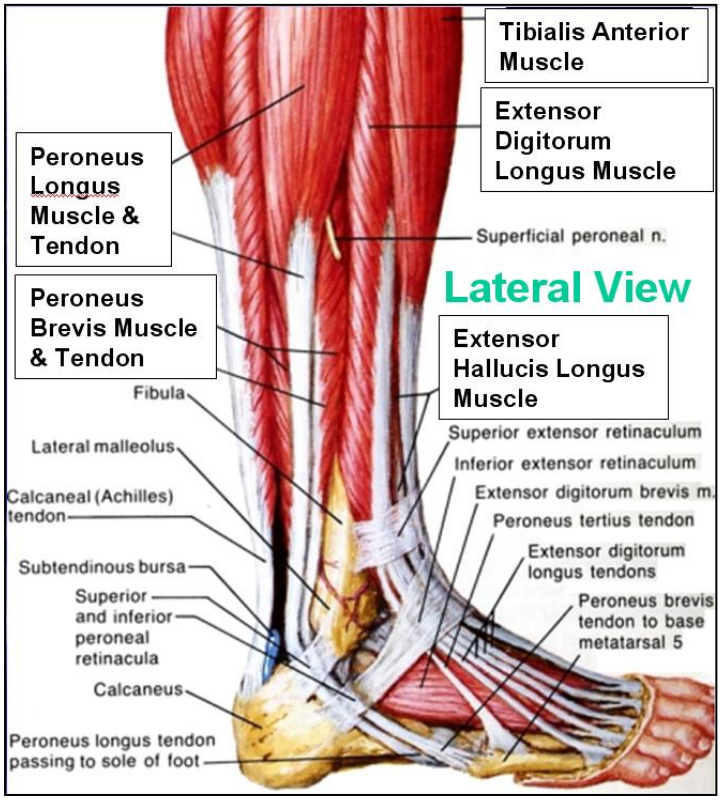

Figure 15 Posterior View of Extrinsic Muscles of the Right Ankle/Foot [22]

Because these muscles insert at different anatomical structures within the foot, the resulting action from the individual muscle forces changes the COP in a unique manner. The goal of this work was to develop a muscle force optimization algorithm that can determine a set of desired muscle forces that will result in an adjustment in the AP and ML COP to closer achieve the desired COP profiles.

For the purpose of this study it has been assumed that the extrinsic muscles of the foot cause actions primarily at the ankle and subtalar joints as shown in Figure 16 (Left). From this figure it can be seen that the ankle joint provides foot range of motion in the dorsiflexion (extension)/plantar flexion directions and the subtalar joint provides inversion (inward tilting)/eversion (outward tilting) of the foot. Figure 16 (Right) further illustrates which muscles would result in which actions as is summarized in Table III.

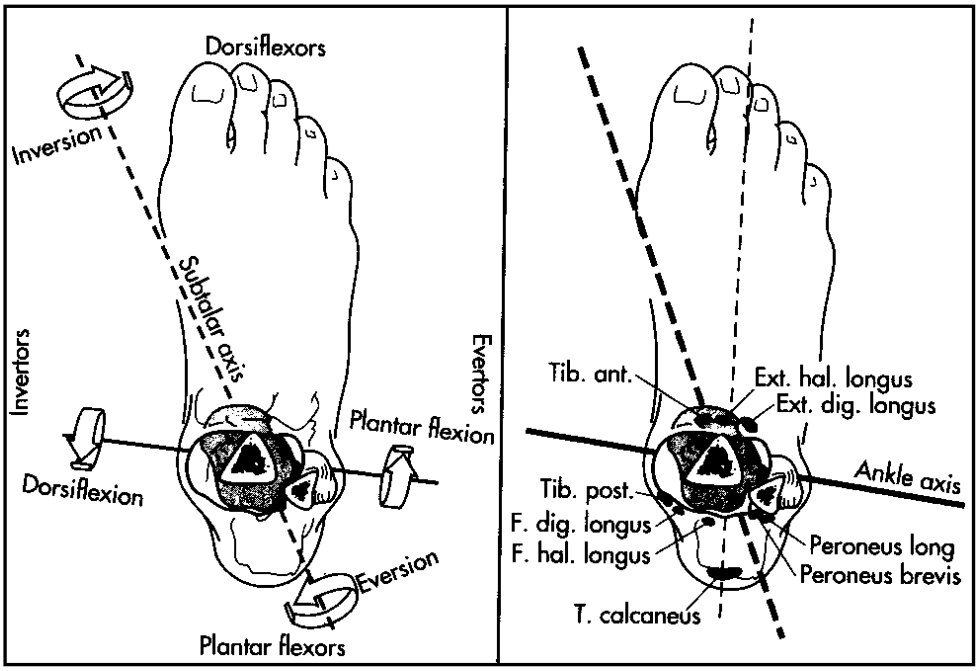

Figure 16 Joints of Ankle/Foot under Investigation [20]

Table III Actions of the Extrinsic Muscles of the Foot/Ankle

Muscle Name	Plantar Flexion	Dorsiflexion	Inversion	Eversion
Triceps Surae	X		X	
Tibialis Posterior	X		X	
Flexor Hallucis Longus	X		X	
Flexor Digitorum Longus	X		X	
Tibialis Anterior		X	X	
Extensor Digitorum Longus		X		X
Extensor Hallucis Longus		X	X	
Peroneus Longus	X			X
Peroneus Brevis	X			X

4.2 Muscle Force Optimization Algorithm Method

The optimization algorithm was developed to compute optimized muscle forces to reduce the error between the measured COP during simulated gait with a cadaver foot and the desired COP. The measured COP is calculated from the force and moment data collected from the force platform. The algorithm attempts to adjust the COP in both AP and ML directions simultaneously. The inputs to the optimization algorithm are:

F_PREV_i	Muscle forces measured during the previous experiment run for the ith muscle[(1)]
VGRF	The desired vertical ground reaction force (VGRF) [(1)]
$COP\_AP_{Desired}$	The desired anterior-posterior COP[(1)]
COP_AP_{Actual}	The anterior-posterior COP measured during the previous run[(1)]
$COP\_ML_{Desired}$	The desired medial-lateral COP[(1)]
COP_ML_{Actual}	The medial-lateral COP measured during the previous run[(1)]

BW	Body weight of specimen donor
FW	Width of foot specimen
FL	Length of foot specimen

(1) Vector consisting of values at each increment of stance

The optimization algorithm takes these inputs along with the moment arms (scaled using foot width and foot length) to develop the objective function constraints. The algorithm then solves the constrained minimization problem to compute new optimized muscle forces. These optimized muscle forces are intended to reduce the error between the desired and actual COP in both the AP and ML directions. The objective function [14] that is minimized by the algorithm is given by:

$$ObjFunction = \sqrt[n]{\sum_{i=1}^{m}\left(\frac{F_i}{A_i}\right)^n} \quad (1)$$

Where:

n = Muscle stress power, value of 3 recommended [14]

m = Total number of extrinsic muscle under test, currently able to test five with the UMS (triceps surae, flexor hallucis longus, peroneus longus, tibialis anterior and tibialis posterior)

F_i = Optimized force of ith muscle

A_i = Cross-sectional area of ith muscle

The objective function given in Equation 1, without additional constraints, would result in a solution representing the case where all muscle forces are zero. Therefore, it is necessary to constrain, or limit the possible solutions to the objective function to that solution which corrects the COP error. The constraints levied upon the objective function

for this work are shown in Equations 2-4 below. Equation 2 provides constraints necessary to correct for COP error in the ML direction and Equation 3 provides the necessary constraint for the AP direction [24]. Equation 4 provides a non-negativity constraint for the muscle forces.

$$\Delta COP\_ML = \sum_{i=1}^{m}\left(\frac{MA\_IN_i}{VGRF}\right)\Delta F_i \tag{2}$$

$$\Delta COP\_AP = \sum_{i=1}^{m}\left(\frac{MA\_DF_i}{VGRF}\right)\Delta F_i \tag{3}$$

$$F_i \geq 0 \tag{4}$$

Where:

ΔCOP_AP = Desired change in COP in anterior-posterior direction

ΔCOP_ML = Desired change in COP in medial-lateral direction

MA_DF_i = Dorsiflexion moment arm of the ith muscle

MA_IN_i = Inversion moment arm of the ith muscle

$VGRF$ = Vertical ground reaction force

ΔCOP_AP = Anterior-posterior COP adjustment:

$$COP\_AP_{Desired} - COP\_AP_{Actual} \tag{5}$$

ΔCOP_ML = Medial-lateral COP adjustment:

$$COP\_ML_{Desired} - COP\_ML_{Actual} \tag{6}$$

ΔF_i = Change in the force between desired/optimized values and previous experiment run values):

$$F_i - F\_PREV_i \tag{7}$$

The Matlab® (Mathworks, Natick Massachusetts) function *fmincon* [25] was used to solve this constrained minimization problem. In order to call this function the linear constraints defined by Equations 2 and 3 must be in the form:

$$Aeq*X = Beq \tag{8}$$

Where *Beq* and *X* are vectors and *Aeq* is a matrix. In the case where five muscles are used these variables become:

$$X = [\, F_1 \;\; F_2 \;\; F_3 \;\; F_4 \;\; F_5 \,] \tag{9}$$

$$Aeq = [\, MA\_DF_1 \;\; MA\_DF_2 \;\; MA\_DF_3 \;\; MA\_DF_4 \;\; MA\_DF_5 \,; \;\; MA\_IN_1 \;\; MA\_IN_2 \;\; MA\_IN_3 \;\; MA\_IN_4 \;\; MA\_IN_5 \,] \tag{10}$$

$$Beq(1) = (COP\_AP_{Desired} - COP\_AP_{Actual})*VGRF + MA\_DF_1*F\_PREV_1 + MA\_DF_2*F\_PREV_2 + MA\_DF_3*F\_PREV_3 + MA\_DF_4*F\_PREV_4 + MA\_DF_5*F\_PREV_5 \tag{11}$$

$$Beq(2) = (COP\_ML_{Desired} - COP\_ML_{Actual})*VGRF + MA\_IN_1*F\_PREV_1 + MA\_IN_2*F\_PREV_2 + MA\_IN_3*F\_PREV_3 + MA\_IN_4*F\_PREV_4 + MA\_IN_5*F\_PREV_5 \tag{12}$$

$$Beq = [\, Beq(1) \;\; Beq(2) \,] \tag{13}$$

The non-negativity constraint is implemented by the variable *lb* (lower bounds):

$$lb = [\, 0.0 \;\; 0.0 \;\; 0.0 \;\; 0.0 \;\; 0.0 \,] \tag{14}$$

Within the optimization algorithm *Fmincon* is called in the following manner for each increment of stance:

[F, fval, lambda, exitflag, output] = fmincon(@(F)ObjFunction(F, A, n),...

F_PREV, [], [], Aeq, Beq, lb, [], [], options); (15)

Where *fval, lamda, exitflag* and *output* are Matlab variables used for debugging purposes.

4.3 Static Ankle Model Method

A static model of the ankle/foot was developed as a foot simulator to allow the analytical evaluation of the muscle force optimization algorithm without necessitating testing with a cadaver foot. The ankle model is a pseudo 2 dimensional (2D) problem that only considers the flat-foot situation where the foot can pivot at both the ankle joint axis and the subtalar joint axis. The foot can also move up or down in the vertical axis to simulate the changing tibia position during gait. Contact points defined at various locations within the outline of the foot are modeled as a non-linear springs. The force at each contact point (*CP_FORCE*) is computed based on how far the deformation penetrates the ground plane at each location. The total deformation (*Z_TOT*) at each contact point is a contribution of the individual deformations due to tibia position (*Z_TIB*), the ankle joint angle (*Z_DF*) and the subtalar joint angle (Z_IN) according to the following expressions:

$$Z\_DF = CP\_DF\_MA * SIN(DF\_ANG * \pi / 180) \quad (16)$$

$$Z\_IN = CP\_IN\_MA * SIN(IN\_ANG * \pi / 180) \quad (17)$$

$$Z\_TOT = Z\_TIB + Z\_DF + Z\_IN \quad (18)$$

Where:

CP_DF_MA = Contact point moment arm distance from ankle axis, cm (Figure 17)

CP_IN_MA = Contact point moment arm distance from subtalar axis, cm (Figure 17)

DF_ANG = Dorsiflexion angle, degrees (Figure 18)

IN_ANG = Inversion angle, degrees (Figure 19)

The force at each contact point is then computed by:

$$\begin{aligned} &\textit{if } Z\_TOT < 0 \textit{ then } CP\_FORCE = A*|Z\_TOT|\text{^}3 \\ &\textit{else } CP\_FORCE=0 \end{aligned} \tag{19}$$

Where:

A = Constant, 50 N/cm^3

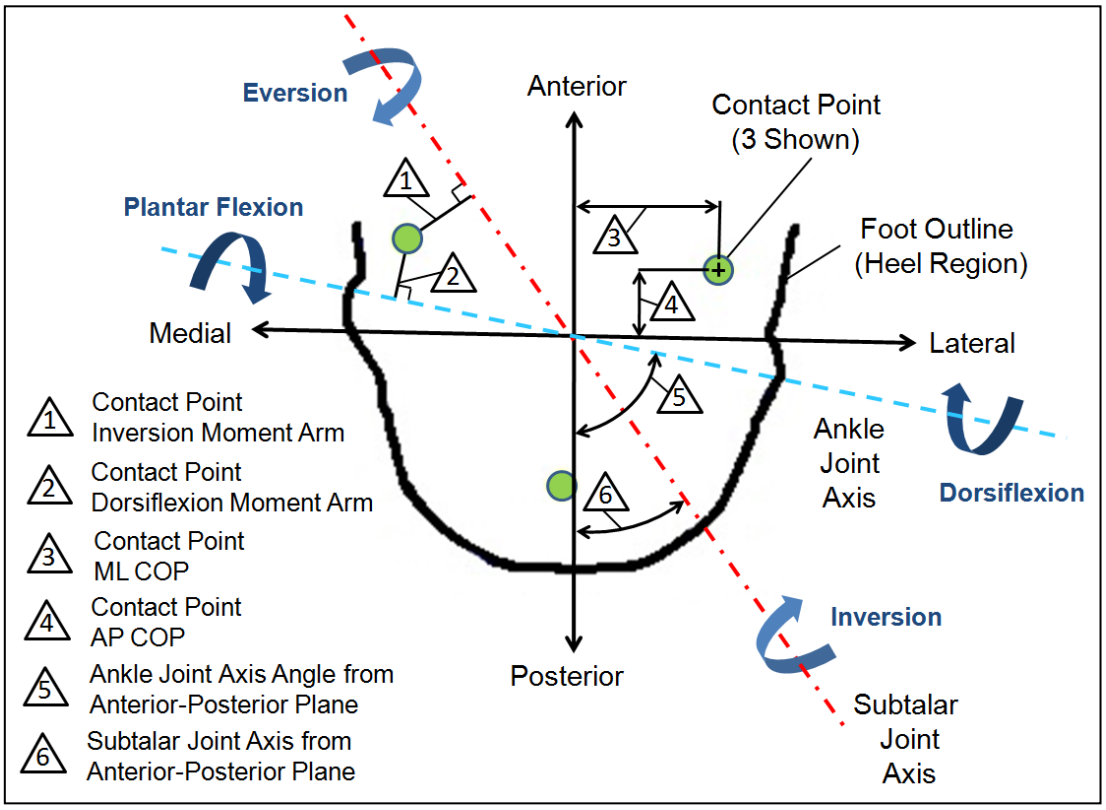

Figure 17 Static Ankle Model Contact Point Geometry

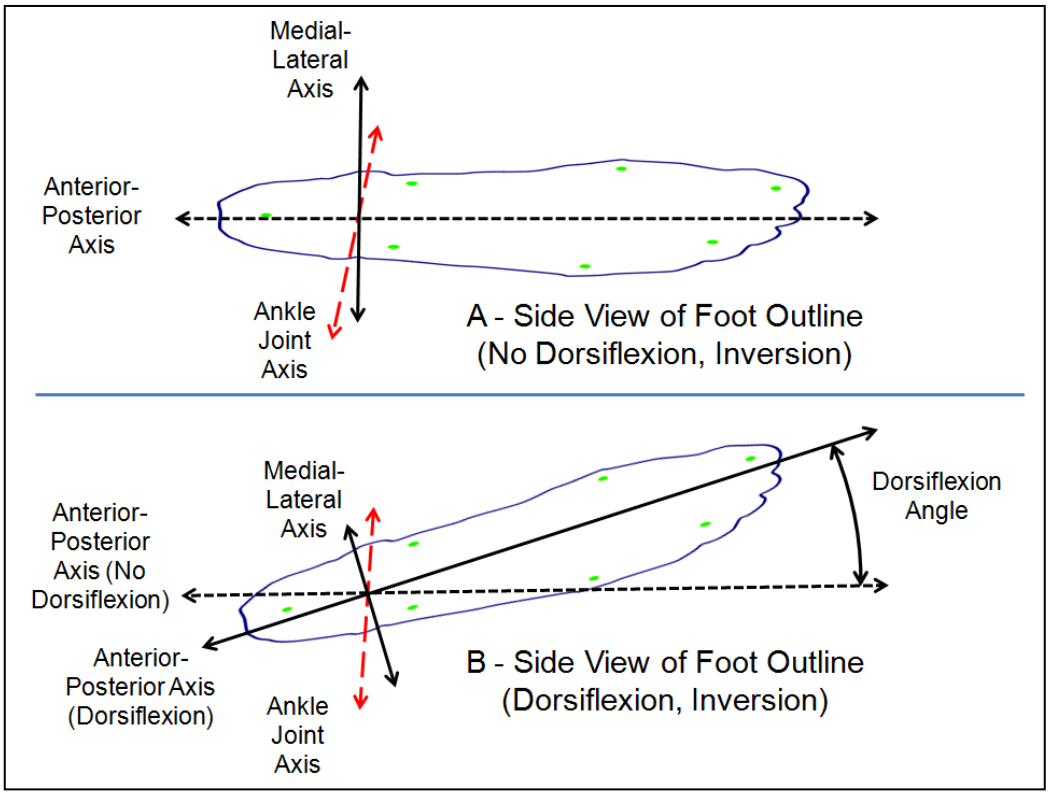

Figure 18 Static Ankle Model Dorsiflexion Angle Definition
(A – No Dorsiflexion, B- Dorsiflexion)

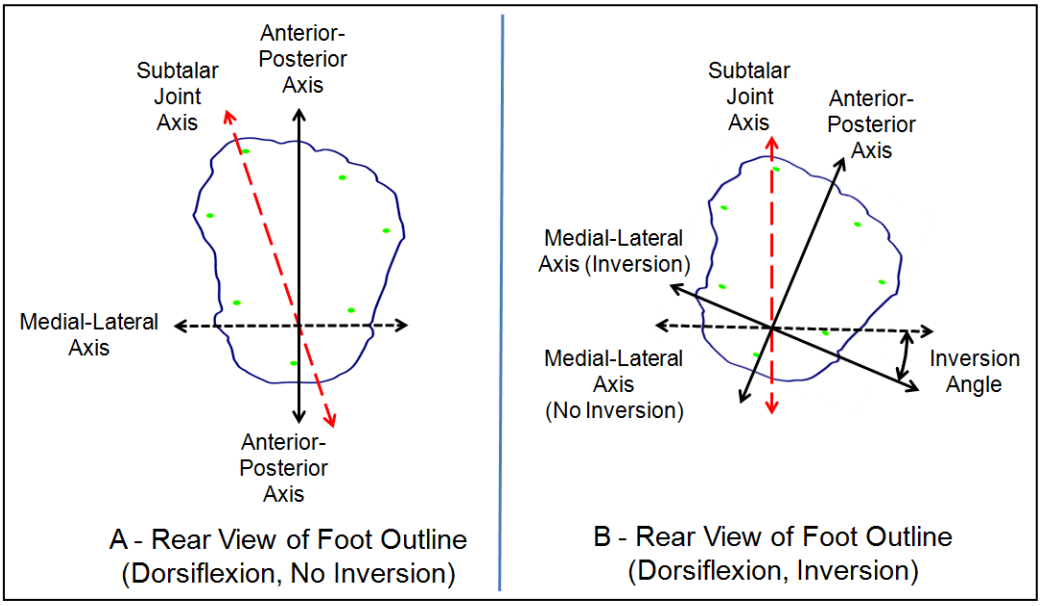

Figure 19 Static Ankle Model Inversion Angle Definition
(A – No Inversion, B- Inversion)

The ankle model was developed to operate within the Matlab® environment for compatibility with the muscle force optimization algorithm and allows easy configuration of the foot/ankle through a simple ASCII text file. Items that can be configured are:

- Foot outline of 2D plantar surface (series of X and Y coordinates)
- Contact point locations (series of X and Y coordinates)
- Muscle moment arms acting on subtalar and ankle joints
- Subtalar joint axis and ankle joint axis locations (lines defined as X and Y coordinates for two end points) [26]
- Desired COP (ML and AP-direction COP at various stance points)
- Initial guess for joint angles (inversion and dorsiflexion angles at various stance points) based on typical walking [20]

The following foot elements are computed from a subset of the configuration data:

- Ankle and subtalar joint axes slope and intercept as depicted in Figure 20
- Contact point (CP) moment arms due to dorsiflexion angle at the ankle joint and inversion angle at the subtalar joint (Figure 17)
- Muscle effective insertion locations (X and Y coordinates for each muscle) as shown in Figure 21

Input data, in addition to the foot/ankle configuration data inputs, for the ankle model are defined in Table IV. The outputs of the ankle models are summarized in Table V.

The ankle model utilizes Matlab's *fsolve* function to solve three simultaneous equations. These equations represent the sum of moments about the ankle joint (Equation

20), the sum of the moments due to the subtalar joint angle (Equation 21) and the sum of forces under the foot (Equation 22):

$$\sum_{m=1}^{M} CP\ Moments(\ Ankle\ Joint) + \sum_{n=1}^{N} Muscle\ Moments(\ Ankle\ Joint\ ) = 0 \quad (20)$$

$$\sum_{m=1}^{M} CP\ Moments\ (Subtalar\ \ Joint) + \sum_{n=1}^{N} Muscle\ Moments\ (Subtalar\ \ Joint) = 0 \quad (21)$$

$$\sum_{m=1}^{M} Contact\ Point\ Force - Body\ Weight = 0 \quad (22)$$

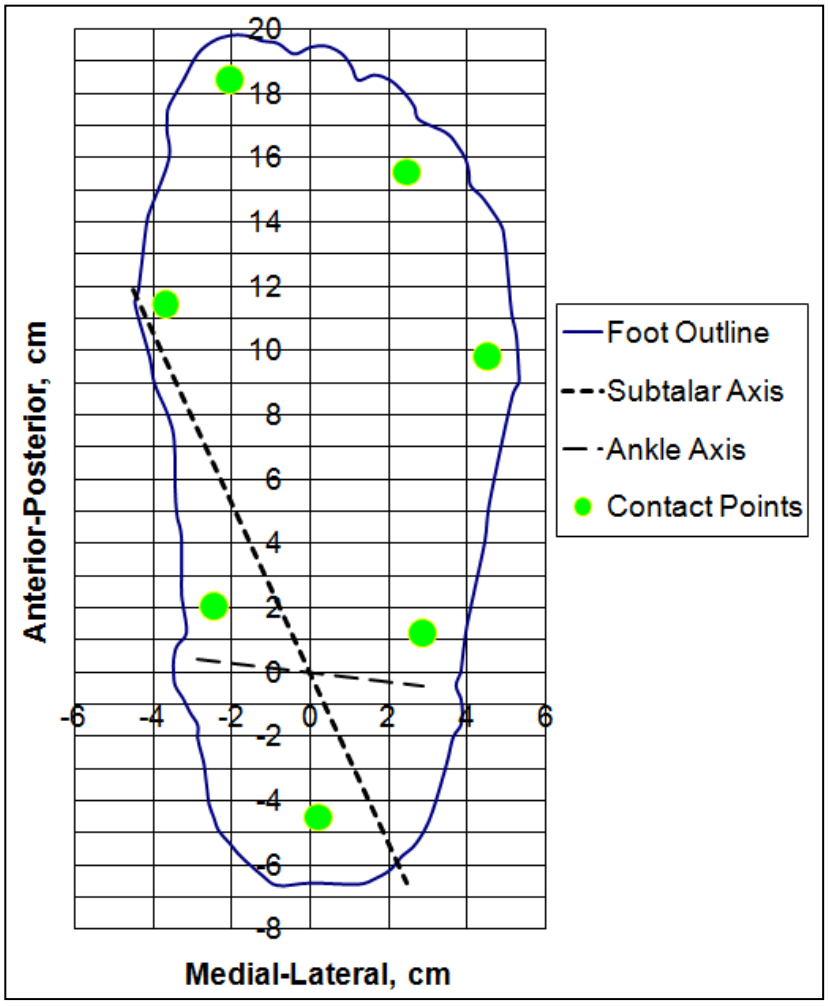

Figure 20 Ankle Model Showing Foot Outline, Contact Points, Ankle Joint Axis and Subtalar Joint Axis

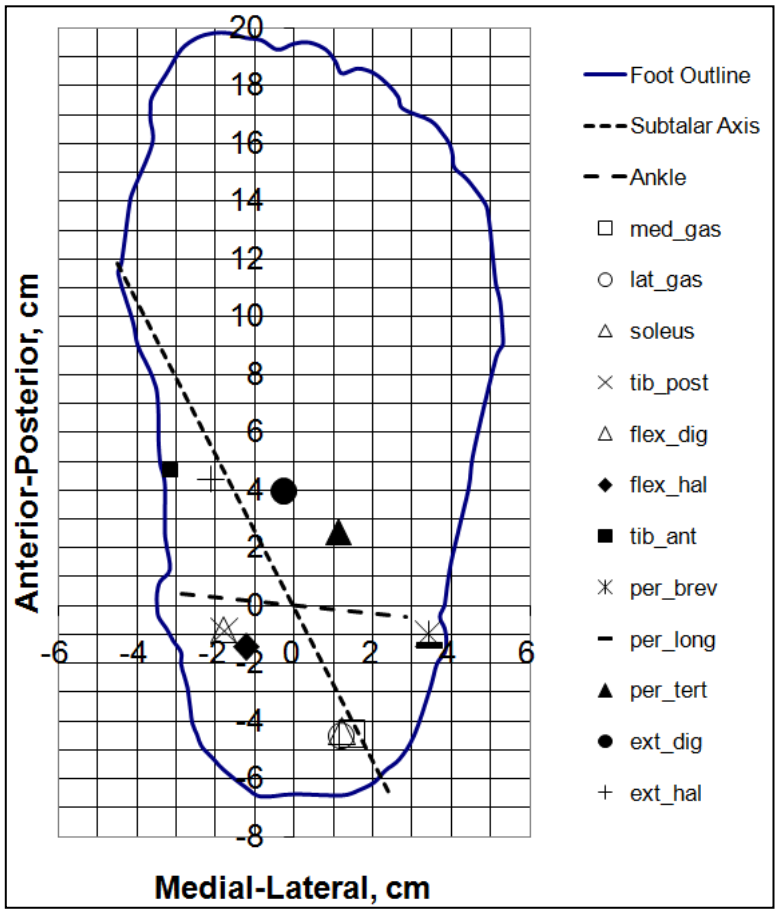

Figure 21 Ankle Model Depicting the Computed Muscle Insertion Location

Table IV Ankle Model Inputs

Name	Description	Units	Format
PER_STANCE	Discrete time elements during which the foot is in contact with the ground	Percent	Vector of length N of real numbers
MuscleForces	Muscle force in engineering units for 10 different muscles (triceps surae, tibialis posterior, flexor digitorum longus, flexor hallucis long us, tibialis anterior, peroneus brevis, peroneus longus, peroneus tertius, extensor digitorum longus, extensor hallucis longus) at each stance point	Newtons	10 x N matrix of real numbers, where N represents the number of stance data points
BodyWeight	Simulated body weight supported by the foot during stance	Newtons	Vector of length N of real numbers

Table V Ankle Model Outputs

Name	Description	Units	Format
CONTACT_ POINT_ FORCE	The simulated force under each foot contact point	Newtons	Vector of length M of real numbers, where M represents the number of contact points defined for the foot
COP_ML	Center of pressure in the medial/lateral direction	cm	Real value
COP_AP	Center of pressure in the anterior/posterior direction	cm	Real value
VGRF	Total vertical GFR acting by the simulated foot	Newtons	Real value
INV_ANGLE	Inversion angle	degrees	Real value
DOR_ANGLE	Dorsiflexion angle	degrees	Real value
TIB_POSN	Tibia position	cm	Real value

The *fsolve* function requires an initial guess for the joint angles and tibia position. The guess values for the angles are those typical values found in literature for normal walking as described previously as part of the configuration. The guess value used for the tibia position is -1.0 cm.

Additionally, the ankle model computes the COP values by summing up the COP contribution due to each of the contact points in both the ML and AP directions according to the following equations:

$$COP\ ML = \sum_{m=1}^{M}\left(ML\ Direction\ Distance\ of\ CP \times CP\ Force\right)/Vertical\ GRF \qquad (23)$$

$$COP\ AP = \sum_{m=1}^{M}\left(\ AP\ Direction\ Distance\ of\ CP \times CP\ Force\right)/Vertical\ GRF \qquad (24)$$

4.4 Muscle Force Optimization Algorithm/Ankle Model Results

The muscle force optimization algorithm was evaluated against the static ankle model to characterize the overall performance before testing with a cadaver foot. A Matlab® function was written that includes the code for the optimization algorithm and code that invokes the ankle model. This function was designed to provide multiple iterations of muscle optimization according to the following logic steps:

1. Read in the initial muscle forces and desired VGRFs for each stance point
2. Determine the resulting COP (call to the ankle model) for that set of muscle forces
3. Calculate the optimized muscle forces with the algorithm
4. Take the optimized muscle forces as the new initial muscle forces for step 1 and repeat steps 1 through 3

Figure 22 identifies the actual COP at each muscle force optimization iteration. Figure 23 identifies the error between the desired COP and the actual COP initially and then after each iteration of the muscle force optimization algorithm. Figure 24 through Figure 26 identify the muscle forces initially and then after the iterations. Figure 27 shows how the ankle joint angle, subtalar joint angle and tibia position (relative to the ground) change due to the iterations.

The mean error and the percent error reduction in COP at each iteration cycle are shown in Table VI. The mean error is the average of the errors at each stance time modeled. The percent error reduction is computed by comparison with the baseline error at each iteration, which essentially computes the amount of original error eliminated by the algorithm at each iteration.

Table VI COP Mean Error and Percent Reduction in Mean Error for Multiple Iterations

Iteration	Mean Error		% Reduction in Mean Error	
	COP Anterior	COP Lateral	COP Anterior	COP Lateral
Baseline	1.24	1.87	--	--
1	0.840	0.321	32.4	82.8
2	0.254	0.360	79.5	80.8
3	0.152	0.266	87.8	85.8
4	0.086	0.232	93.0	87.6
5	0.071	0.226	94.2	87.9

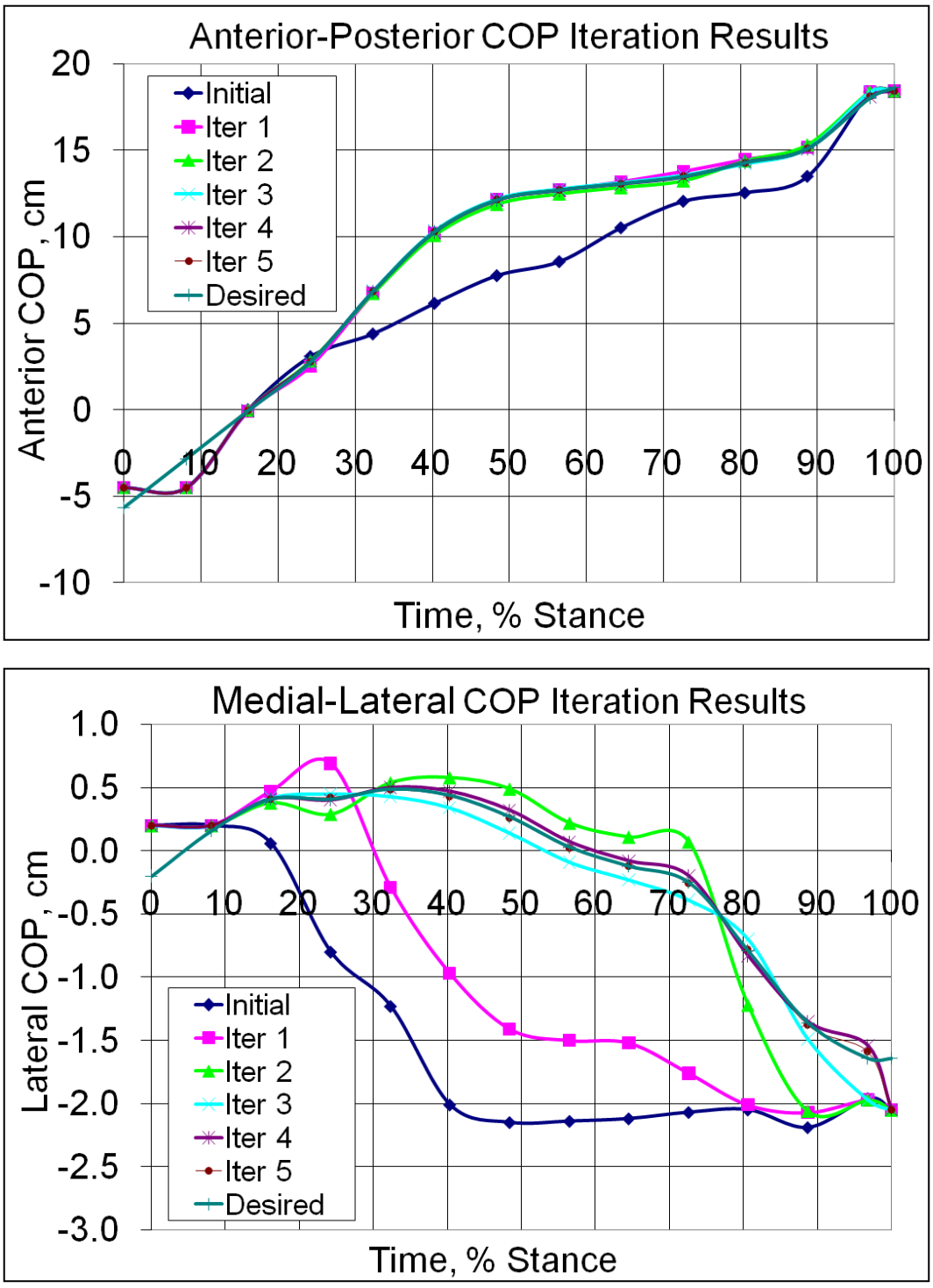

Figure 22 COP for each Optimization Iteration (AP: Top, ML: Bottom)

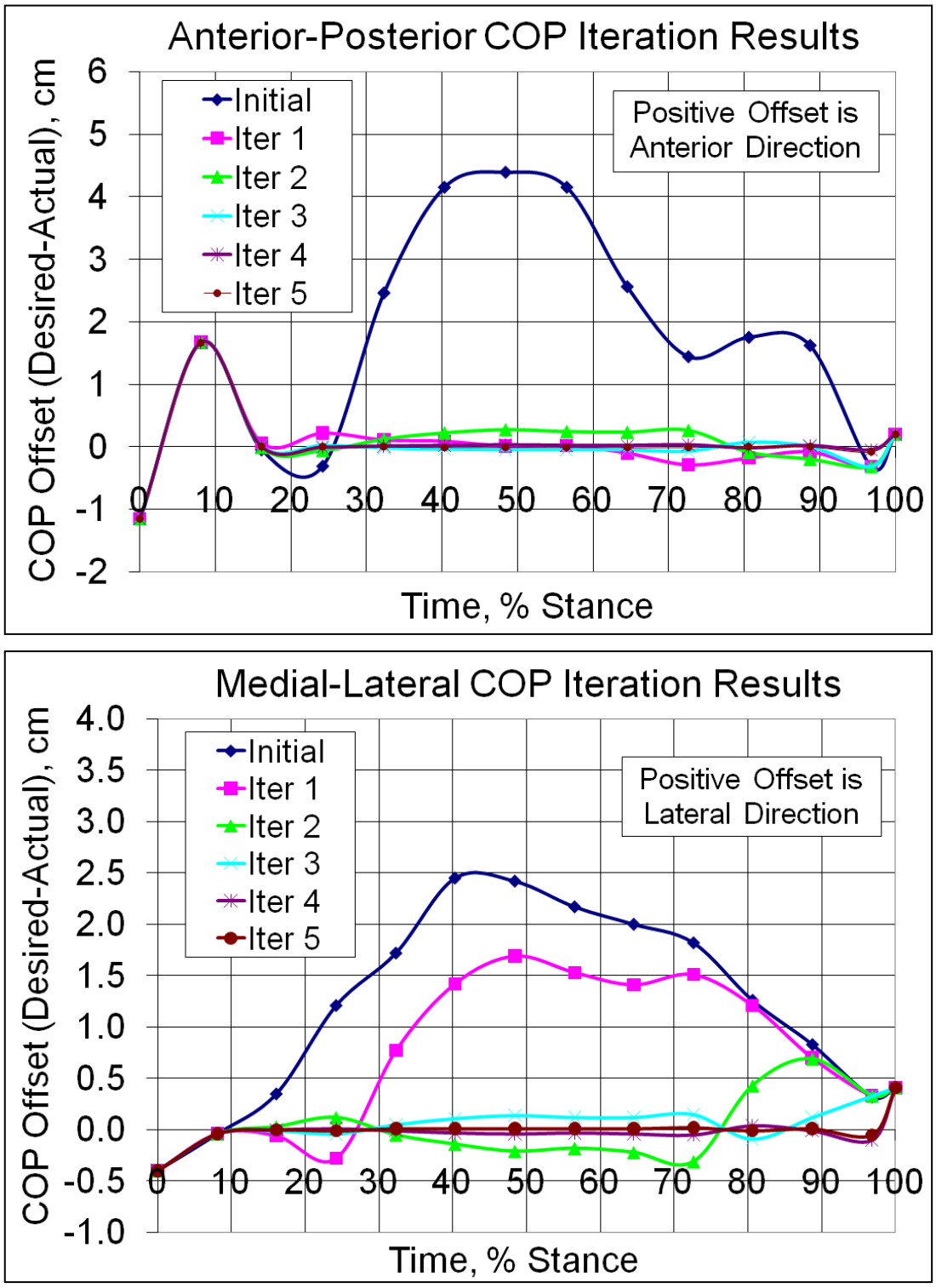

Figure 23 COP Offset for each Optimization Iteration (AP: Top, ML: Bottom)

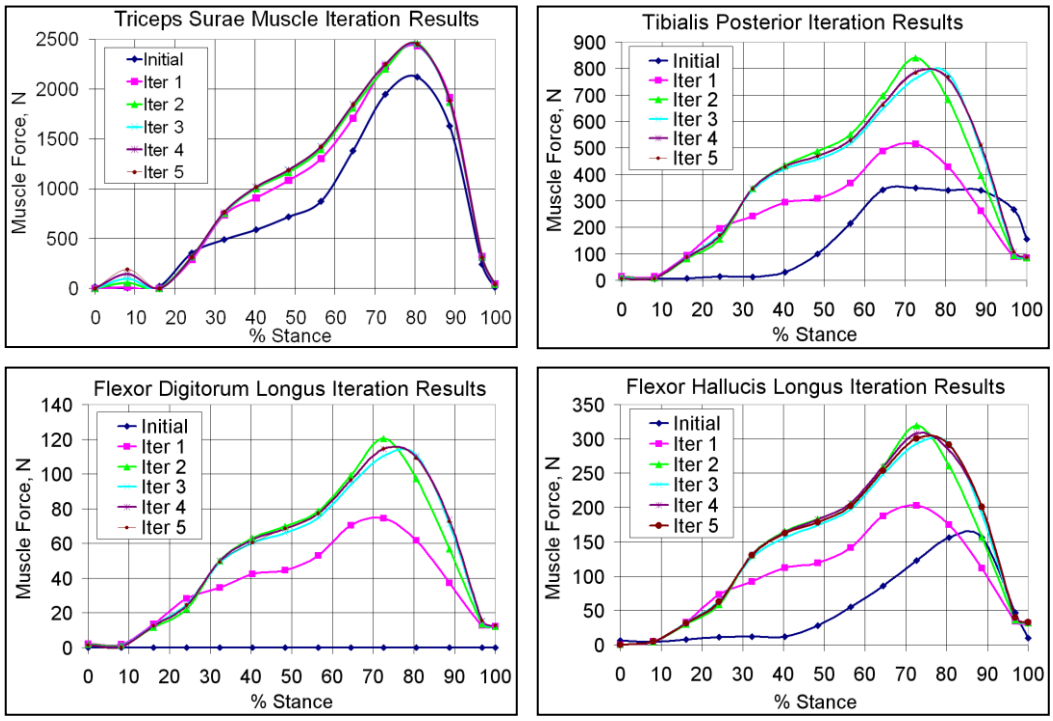

Figure 24 Flexor Muscle Forces for each Optimization Iteration

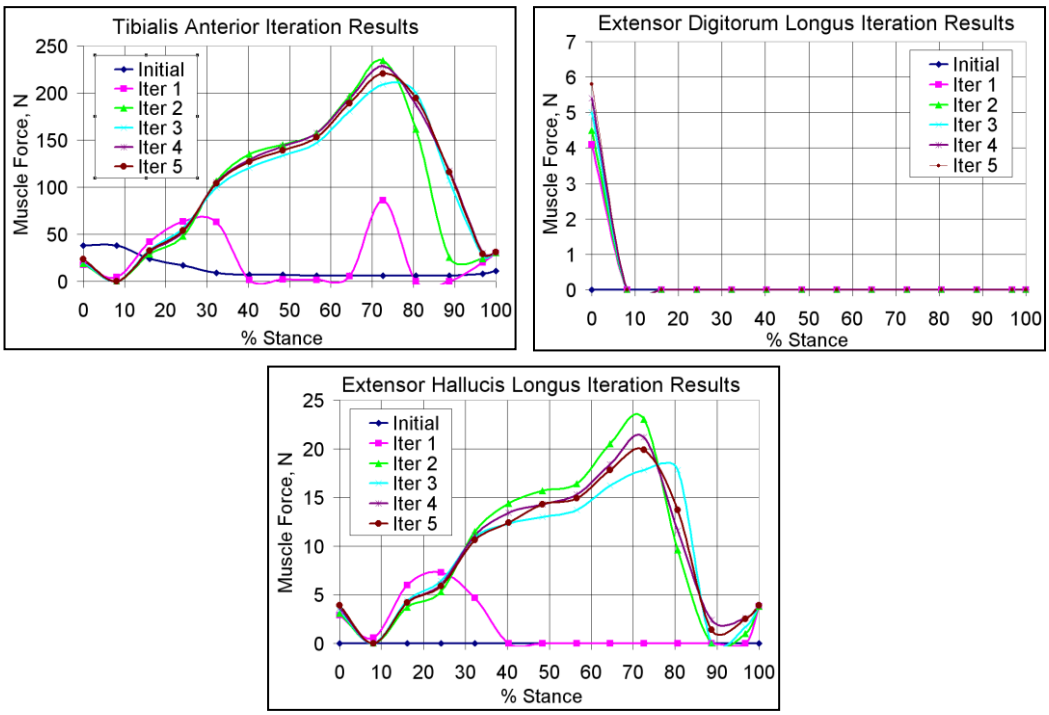

Figure 25 Extensor Muscle Forces for each Optimization Iteration

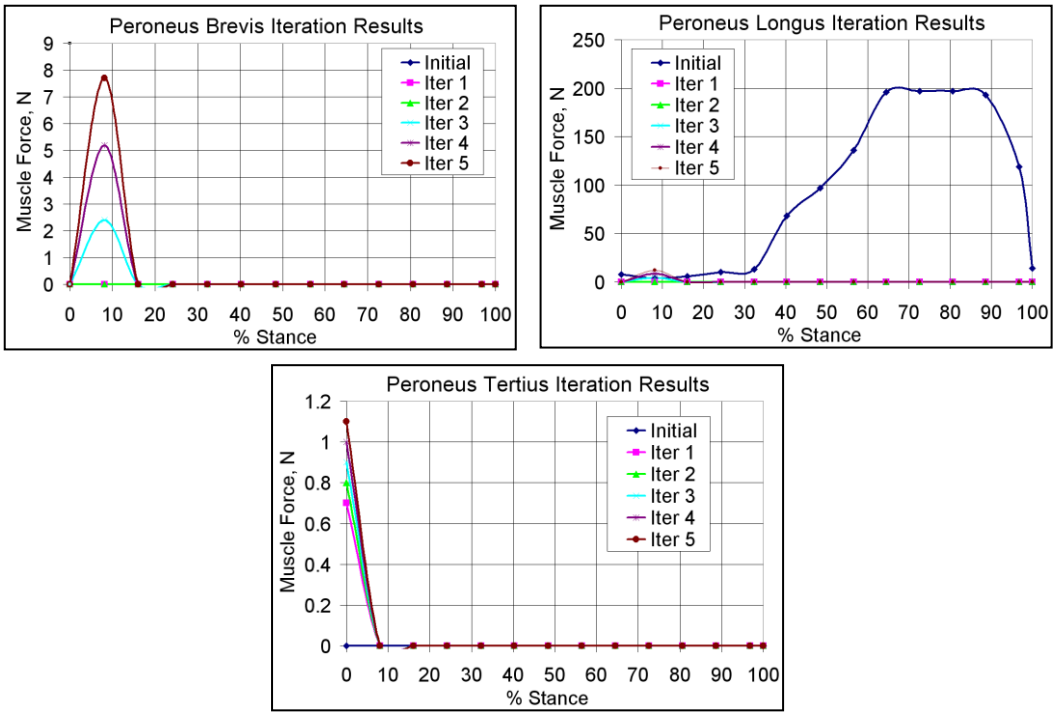

Figure 26 Everter Muscle Forces for each Optimization Iteration

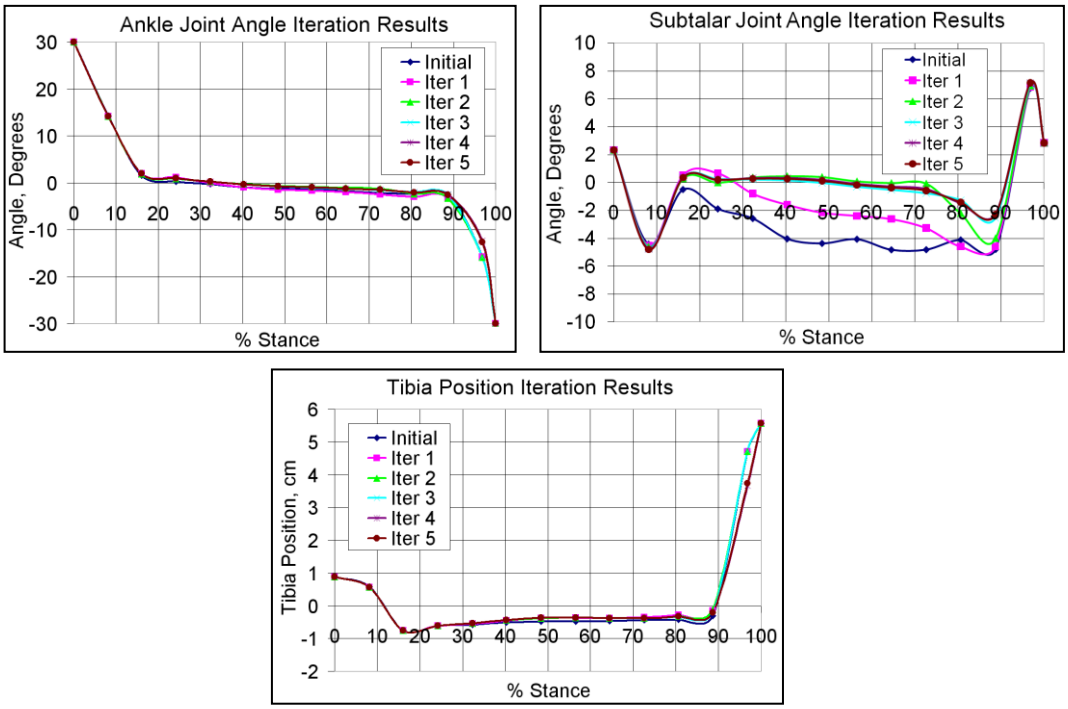

Figure 27 Ankle Joint Angle, Subtalar Joint Angle and Tibia Position for each Optimization Iteration

4.5 Muscle Force Optimization Algorithm/Ankle Model Discussion

The ankle model has been demonstrated to be a valuable tool for the debugging and evaluating the performance of the muscle force optimization algorithm in spite of being a very simple pseudo 2D representation of the foot/ankle. The muscle force optimization algorithm essentially eliminates error between the desired and actual COP within four iterations when tested against the ankle model as shown in Figure 22. As seen from Table VI, after four iterations the mean error in the anterior and lateral COP was reduced by 93.0% and 87.6%, respectively.

From viewing the optimized muscle forces resulting from each iteration (Figure 24 through Figure 26), it can be seen qualitatively that muscle force adjustments are being made to correct the errors at the previous iteration. For example, if we consider the triceps surae muscle, the ML-direction COP offset (desired – actual) shows significant positive value (over 4 cm in the lateral direction in some regions) identifying that higher muscle force would be required to achieve this amount of lateral movement in the COP. Since the triceps surae muscle group will invert the foot, it will result in a shift in the COP in the lateral direction. Similarly, the AP-direction COP offset is also positive (as high as 2 cm in anterior direction) signifying that higher muscle force will make the necessary adjustment by shifting the force in the anterior direction since the triceps surae muscle group will plantar flex the foot.

It was observed that the optimized muscle forces for tibialis anterior and extensor hallucis longus were significantly increased throughout stance. This is one outcome of the optimization approach that minimizes the cube of the muscle stresses that may contradict what is reported in literature with respect to surface EMG measurements of

these muscles during walking [27]. EMG seems to indicate that extensors are active to setup for heel strike and swing phase, but inactive during the majority of stance phase. This indicates that additional constraints may be required for the muscle force optimization algorithm to augment those implemented during this research effort.

CHAPTER V

EVALUATION OF A MUSCLE FORCE OPTIMIZATION ALGORITHM WITH A CADAVER FOOT

5.1 Muscle Force Optimization Algorithm Test Overview

Evaluation of the muscle force optimization algorithm has been performed using the UMS to simulate walking with a cadaver feet. A special Matlab® function was prepared to adapt the muscle force optimization algorithm to interface with the LabVIEW application software previously written for foot walking simulations. The inputs to this function are defined in Table VII. The output of this function is a set of optimized muscle forces at each discrete stance time.

Three frozen cadaveric specimens (Table VIII) were used for this study. Feet were dissected to expose nine tendons: triceps surae, tibialis posterior, flexor hallucis longus, flexor digitorum longus, peroneus longus, peroneus brevis, tibialis anterior, extensor digitorum longus and extensor hallucis longus. All remaining soft tissue was cleaned from the proximal end of the tibia and fibula in order to mount the bones within an 2 inch OD aluminum tube using a low temperature melting point metal alloy (Wood's metal, CAS# 76093-98-6), as a potting substrate.

Table VII Muscle Force Optimization Algorithm Inputs

Name	Description	Units	Format
Foot_Length	Maximum foot length measured from tip of 1st toe to back of heel. Used to scale ankle joint moment arms	mm	Real number
Foot_Width	Maximum width of foot measured across the metatarsal head region. Used to scale subtalar joint moment arms	mm	Real number
Total_Body_Mass	Total body mass of subject that donated the cadaver foot. Used to compute muscle cross-sectional areas	kg	Real number
Percent_Stance	The set of discrete time values during the simulated stance	% Stance	Vector of real numbers
Muscle_Forces_ Actual	Muscle Forces from previous run at various stance positions	N	10 x N matrix of real numbers, where N represents the number of stance data points
Muscle_Gains	Gain value to allow linear scaling of moments arms. Also, allows elimination of some muscles or time values by entering zero (0) for gain.	Not Applicable	10 x N matrix of real numbers, where N represents the number of stance data points
COP_Actual	Previous measured values for COP in ML and AP directions as measure from the force platform	cm	2 x N matrix of real numbers, where N represents the number of stance data points
COP_Desired	Desired (target) values for COP in ML and AP directions	cm	2 x N matrix of real numbers, where N represents the number of stance data points
VGRF_Desired	Desired (target) vertical ground reaction force	N	Vector of length N of real numbers
Exponent_n	This is exponent used in the objective function. This is the order of the muscle stress (muscle force/muscle cross-sectional area) typically 2 or 3 are reported for this value	Not Applicable	Real number

Table VIII Cadaver Foot Specimen Summary

Specimen ID	Age, years	Sex	Side	Donor Weight, kg	Recovery Time, hrs	Cause of Death
63496-L	49	Male	Left	45.4	15.2	Respiratory Arrest
63496-R	49	Male	Right	45.4	15.2	Respiratory Arrest
63529-L	67	Female	Left	60.4	7.3	Pancreatic Cancer

Cadaver specimens were tested in the Cleveland Clinic's UMS facility (Figure 28). The detailed components and capabilities of the UMS have been published previously [19]. Kinematic and kinetic data required as inputs to the UMS to provide walking patterns, desired ground reaction forces and desired center of pressure were collected as previously described [21] for a similar experiment where normal gait was simulated within the UMS. Target ground reaction forces (Figure 11) and target COP (Figure 9) were shown previously in this current work.

Muscle forces were simulated with the UMS-provided Multi-Tendon Actuator System (developed as part of this work) using optimized force profiles previously [19] found to achieve the desired/target superior force (VGRF) within ±10% during simulated walking. The optimized muscle forces were derived initially by linear scaling from EMG values [27] based on muscle cross-sectional area obtained in literature [28]. Assuming that the triceps surae muscle group generates a peak normalized force 220 %BW, the peak force for other muscles were estimated by the ratio of muscle cross-sectional areas to triceps surae cross-sectional area. The muscle EMG-derived muscle force profiles are shown in Figure 29 (solid lines). The optimized muscle force profiles (dashed lines), shown in this same figure, represent the resulting force profiles that were developed during cadaver foot testing where the goal was to achieve the superior force/VGRF

within ±10% of the target force during evaluation of tibial and calcaneal bone strain during simulated walking [19]. The optimized profiles were achieved by taking the EMG-derived profiles as a starting point for the simulation and then using a simple fuzzy-logic based controller to individually adjust muscles profiles until this superior force target was achieved.

Figure 28 Universal Musculoskeletal Simulator Configured for Foot Studies

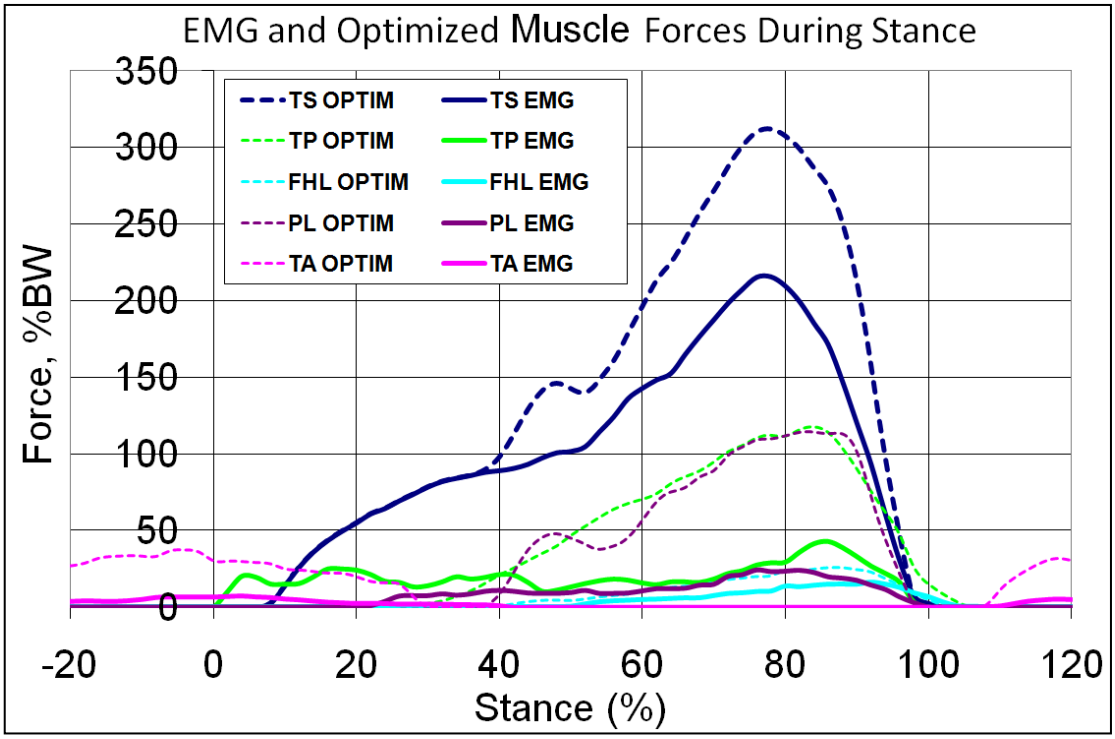

Figure 29 EMG-derived and Target (Optimized) Muscle Force Profiles for Simulated Walking within the UMS

5.2 Muscle Force Optimization Algorithm Test Results for Cadaver Specimen 63496-R

The force optimization control algorithm was set to limit the change in muscle optimization to the range of 22 to 64% stance to focus on the mid stance region where the foot is essentially flat on the ground. Figure 30 and Figure 31 display the results of three iterations of muscle force optimization on the anterior and medial COP, respectively. Figure 32 provides the resulting muscle forces, at each iteration, in addition to the initial forces (baseline). The change in ground reaction forces that result from the change in muscle forces is shown in Figure 33. The cumulative percent reduction in the COP mean error (desired - actual) is shown in Table IX.

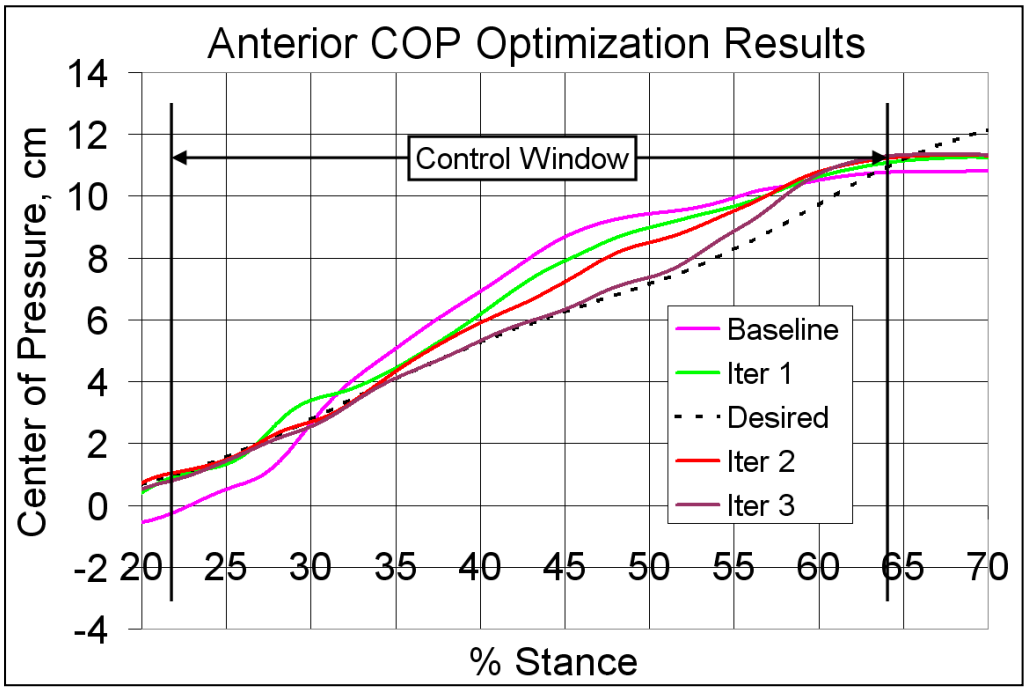

Figure 30 Anterior COP Optimization Results (Specimen 63496-R)

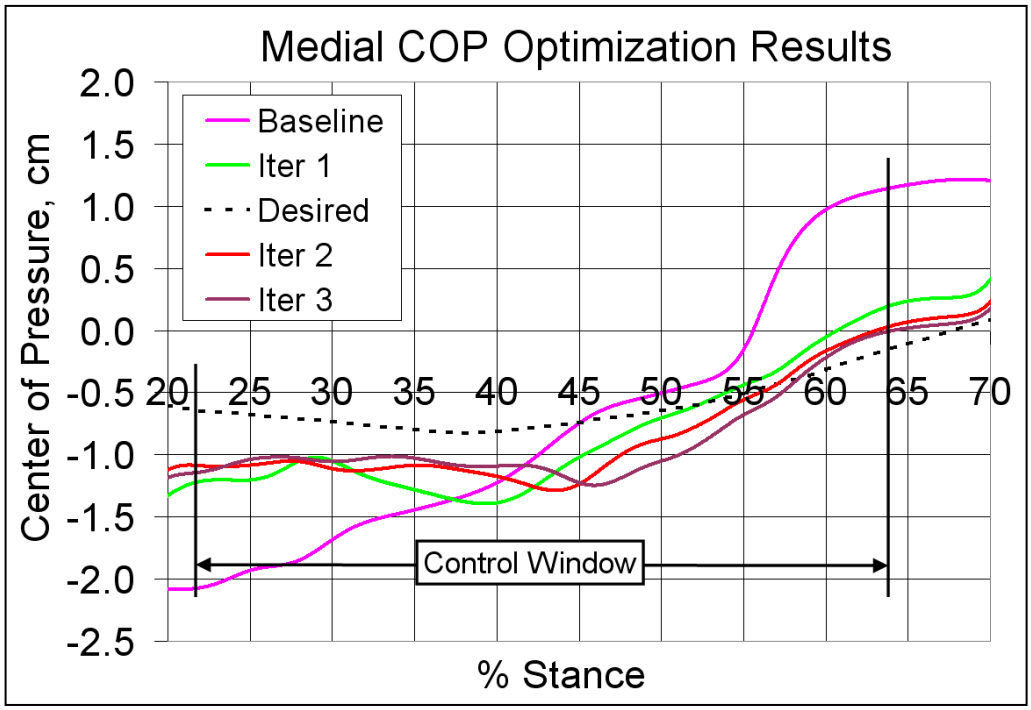

Figure 31 Medial COP Optimization Results (Specimen 63496-R)

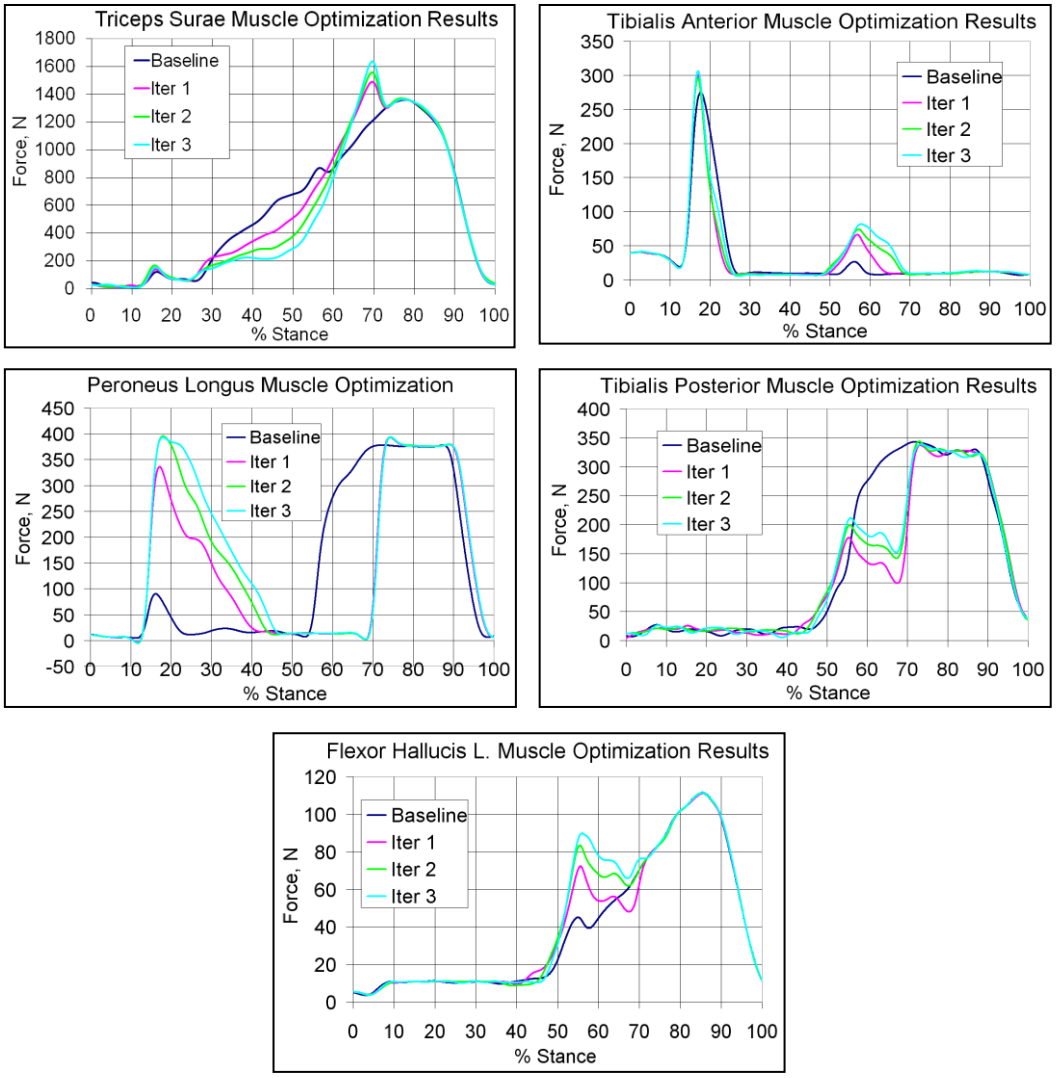

Figure 32 Muscle Forces Optimization Results (Specimen 63496-R)

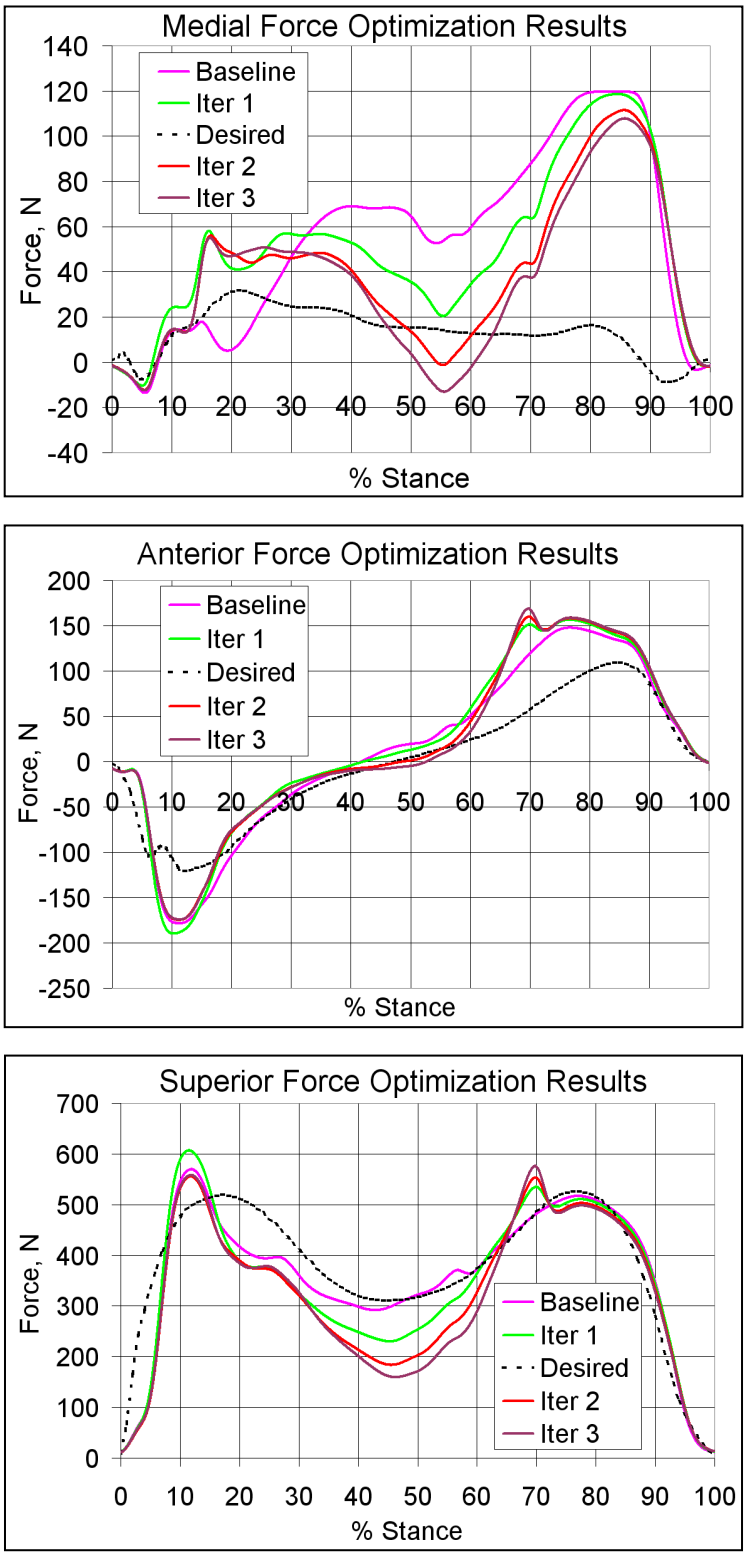

Figure 33 Ground Reaction Forces Optimization Results (Specimen 63496-R)

Table IX Percent Reduction in Mean COP Error Resulting from Muscle Optimization (Cadaver Specimen: 63496-R)

% Stance Range	Iteration 1		Iteration 2		Iteration 3	
	COP Anterior	COP Medial	COP Anterior	COP Medial	COP Anterior	COP Medial
22-64	32.3	75.6	50.1	78.4	78.7	78.3
22-30	70.2	50.0	94.3	56.2	84.6	58.8
31-40	50.0	52.4	68.5	68.5	94.0	74.8
41-50	29.1	87.8	54.1	82.7	93.4	81.6
51-60	11.7	93.4	20.5	93.4	58.9	88.4
61-64	-52.8	-15.7	-110	37.3	-127.4	48.9

5.3 Muscle Force Optimization Algorithm Test Results for Cadaver Specimen 63496-L

The force optimization control algorithm was set to limit the change in muscle optimization to the range of 36 to 92% stance to focus on the mid stance region where the foot is essentially flat on the ground. Figure 34 and Figure 35 display the results of two iterations of muscle force optimization on the anterior and medial COP, respectively. Figure 36 includes the resulting muscle forces, at each iteration, in addition to the initial forces (baseline). The change in ground reaction forces that result from the change in muscle forces is shown in Figure 37. The percent reduction in the COP mean error is shown in Table X.

Table X Percent Reduction in Mean COP Error Resulting from Muscle Optimization (Cadaver Specimen: 63496-L)

% Stance Range	Iteration 1		Iteration 2		Iteration 3	
	COP Anterior	COP Medial	COP Anterior	COP Medial	COP Anterior	COP Medial
37-92	17.8	37.9	40.1	53.6	32.8	71.1
37-40	-121	-13.5	-144	37.8	72.4	85.9
41-50	38.7	87.9	81.9	97.7	85.3	98.6
51-60	-8.1	50.2	42.7	86.4	-2.77	93.6
61-70	-7.7	55.1	-34.5	69.8	-96.5	90.7
71-80	57.7	36.5	35.8	28.5	11.0	64.1
81-92	-24.5	-203	-40.1	-173.3	-36.1	-93.1

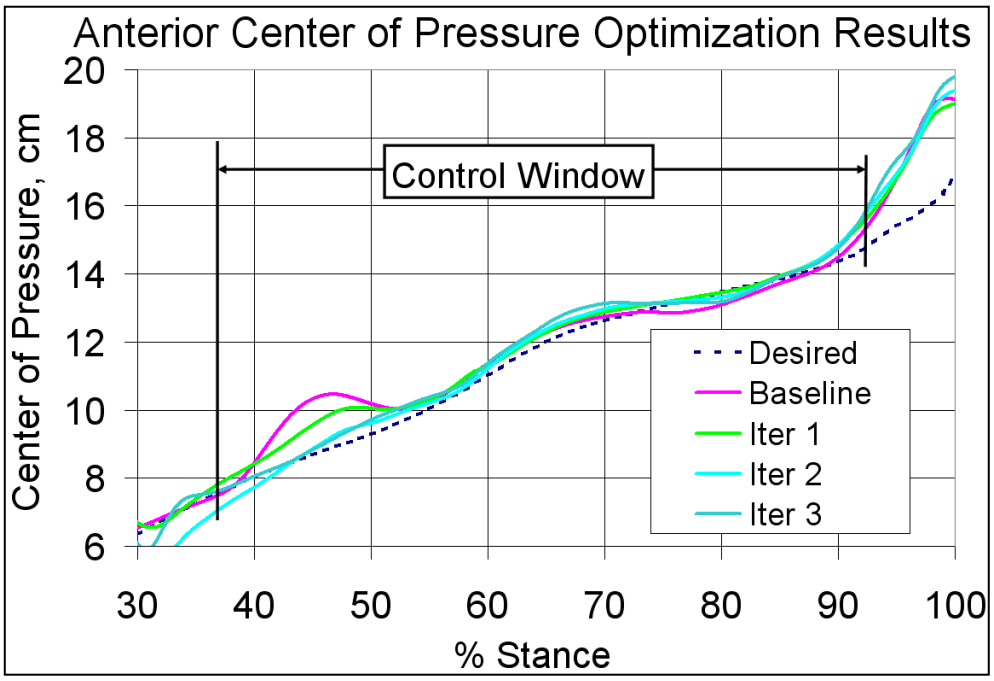

Figure 34 Anterior COP Optimization Results (Specimen 63496-L)

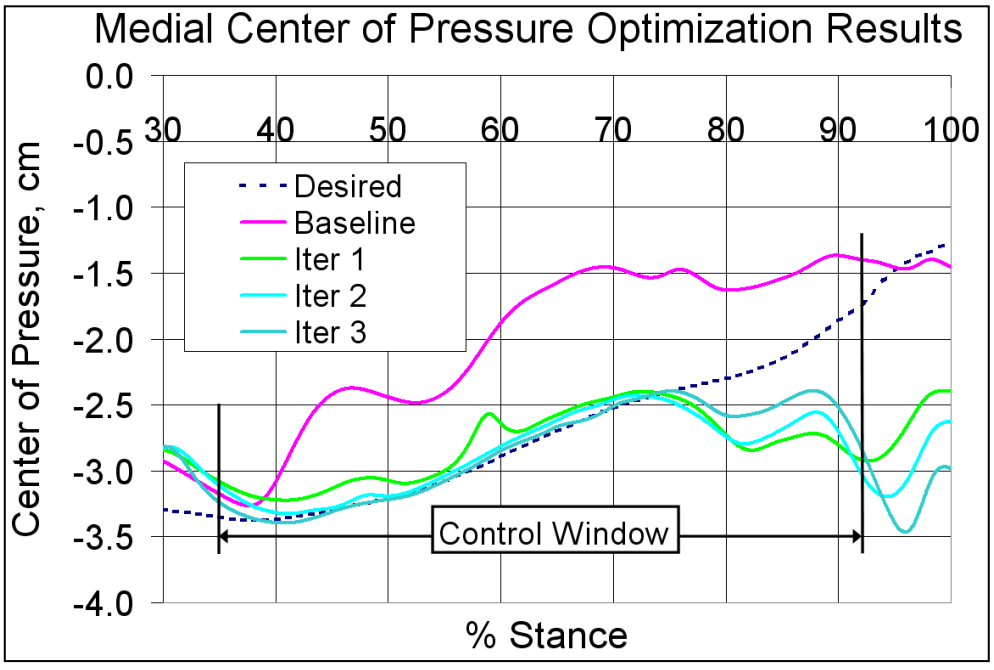

Figure 35 Medial COP Optimization Results (Specimen 63496-L)

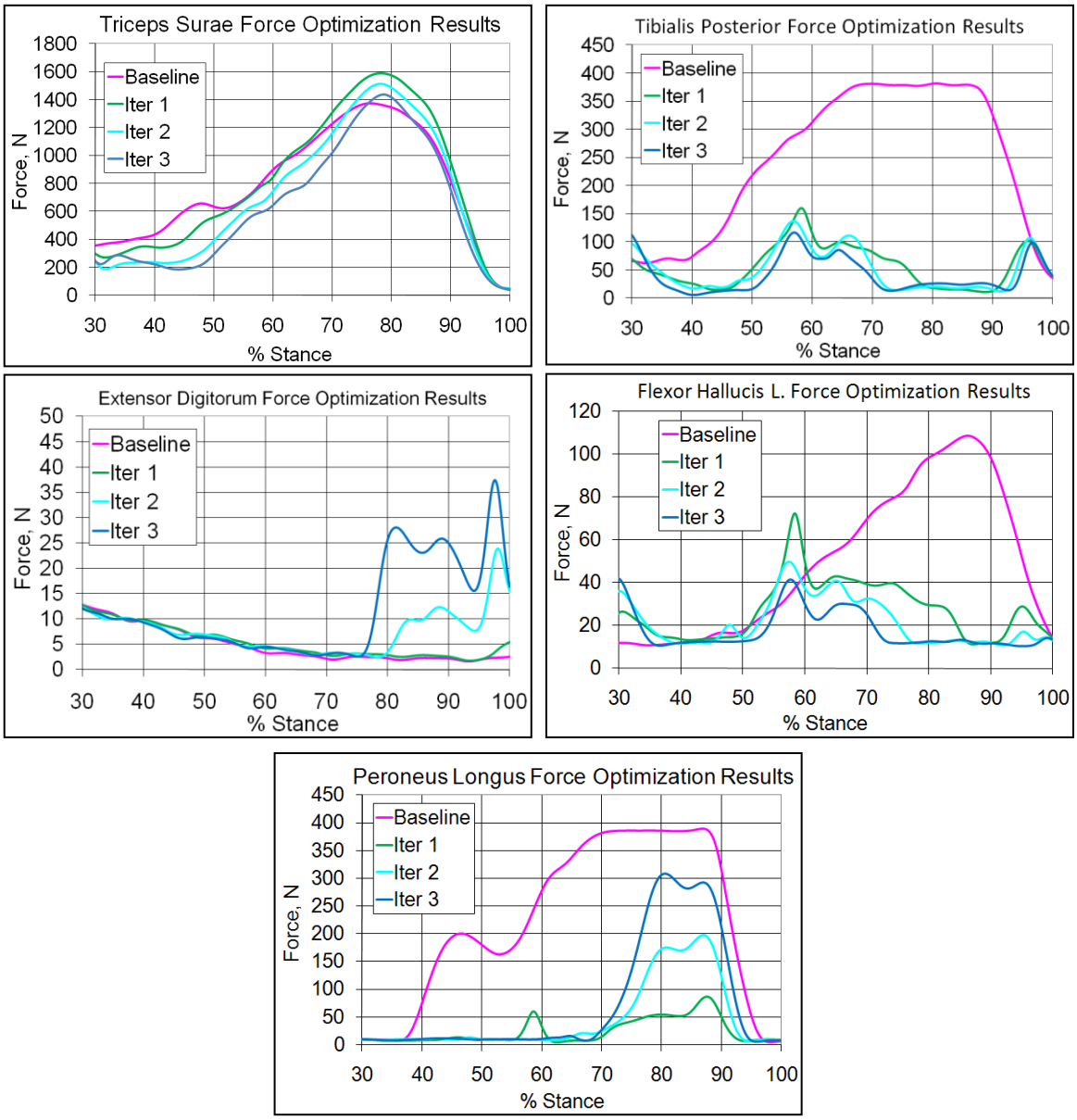

Figure 36 Muscle Forces Optimization Results (Specimen 63496-L)

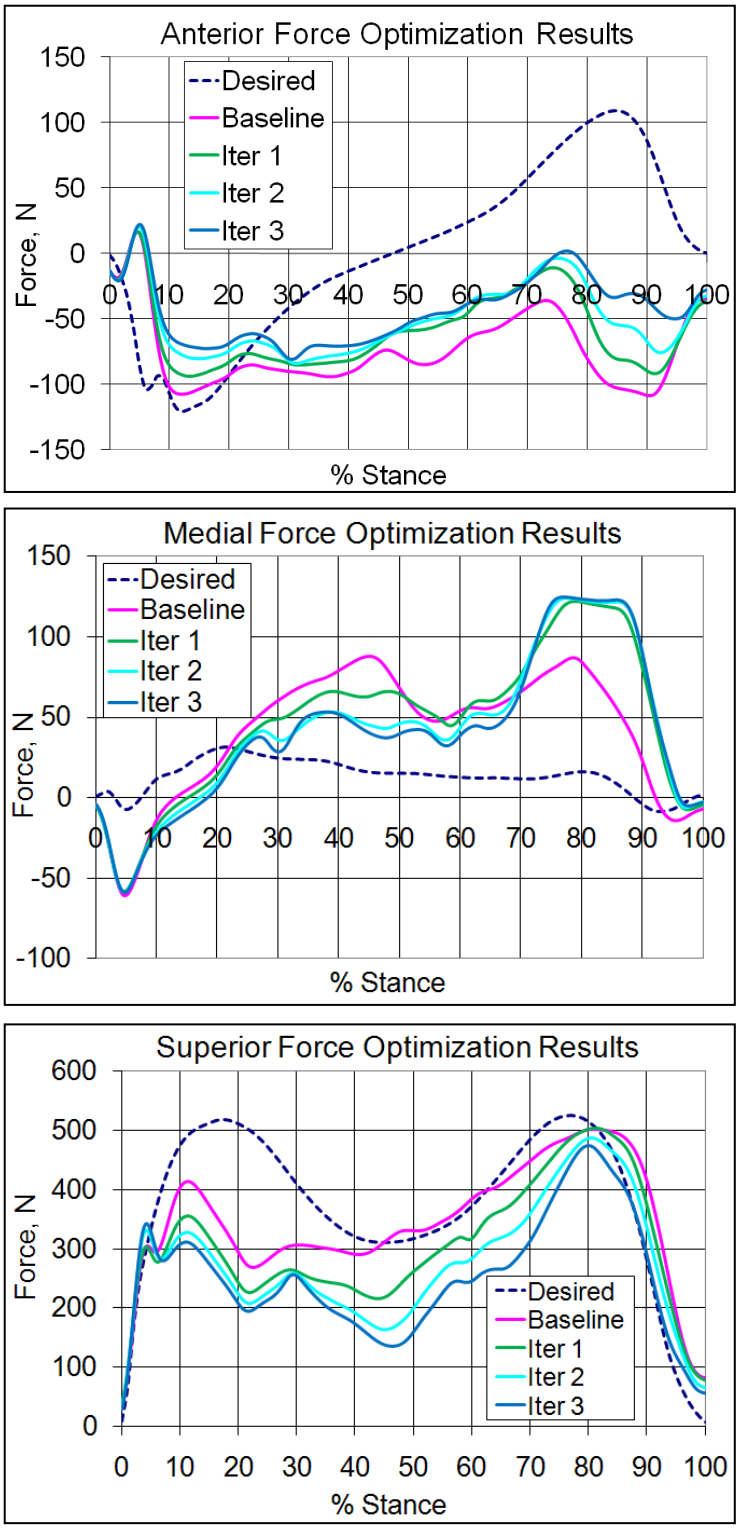

Figure 37 Ground Reaction Forces Optimization Results (Specimen 63496-L)

5.4 Muscle Force Optimization Algorithm Test Results for Cadaver Specimen 63529-L

The force optimization control algorithm was set limit the change in muscle optimization to the range of 36 to 98% stance to focus on the mid stance and terminal stance regions. Figure 38 and Figure 39 display the results of two iterations of muscle force optimization on the anterior and medial COP, respectively. Figure 40 includes the resulting muscle forces, at each iteration, in addition to the initial forces (baseline). The change in ground reaction forces that result from the change in muscle forces is shown in Figure 41. The percent reduction in the COP mean error is shown in Table XI.

Table XI Percent Reduction in Mean COP Error Resulting from Muscle Optimization (Cadaver Specimen: 63529-L)

Stance Range, %	Iteration 1		Iteration 2		Iteration 3	
	COP Anterior	COP Medial	COP Anterior	COP Medial	COP Anterior	COP Medial
Overall	21.3	85.8	28.8	93.8	32.9	89.8
36-40	52.0	92.9	78.5	95.8	94.9	98.3
41-50	20.7	88.1	66.4	95.7	83.0	97.4
51-60	33.3	97.9	38.8	93.3	77.8	95.7
61-70	34.6	68.6	4.63	88.2	39.9	88.5
71-80	48.9	35.6	18.8	90.8	-23.9	82.5
81-90	7.10	84.7	6.92	98.3	-10.3	82.9
91-97	-7.66	92.2	0.145	91.0	-20.2	84.2

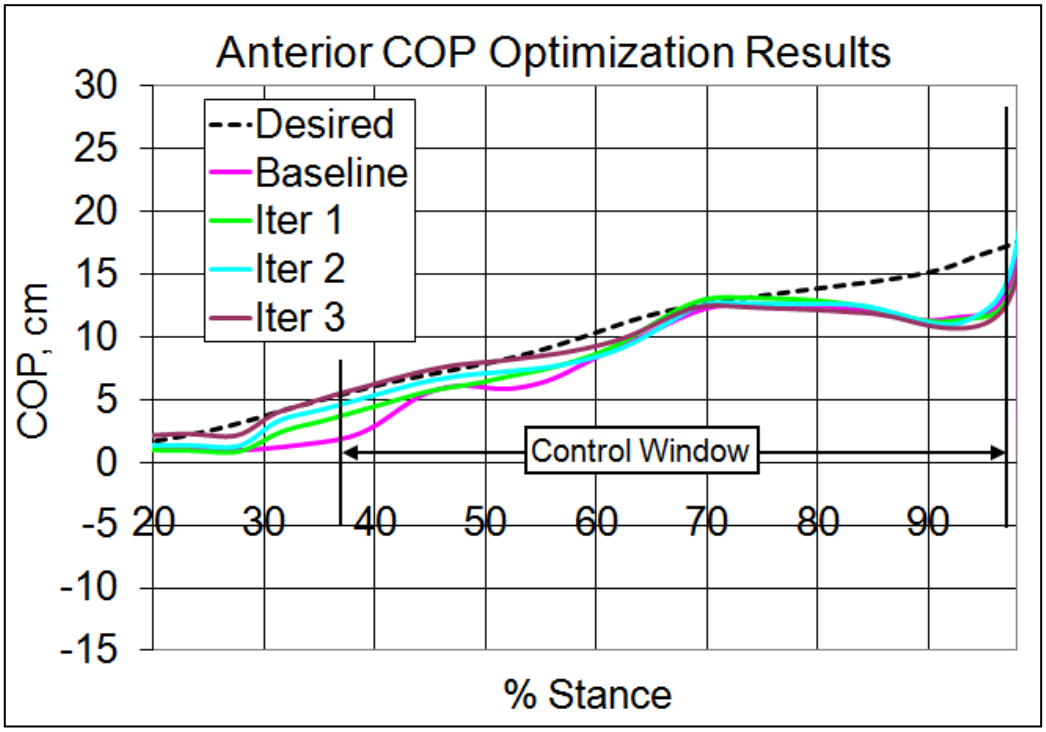

Figure 38 Anterior COP Optimization Results (Specimen 63529-L)

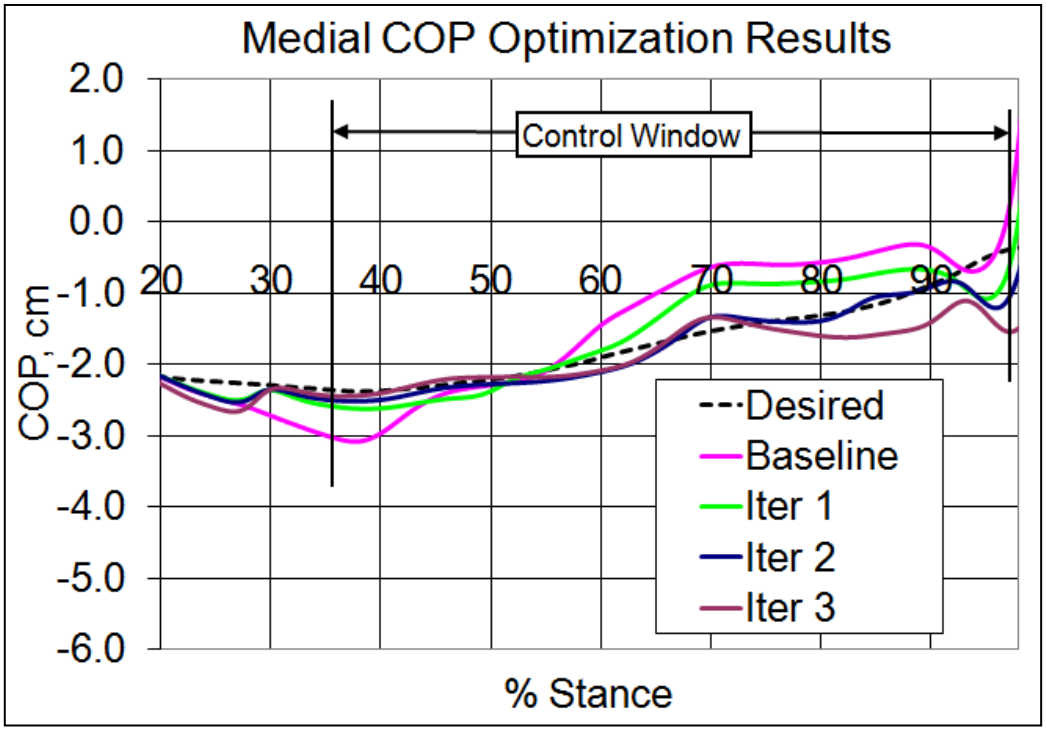

Figure 39 Medial COP Optimization Results (Specimen 63529-L)

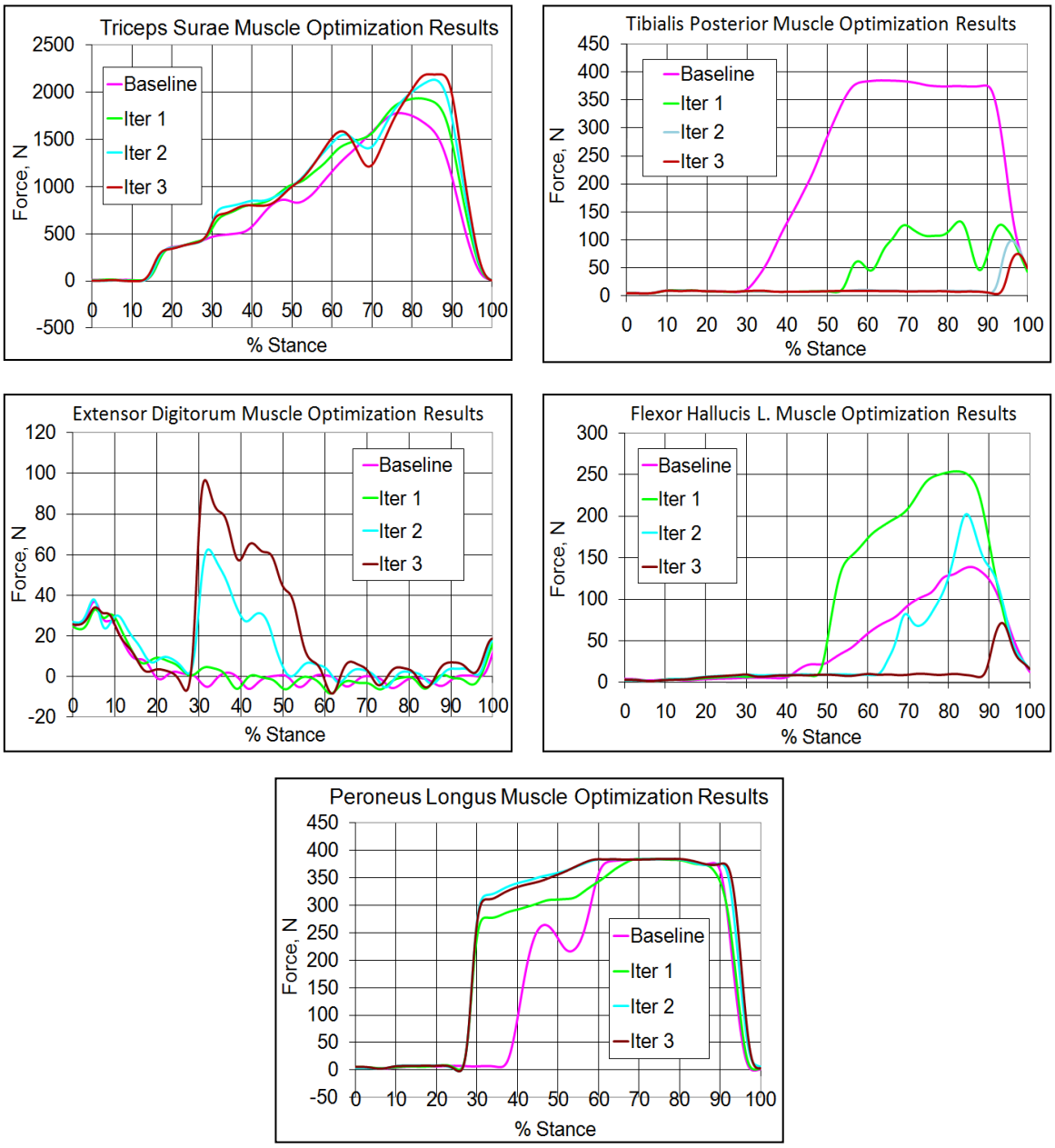

Figure 40 Muscle Forces Optimization Results (Specimen 63529-L)

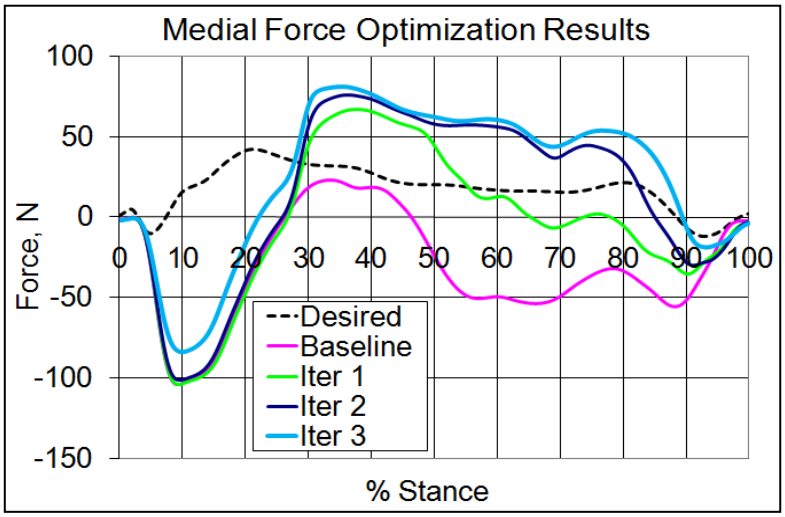

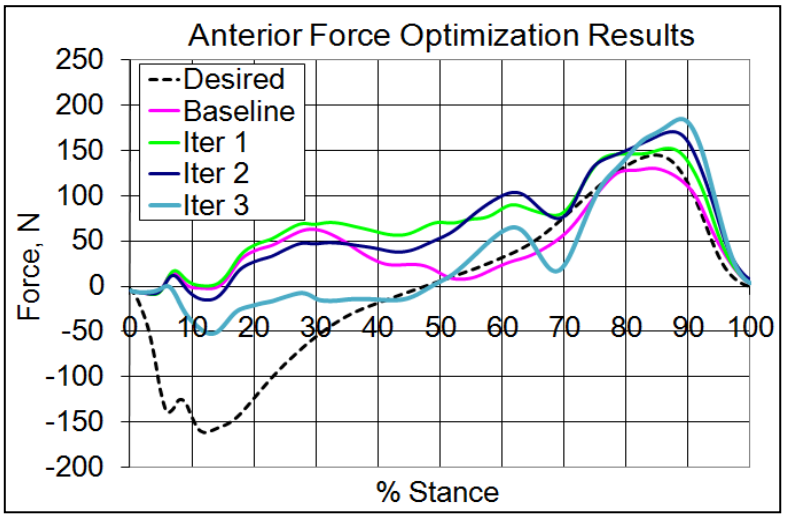

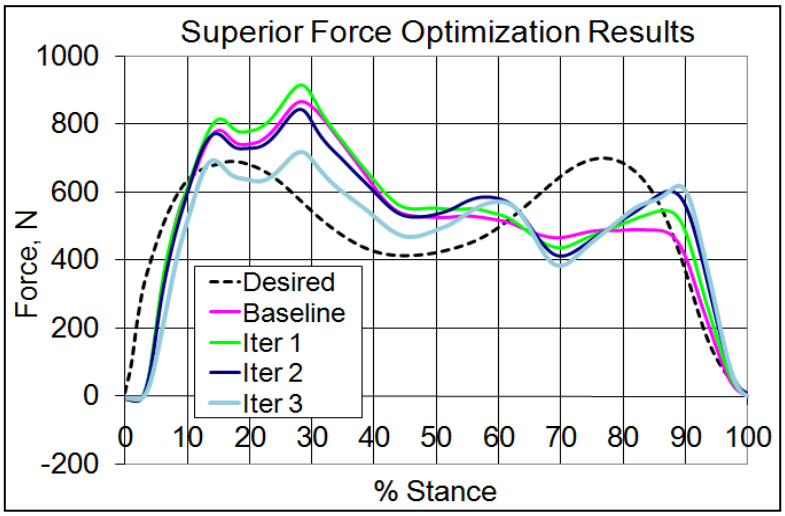

Figure 41 Ground Reaction Forces Optimization Results (Specimen 63529-L)

5.5 Muscle Force Optimization Algorithm Cadaver Foot Testing Discussion

Testing with cadaver feet has demonstrated that this algorithm is able to optimize muscle forces to simultaneously improve AP and ML COP.

For the three feet tested, improvement to COP is greatest in the mid stance portion of gate and especially in the range of 41-50% stance where the anterior and medial percent reduction in the mean error ranged from 83.0% to 93.4% for AP COP and from 81.6% to 98.6% for ML COP after three iterations. This result is consistent with the derivation of the optimization algorithm, as it assumes a flat foot situation, ignoring the forefoot joint. Therefore, this finding seems to confirm that for the heel strike and terminal stance regions, where the flat foot condition does not hold true, the objective function constraints are not valid. Additionally, the muscle moment arms are assumed constant, but at extreme ankle and subtalar joint angles, this assumption may not be valid. This might also be a contributing factor to the algorithm's inability to correct COP in terminal stance.

Optimization of the COP was shown to have a marked impact on the ground reaction forces, but the impact was not consistent across the feet tested. For instance, even though all three cadaver gait simulations started with the superior force within ±10% of the target set point (the area of interest for this investigation: 50% to 100% stance), but after the iterations of muscle optimization the superior force of specimen 63529-L was improved (closer to desired value) but specimens 63496-L and 63496-R showed the opposite result. Similar inconsistencies are seen in the anterior forces that result due to the optimization iterations. Anterior forces are greatly improved through

mid stance for specimen 63529-L but this is not the case for the other specimens. The medial force does show a general improvement due to the muscle force optimization.

Variations between specimens in the observed ground reaction forces due to optimization cycles may be due to the following:

- Normalization techniques [19] applied during this testing may not be entirely appropriate as they are used to scale force platform trajectories, ground reaction force targets, muscle moment arm lengths, muscle cross-sectional area, etc.
- Use of extensor muscles during stance (tibialis anterior for right feet, extensor digitorum longus for left feet) may be complicating the ground reaction force patterns as these antagonist muscles would generally not be active during stance per reported EMG patterns [27]
- Misalignment that may have been introduced when the feet were potted in the mounting tube may have caused the foot to contact the force platform in unnatural position as compared to the foot orientation measured during contact with the force platform by the subject in the gait lab

CHAPTER VI

EFFECT OF INDIVIDUAL EXTRINSIC MUSCLES OF THE FOOT/ANKLE ON THE CENTER OF PRESSURE DURING SIMULATED STANCE PHASE OF GAIT

Testing has been performed with six cadaver feet (right side) to study the individual muscle effect on COP. This has been accomplished by running a robotic gait simulation with five muscles active as a baseline and then deactivating the muscle of interest and noting the difference in COP. This difference can be attributed to the individual muscle deactivated. Two different sets of five muscles were investigated according to Table XII. Six right-side cadaver lower leg specimens (Table XIII) were used to evaluate individual muscle contributions to COP. Also, gait was simulated at different levels of %BW for each specimen as shown in Table XIV. Since the ground reaction forces and force platform trajectories are scaled for %BW, theoretically the COP change should not be affected by the level of %BW tested. Simulations at lower %BW offer the advantage of reducing the risk of damaging the cadaver specimen due to excessive loading.

Table XII Muscles Simulated during COP Measurements

Muscle Set	Simulated Muscles						
	TS	TP	PL	PB	FHL	FDL	EDL
1	X	X	X		X		X
2	X	X		X		X	X

Table XIII Cadaver Specimen Summary for COP Measurements

Specimen ID	Age, years	Sex	Weight, Kg	Foot Width, cm	Foot Length, cm	Cause of Death
051310-R	56	Female	91.0*	8.64	22.8	Unknown
081810-R	52	Female	100*	9.57	23.4	Unknown
63494-R	65	Male	115	9.77	24.0	Diabetes
63529-R	67	Female	60.5	9.23	23.6	Pancreatic Cancer
8082330-R	70	Male	86.4	9.79	26.8	Respiratory Failure
9061439-R	83	Female	46.8	8.43	24.2	Natural Causes

(*) – Approximate value

Table XIV Cadaver Specimen Summary for COP Measurements

Specimen ID	Percent Body Weight (%BW)										
	40	50	60	65	70	75	80	85	90	95	100
051310-R	--	1	1	--	--	--	1	--	2	--	--
081810-R	1	2	1	--	1	--	2	--	1	--	--
63494-R	--	--	2	--	--	-	1	--	2	--	1
63529-R	--	--	--	--	--	--	--	--	--	--	1
8082330-R	--	1	--	--	--	--	1	--	1	--	1
9061439-R	--	--	--	1	--	2	--	1	2	1	2

6.1 Triceps Surae Muscle Group Contribution to Center of Pressure

Figure 42 and Figure 43 provide the results for the average anterior and medial direction COP change, respectively, resulting from simulated triceps surae muscle group. Figure 44 shows the muscle forces that were simulated during COP measurements. For triceps surae both muscle sets were tested.

The triceps surae muscle group was shown to behave as a strong plantar flexor causing a 24%FL peak anterior shift in COP below 70% stance and no significant shift above 70% stance. It acts as a weak everter causing a 5% FW peak medial COP shift at times before 65% stance and acts like a strong inverter causing a 21%FW lateral shift in COP at stance times above 65% stance. Muscle Set 1 revealed a much larger magnitude of lateral COP shift due to peroneus longus than was observed with Muscle Set 2 utilizing peroneus brevis. This seems to indicate that the foot posture between the two muscle sets is significantly different during the simulated gait. The COP test results for the triceps surae muscle provides meaningful insight to the behavior of the optimization algorithm. For instance, when testing specimen 63496-L, the large error in medial COP was greatly reduced below 70% stance by reducing the triceps surae force through optimization causing a lateral shift in the COP (Figure 45). In contrast, increasing the triceps surae force above 70% stance resulted in a substantial lateral shift in the COP as would be predicted by these results.

6.2 Tibialis Posterior Muscle Contribution to Center of Pressure

Figure 46 and Figure 47 provide the results for the average anterior and medial direction COP change, respectively, resulting from simulated tibialis posterior muscle. Figure 48 shows the muscle forces that were simulated during COP measurements.

Plateau regions for tibialis posterior represents muscle force hard limits placed on this tendon to minimize the chance of breaking this tendon during the simulation. For tibialis posterior both muscle sets were tested. For some testing, tibialis posterior force was limited to approximately 700 Newtons as a precautionary measure to protect the specimen under test as failure of this tendon occurred in previous specimens above this level. The results of the tibialis posterior muscle testing reveals that there is actually a small posterior shift in the COP, particularly in the mid stance region, due to this muscle. This might be due to the insertion at the navicular bone that acts to lift the arch of the foot, and act like a dorsiflexor. Starting at about 60% stance, the action of the tibialis posterior is to shift the COP in the medial direction and hence acts like an everter. The magnitude of the COP increases in terminal stance. No significant difference observed between the two muscle sets (Muscle Set 1 using peroneus longus/flexor hallucis longus or Muscle Set 2 using peroneus brevis/flexor digitorum longus). These results indicate that this muscle would not be effective to provide plantar flexion during simulated gait, but would be effective to provide a medial-direction COP shift.

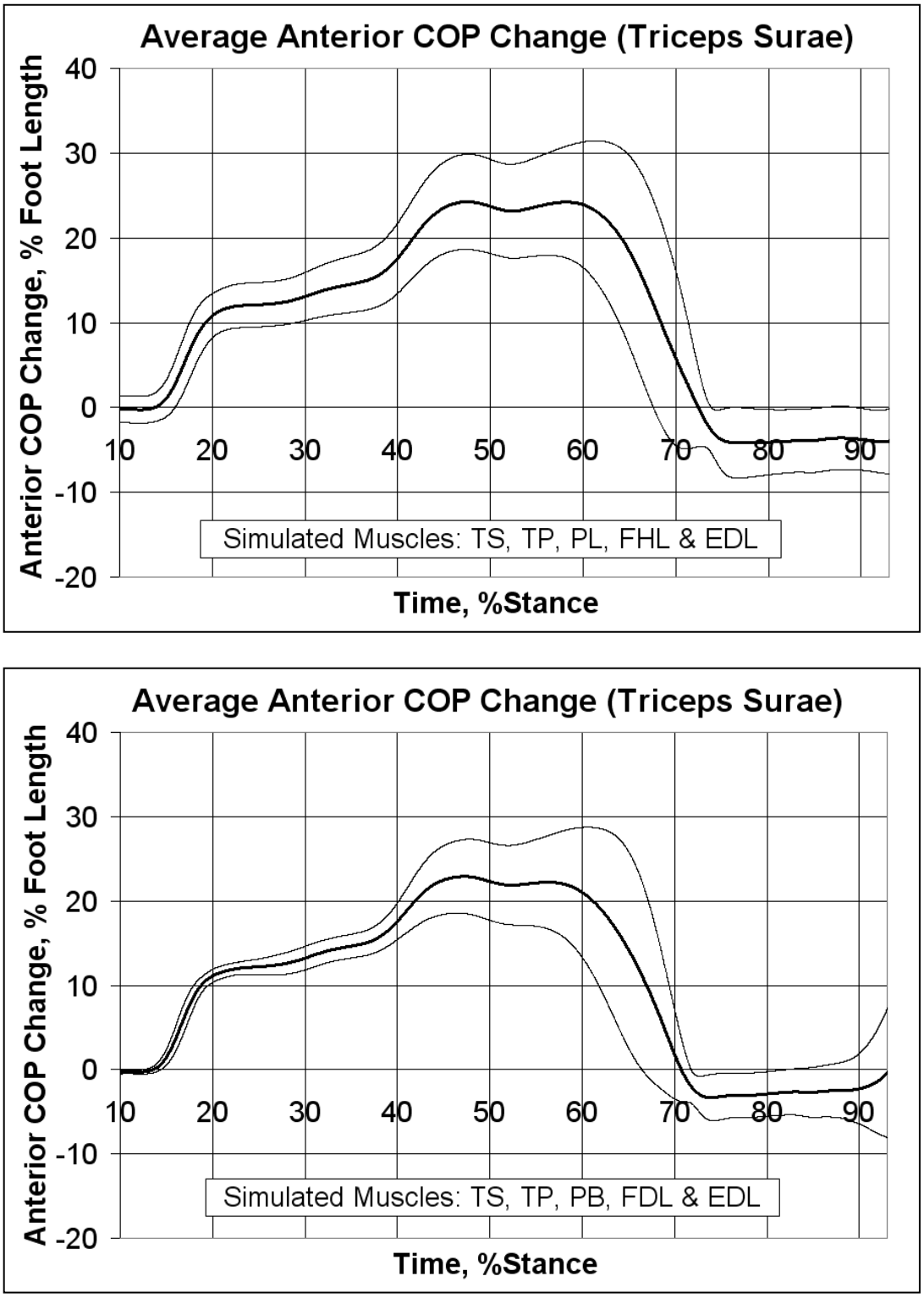

Figure 42 Activated Triceps Surae AP COP Results Showing Mean±1SD
(Top: Muscle Set 1, Bottom: Muscle Set 2)

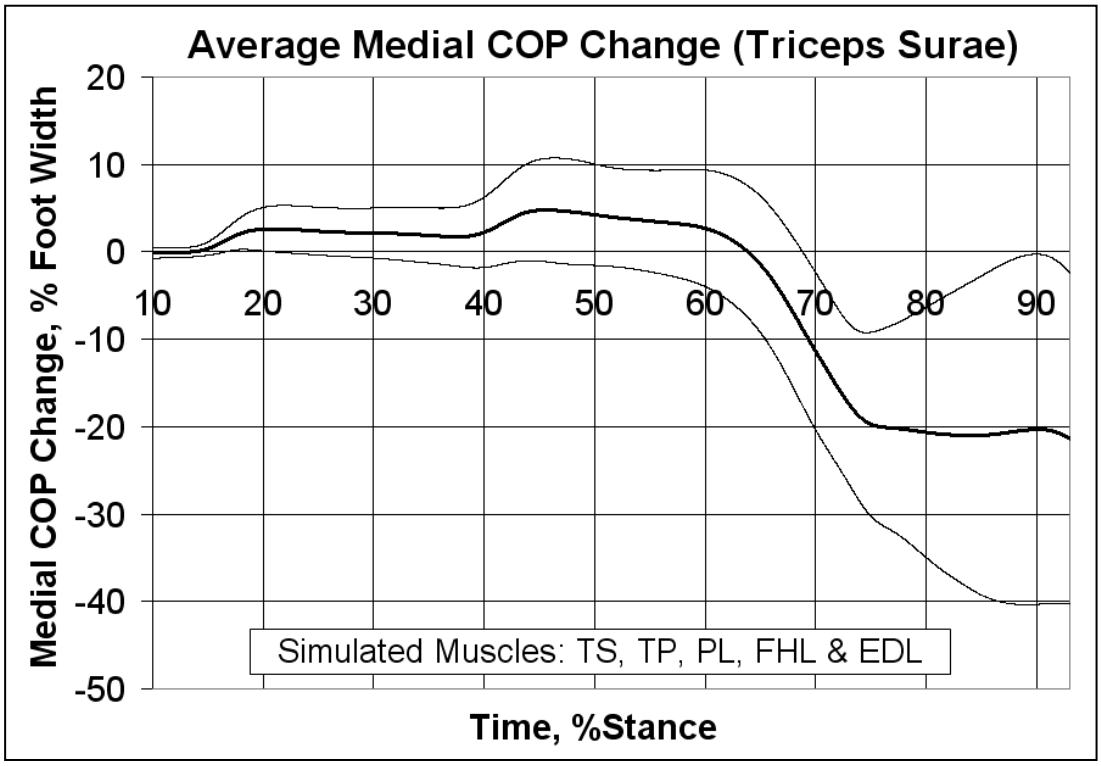

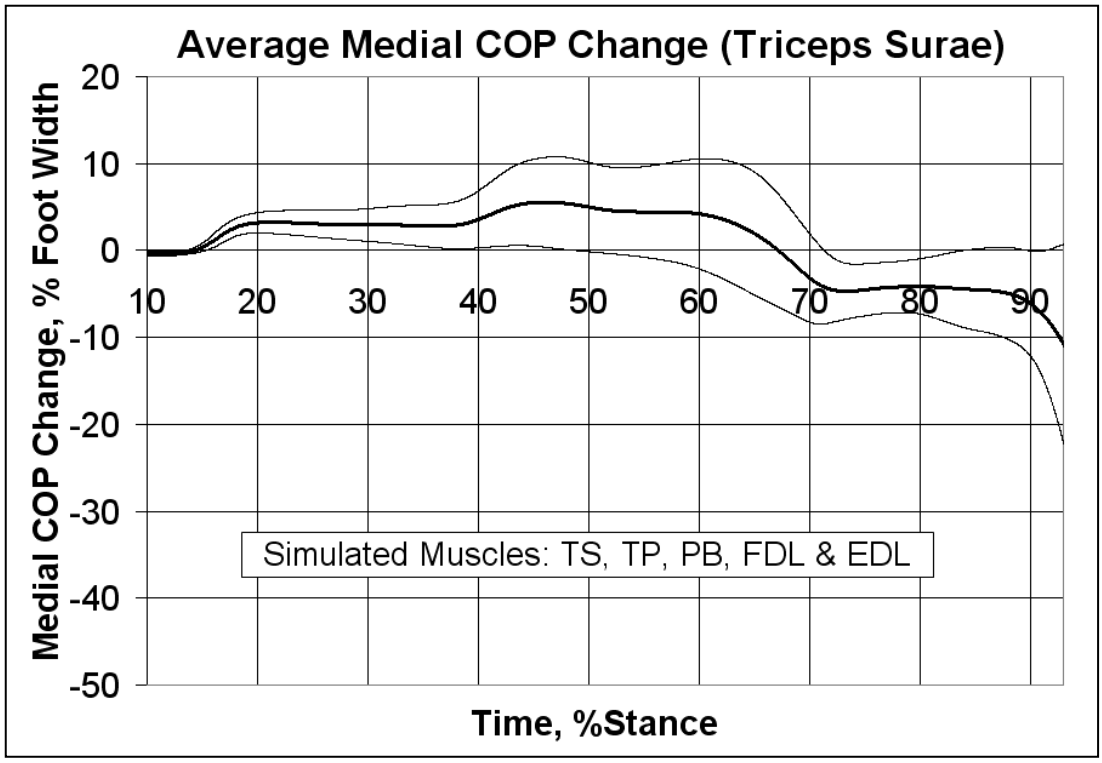

Figure 43 Activated Triceps Surae ML COP Results Showing Mean ±1SD
(Top: Muscle Set 1, Bottom: Muscle Set 2)

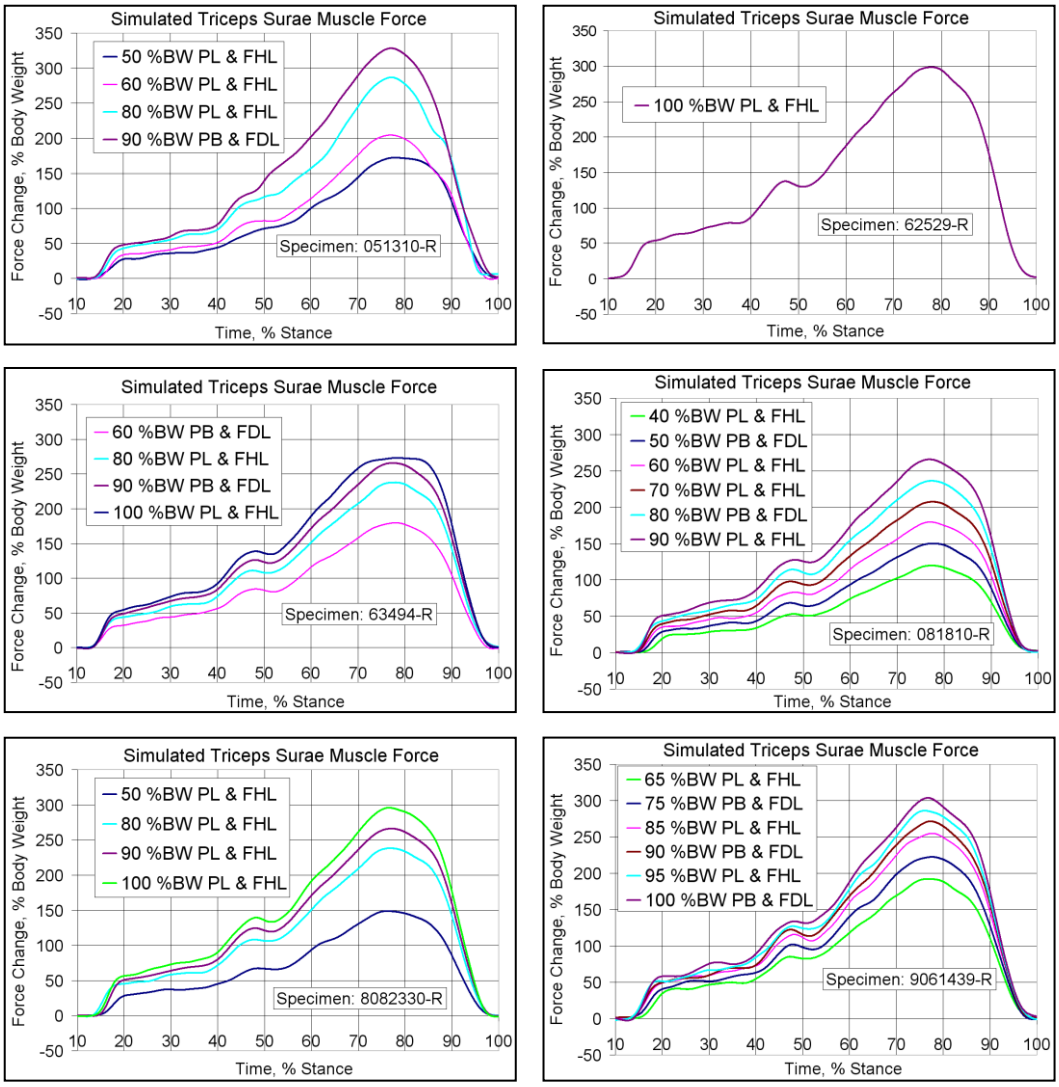

Figure 44 Triceps Surae Muscle Force Simulated for each Specimen

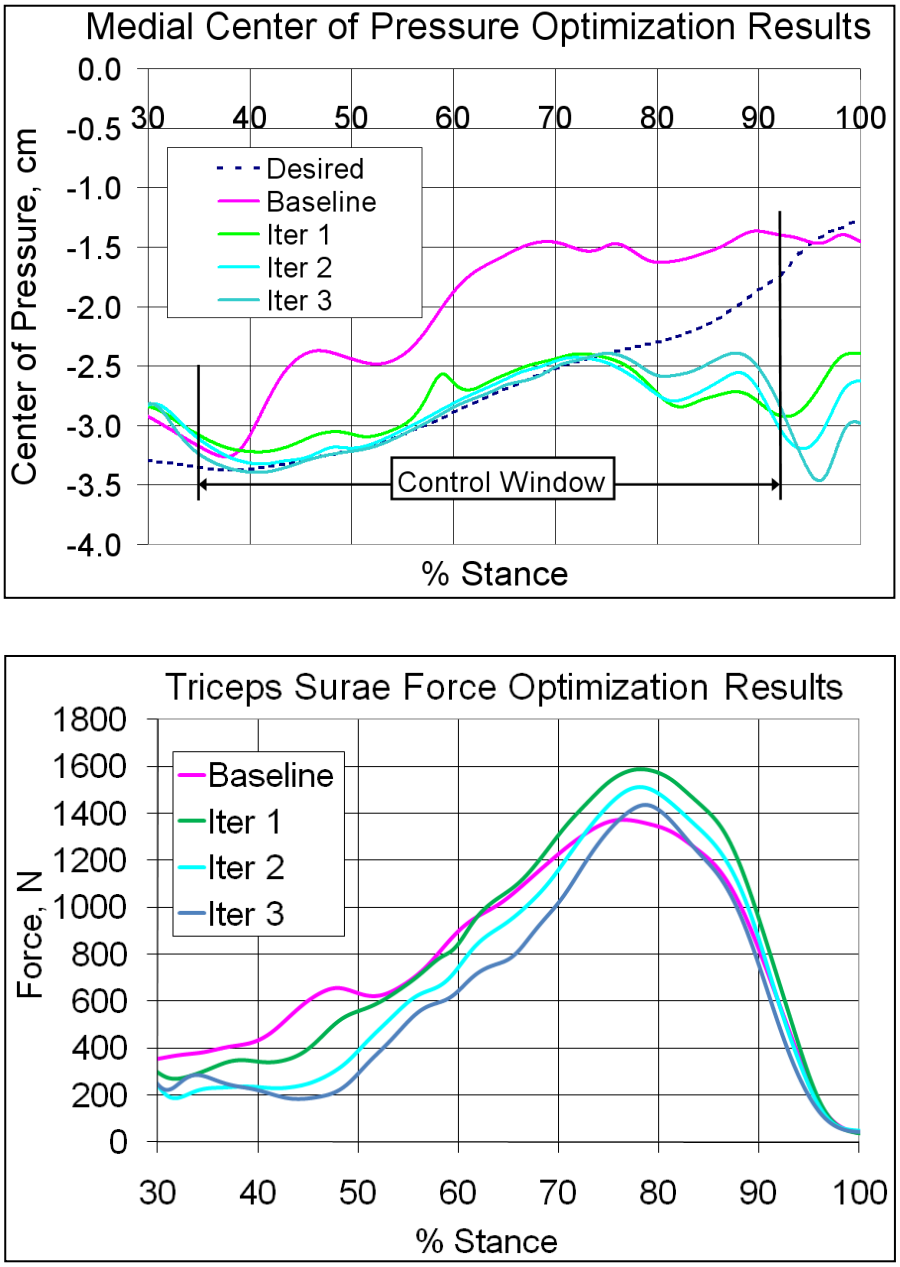

Figure 45 ML COP Optimization Results for Specimen 63496-L

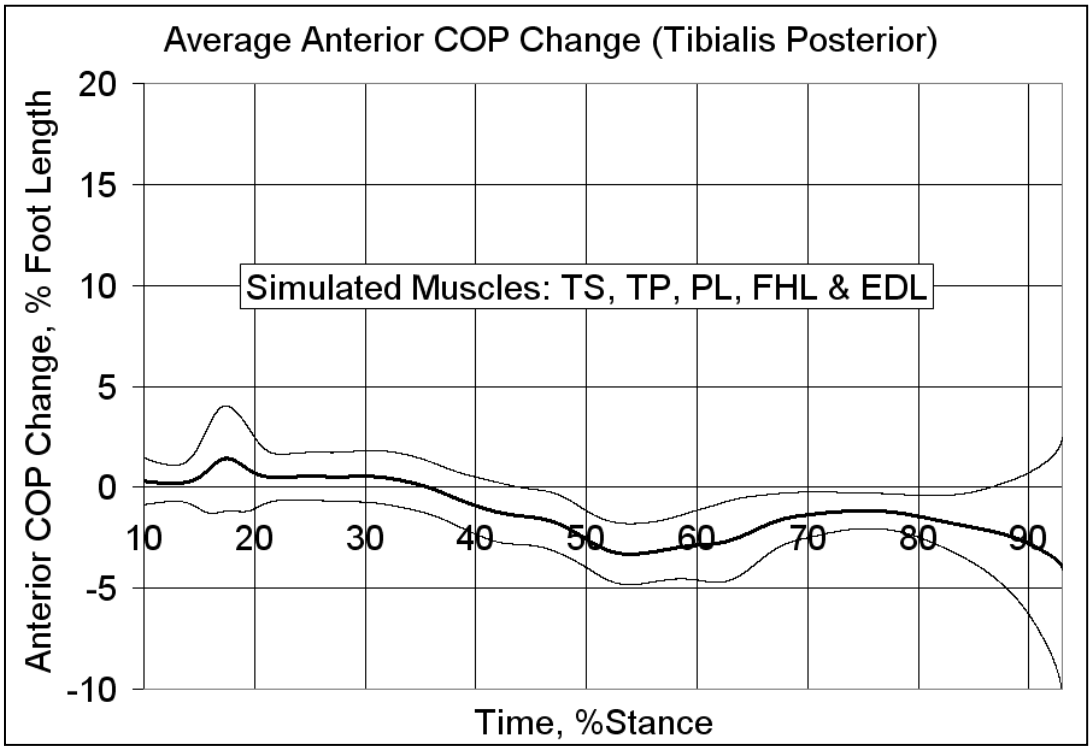

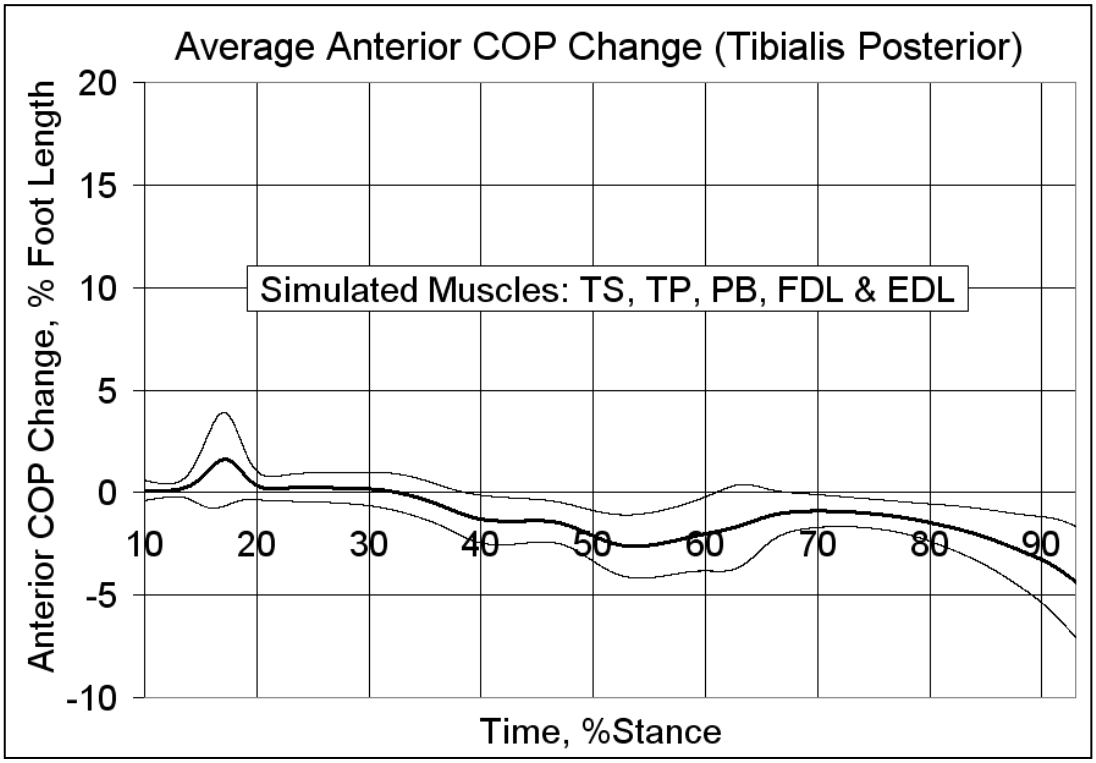

Figure 46 Activated Tibialis Posterior AP COP Results Showing Mean ±1SD (Top: Muscle Set 1, Bottom: Muscle Set 2)

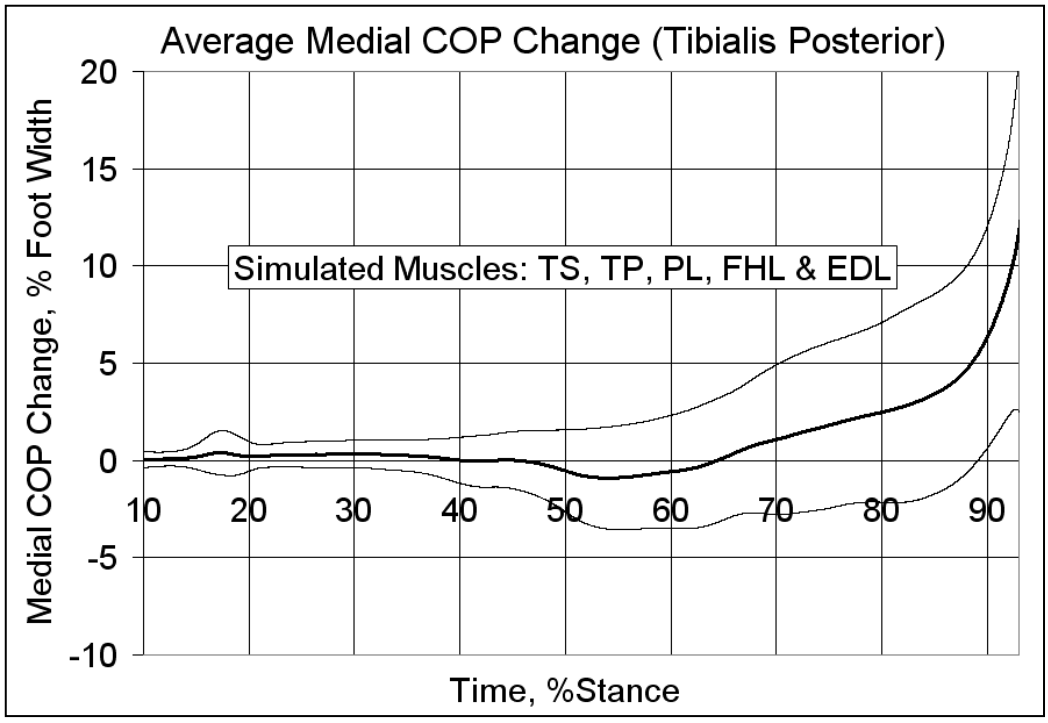

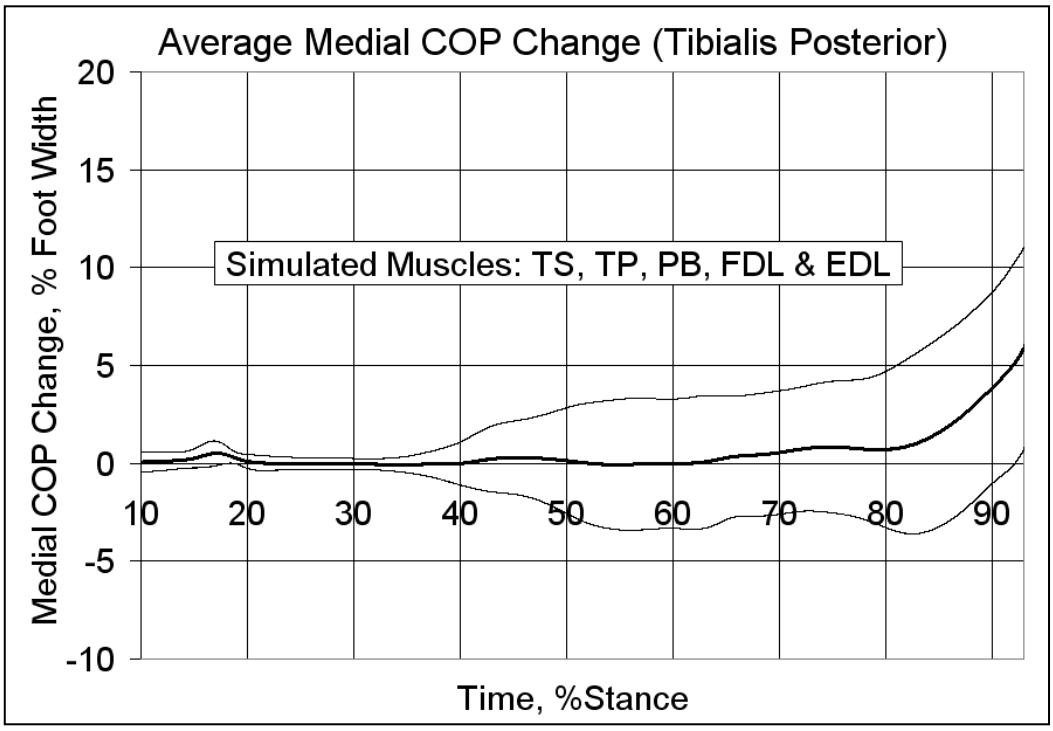

Figure 47 Activated Tibialis Posterior ML COP Results Showing Mean ±1SD (Top: Muscle Set 1, Bottom: Muscle Set 2)

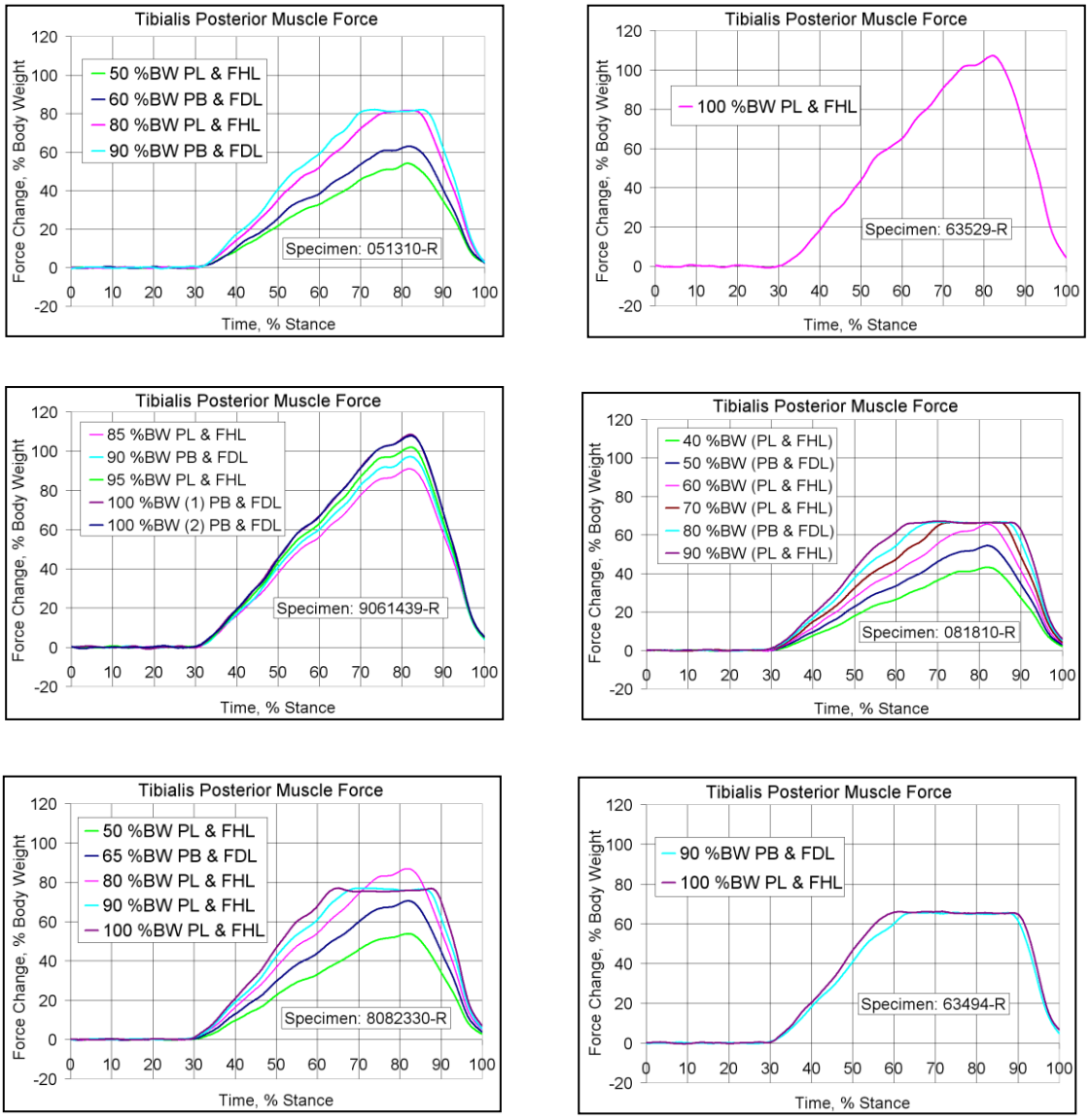

Figure 48 Tibialis Posterior Muscle Force Simulated for each Specimen

6.3 Peroneus Longus Muscle Contribution to Center of Pressure

Figure 49 and Figure 50 provide the results for the average anterior and medial COP change due to simulated peroneus longus, respectively. Figure 51 shows the simulated peroneus longus muscle forces that resulted in the COP change. In many cases the peroneus longus force did not achieve the desired set point because the load cell was limited to an upper limit of 440 Newtons. The peroneus longus muscle testing confirmed that this muscle acts like a plantar flexor and shifts the COP in the anterior direction in the ranges of 40 to 75% stance and above 85% stance. Testing also confirmed this muscle as a strong everter, causing a medial increase to the COP above 40% stance.

6.4 Peroneus Brevis Muscle Contribution to Center of Pressure

Figure 52 and Figure 53 provide the results for the average anterior and medial direction COP change, respectively, resulting from simulated peroneus brevis muscle. Figure 54 shows the muscle forces that drove the COP measured change. In many cases the peroneus brevis force did not achieve the desired set point because the load cell was limited to an upper limit of 440 Newtons. Peroneus brevis was shown to provide similar COP change patterns as peroneus longus. Peroneus brevis did result in a slightly higher anterior COP shift and approximately half the medial COP shift of peroneus longus.

6.5 Flexor Hallucis Longus Muscle Contribution to Center of Pressure

Figure 55 and Figure 56 provide the results for the average anterior and medial direction COP change, respectively, resulting from simulated flexor hallucis longus. Figure 57 shows the simulated muscle forces that caused the change in COP. Flexor

hallucis longus activity showed a slight shift in anterior COP above 60% stance, a gradual medial shift between 50% and 90% stance and larger medial shift above 90% stance. This medial shift is expected, since this muscle is located under the large toe on the medial side of foot and since it is a plantar flexor, increased muscle activity would be expected to increase the anterior COP. The magnitude of the COP change was very small, due to the low muscle force profiles tested. Specimen 051310-R was not used for this testing because simulations were performed with the wrong muscle profile.

6.6 Flexor Digitorum Longus Muscle Contribution to Center of Pressure

Figure 58 and Figure 59 provide the results for the average anterior and medial direction COP change, respectively, resulting from simulated flexor digitorum longus muscle. Figure 60 shows the muscle forces that contributed to this COP change. Testing of the flexor digitorum longus revealed slight anterior COP shift above 50% stance and a slight lateral shift in COP from 50 to 90% stance. Above 90% stance a medial shift in COP was observed as would be expected during terminal stance. Specimen 051310-R was not used for this testing because simulations were performed with the wrong muscle profile.

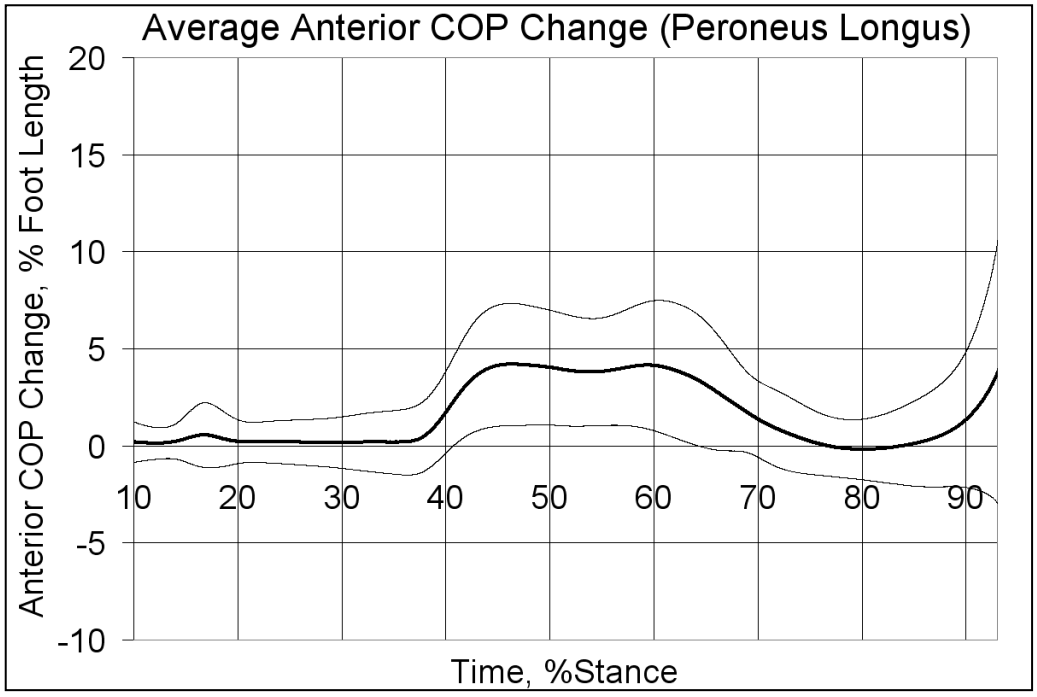

Figure 49 Activated Peroneus Longus AP COP Results Showing Mean ±1SD

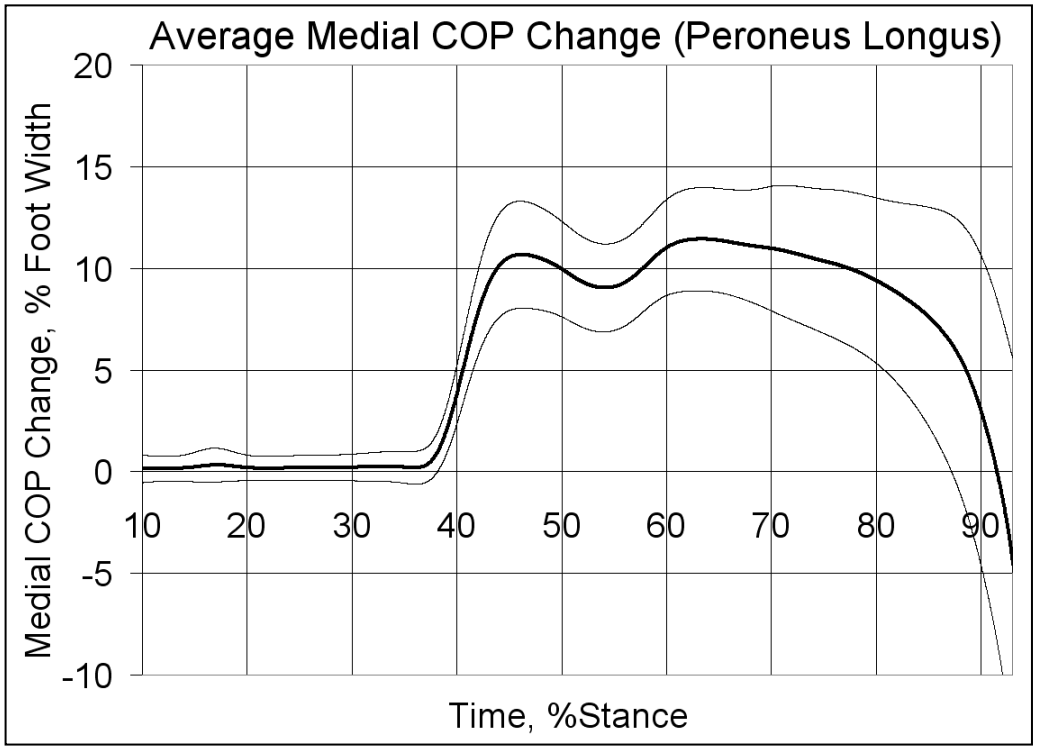

Figure 50 Activated Peroneus Longus ML COP Results Showing Mean ±1SD

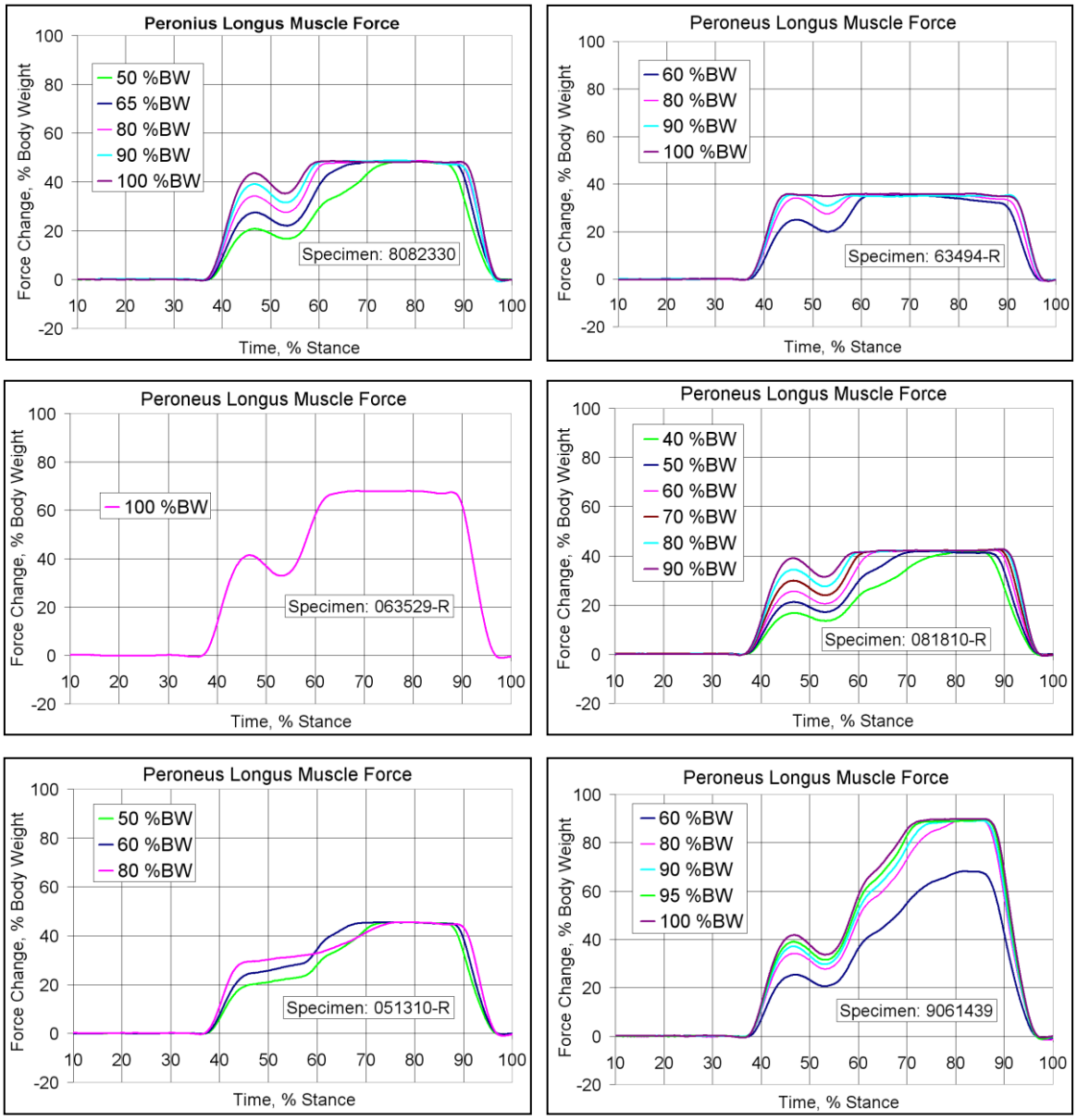

Figure 51 Peroneus Longus Muscle Force Simulated for each Specimen

.

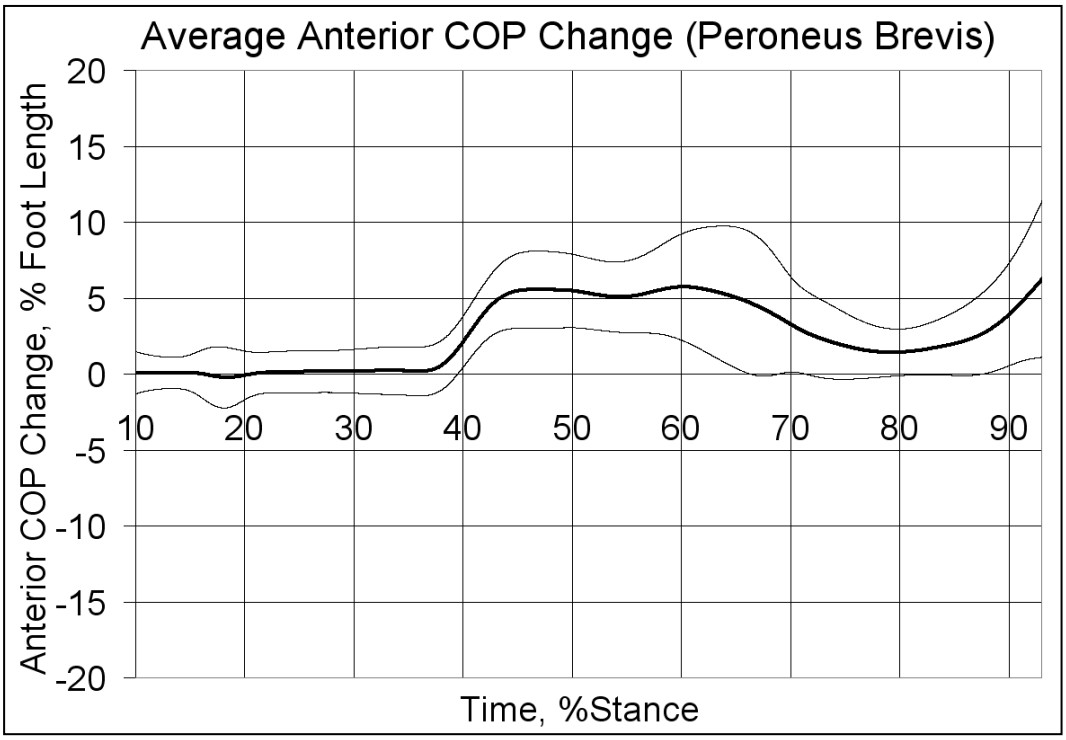

Figure 52 Activated Peroneus Brevis AP COP Results Showing Mean ±1SD

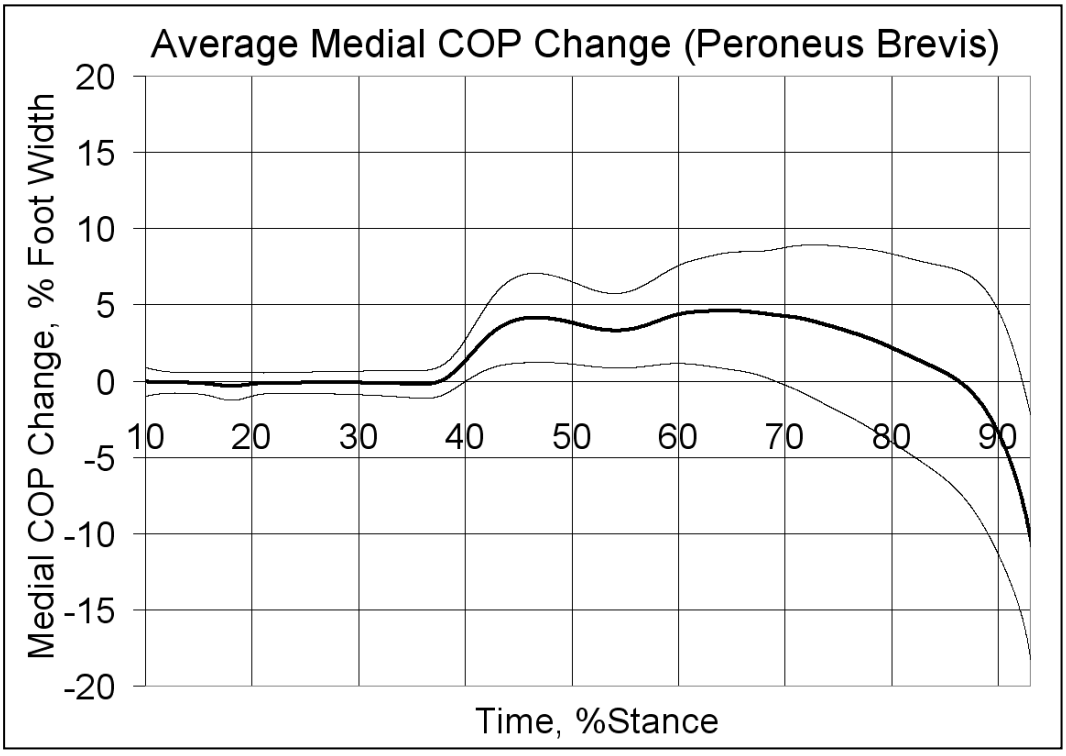

Figure 53 Activated Peroneus Brevis ML COP Results Showing Mean ±1SD

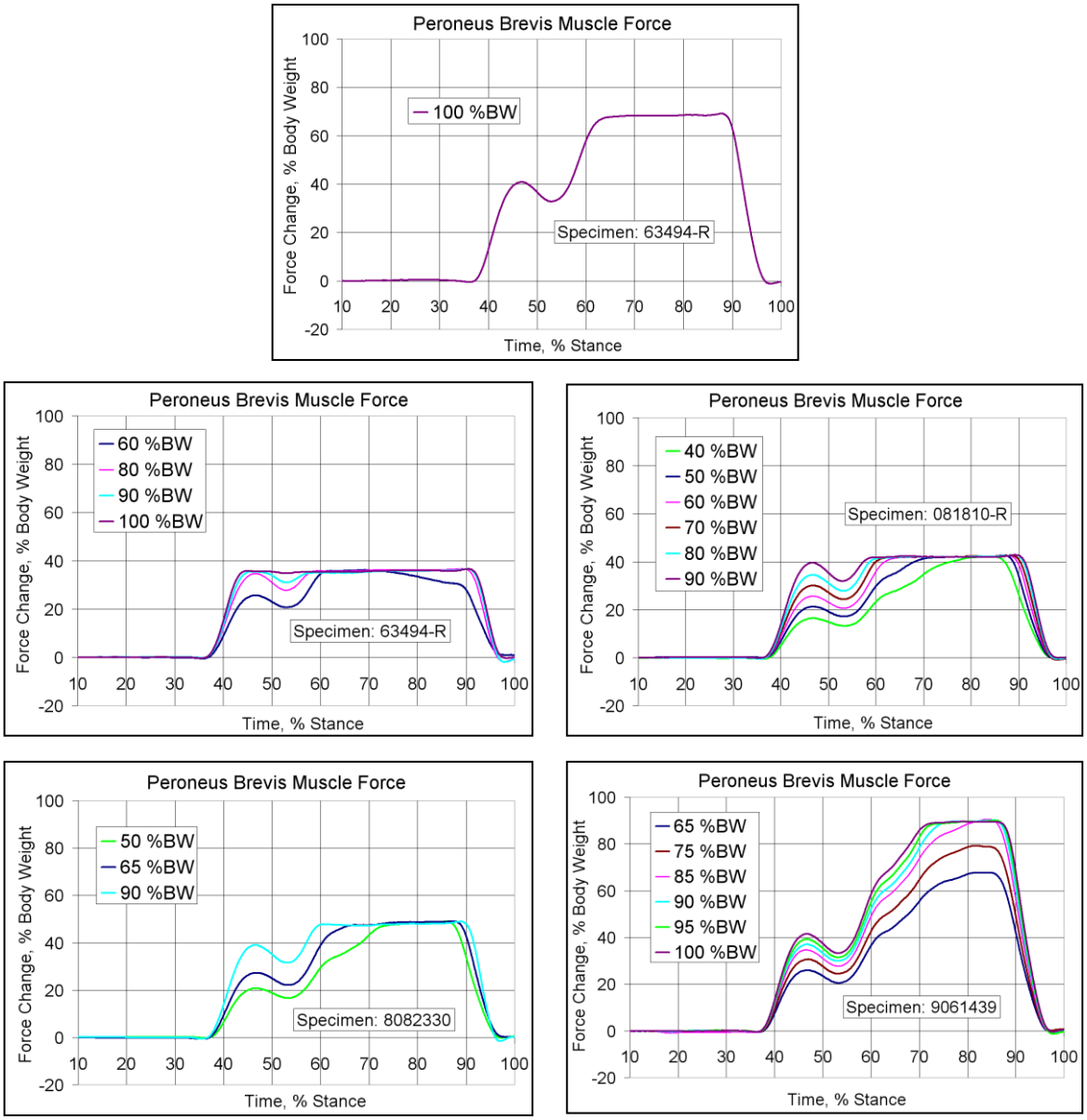

Figure 54 Peroneus Brevis Muscle Force Simulated for each Specimen

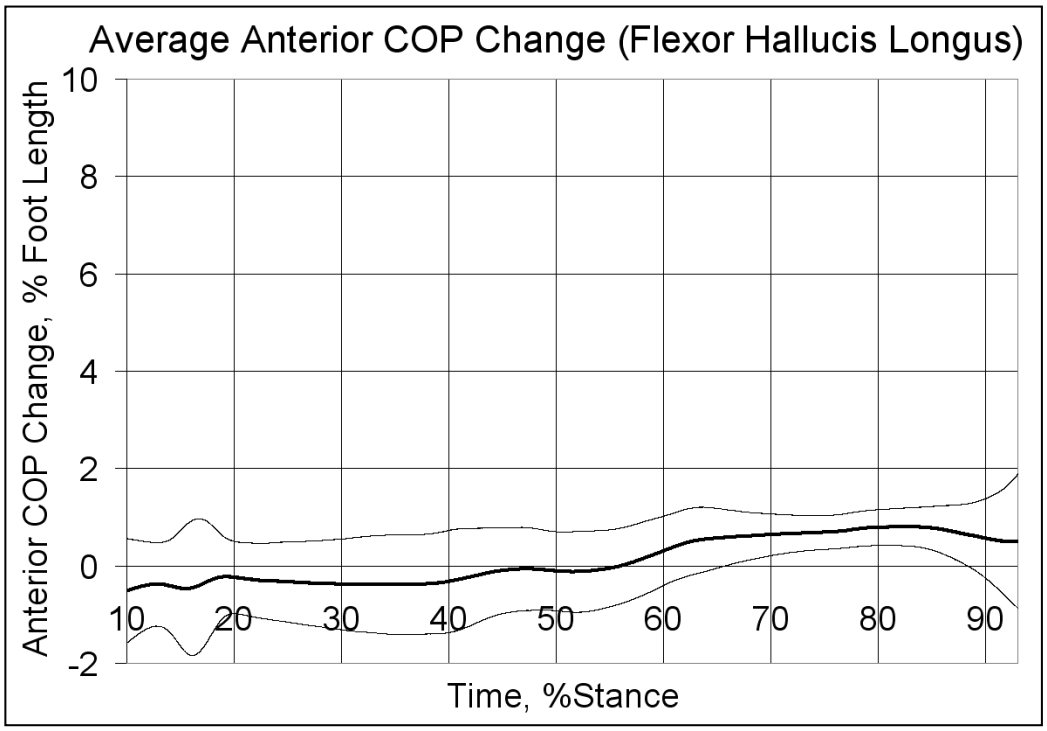

Figure 55 Activated Flexor Hallucis Longus AP COP Results Showing Mean ±1SD

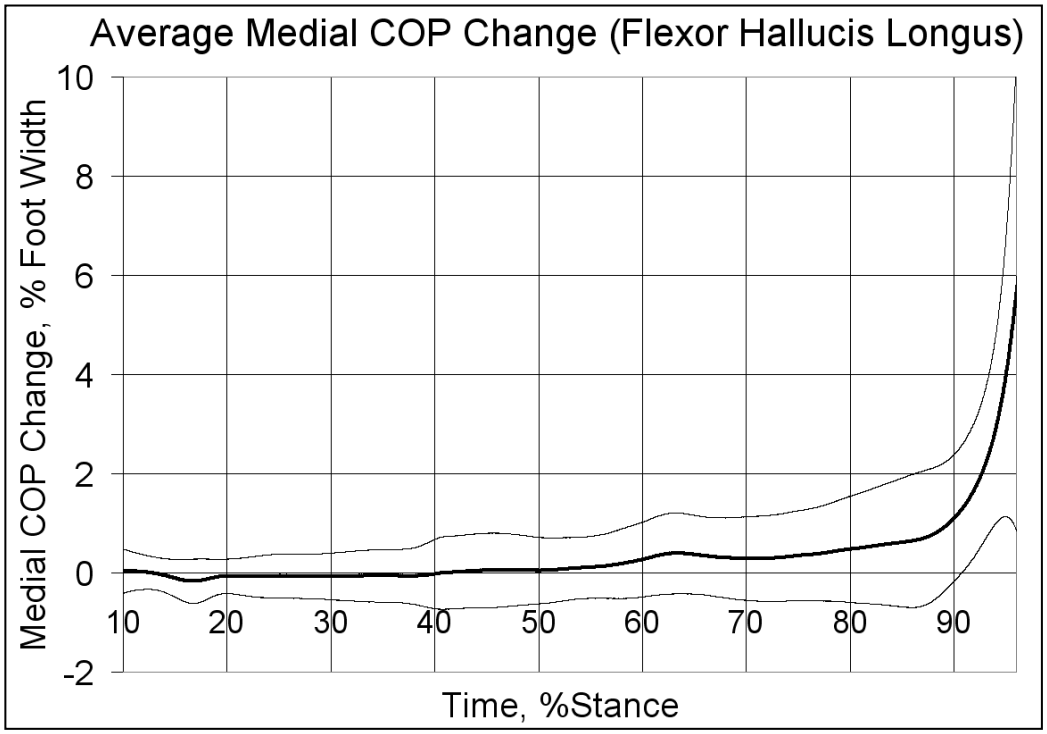

Figure 56 Activated Flexor Hallucis Longus ML COP Results Showing Mean ±1SD

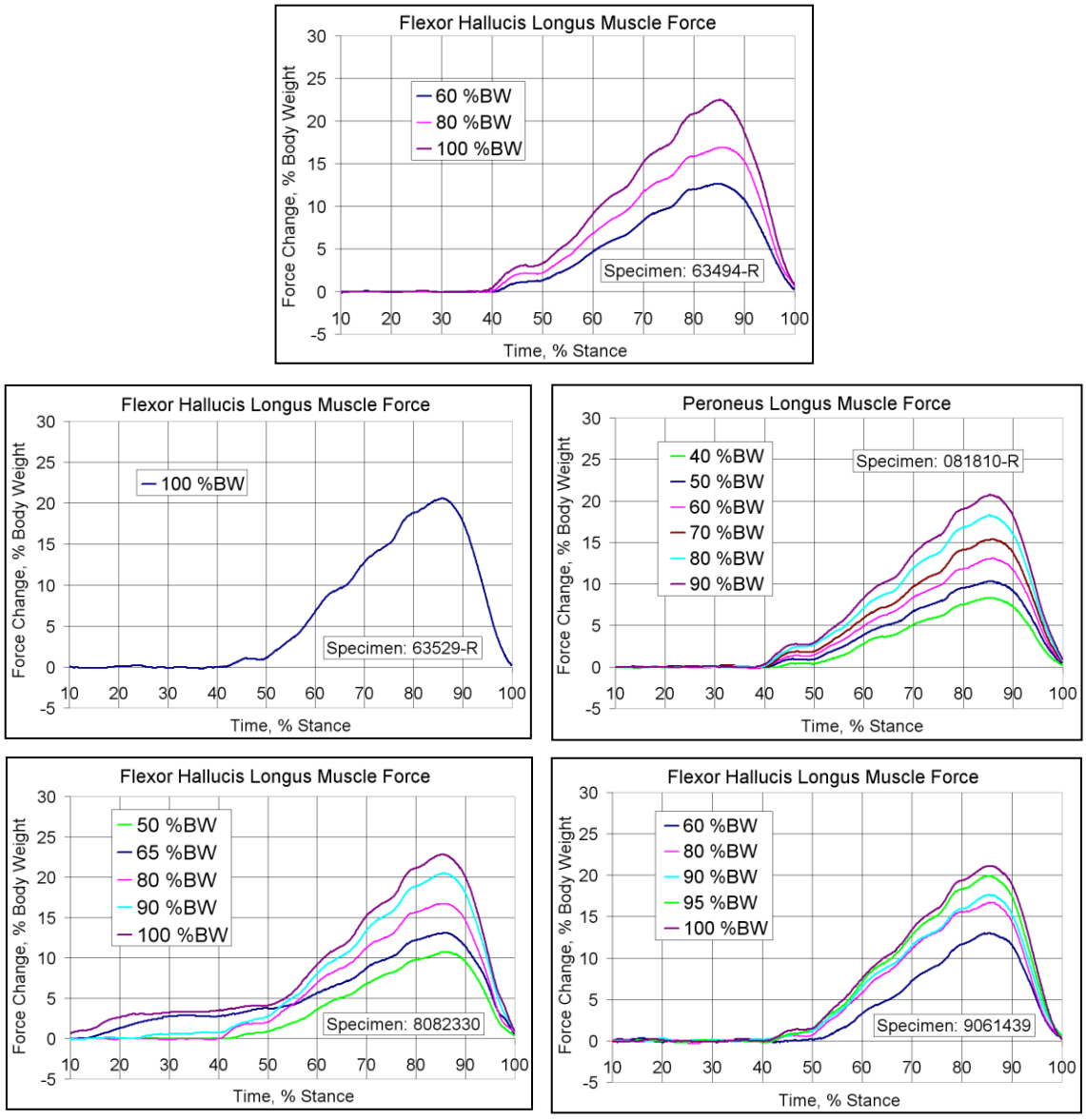

Figure 57 Flexor Hallucis Longus Muscle Force Simulated for each Specimen

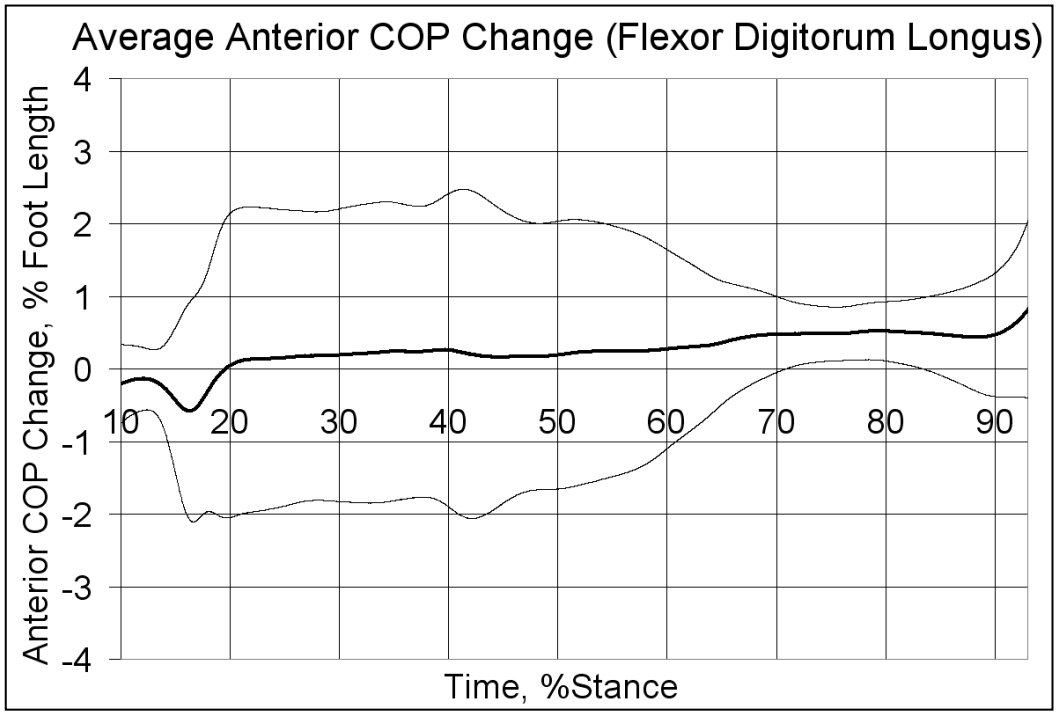

Figure 58 Activated Flexor Digitorum Longus AP COP Results Showing Mean ±1SD

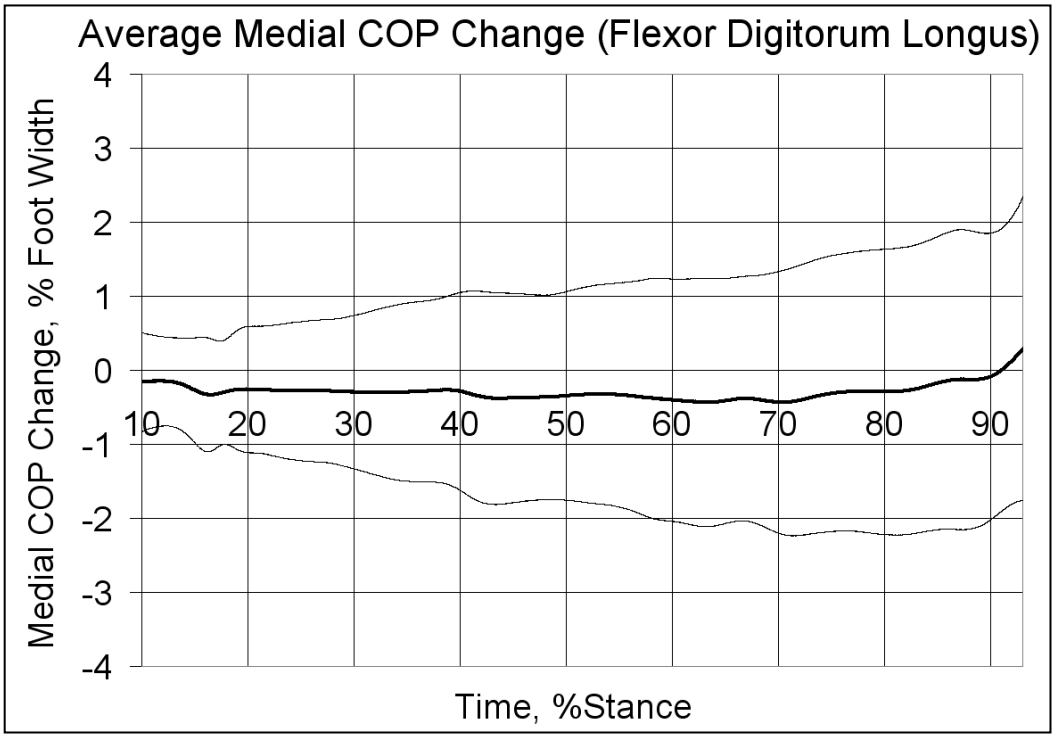

Figure 59 Activated Flexor Digitorum Longus ML COP Results Showing Mean ±1SD

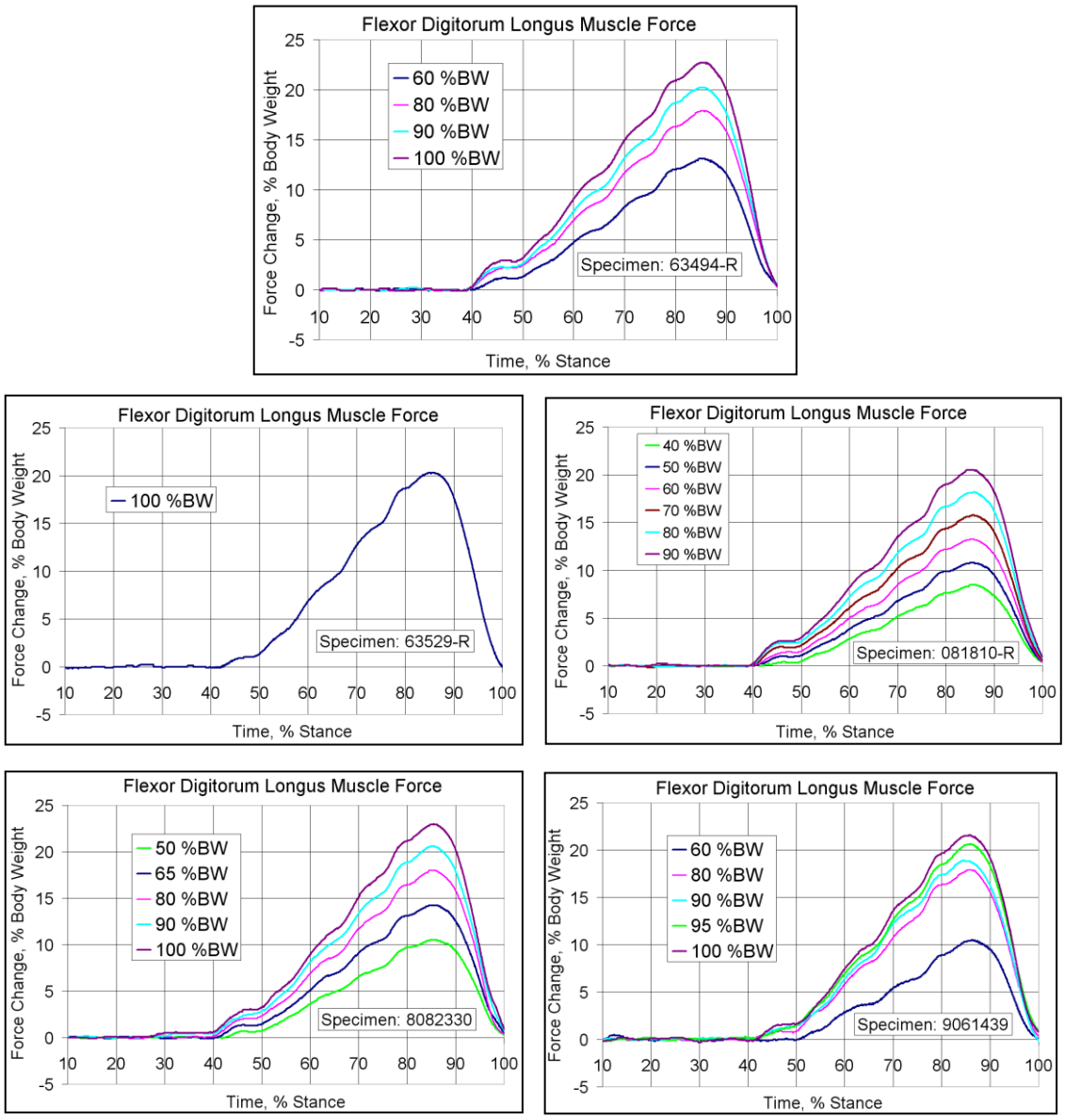

Figure 60 Flexor Digitorum Longus Muscle Force Simulated for each Specimen

CHAPTER VII

SUMMARY AND DISCUSSION

In summary, this research that has been performed has provided the following contributions:

1. A general use multi-tendon actuator capable of supporting musculoskeletal research within the UMS platform at the Cleveland Clinic
2. An algorithm that performed optimization of muscle forces using the unique combination of minimizing cubed muscle stresses and applying quadratic sequential programming techniques:
    - Inputs are body weight simulated, foot width, foot length, the forces measured during the previous experiment for 10 extrinsic muscles (triceps surae, tibialis posterior, flexor digitorum longus, flexor hallucis longus, tibialis anterior, peroneus brevis, peroneus longus, peroneus tertius, extensor digitorum longus, extensor hallucis longus) at each stance point and the measured medial and anterior COP from the previous experiment
    - Outputs are the target muscle forces for the next experiment to reduce the error between the desired and measured COP

3. A static model of the foot/ankle for development and evaluation of the optimization algorithm
4. Incorporation of the optimization algorithm into the UMS
5. Insight on how individual muscles contribute to the center of pressure during gait

Subsequent sections below provide conclusions and discussions for each of these research areas.

7.1 Multi-Tendon Actuator System

Four linear actuators were developed and integrated with the previously existing rotary actuator within the Cleveland Clinic's UMS to allow the simulation of up to five muscles or muscle groups simultaneously. The design of brackets, pulleys, wire-rope cables and electrical cables provided a very flexible mounting configuration for the linear tendon actuators. Actuators positions were easily adjusted by loosening four screws on the mounting bracket allowing the assembly to slide over the surface of the t-slotted frame structure to eliminate excess slack in the wire rope cables attaching to the tendons. The intent of this design was to support any joint system under investigation offering a significant advantage to previous dynamic simulators and was found to be easily adapted to the foot/ankle experiments described herein.

Tendon actuators were operated under force direct feedback control through using load cells as the control input. During the foot/ankle experiments at certain times the absolute error between the target and actual tendon forces revealed a larger than expected variability during research conducted previously [19, Appendix A]. The largest error was observed at the last 10% of stance where the ankle and subtalar joints angles are changing rapidly. Some of this error has been attributed to reaching hard limits in the actuator

stroke preventing the actuator from achieving the desired force target. Extra care was taken for walking simulations conducted during this research to monitor actuator travel to maintain the actuator positions such that the end limits were not reached. In contract with the absolute error limitations, the previous tests demonstrated excellent repeatability from one simulation to the next when the target tendon forces were the same.

Synchronization error of the linear actuators to an event trigger generated when the robot motion was initiated was determined to be 5.2 ± 1.4 ms compared to the existing rotary actuator synchronization of 4.1 ± 1.0 ms. With the 7.12 second stance time simulated during the experiments conducted in this research, this synchronization error was considered insignificant (0.07% of stance time).

7.2 Muscle Force Optimization Algorithm Initial Evaluation using the Static Ankle/Foot Model

Foot/ankle model configuration elements are entered through an ASCII file for ease of configuration. Configurable items are:

- Foot outline of 2D plantar surface (series of X and Y coordinates)
- Contact point locations (series of X and Y coordinates)
- Locations of subtalar joint and ankle joint axes (lines defined as X and Y coordinates for two end points)
- Desired COP (ML and AP-direction COP at various stance points)
- Muscle effective insertion locations (X and Y coordinates for each of the 10 extrinsic muscle)

- Initial guess for joint angles (inversion and dorsiflexion angles at various stance points) based on typical walking

Static model inputs for each stance point simulated are the forces for 10 extrinsic muscles and body weight (target superior GRF). Outputs of the model at each stance point are the forces at each contact point, predicted AP and ML COP, total superior GRF, inversion angle, dorsiflexion angle and tibia position (distance from simulated ground). The ankle model was shown to be numerically stable for all input condition tested providing a valuable tool for debugging the muscle force optimization algorithm.

The algorithm, when tested using the static model, showed that the percent reduction in mean COP error was 93.0% for anterior COP and 87.6% for medial COP after 4 iterations

7.3 Integration and Testing of the Optimization Algorithm with the UMS

LabVIEW code, native to the previously developed UMS foot application software, was developed for seamless integration of the muscle force optimization algorithm. The algorithm was designed for easy configuration to simulate any number of muscles (5 muscles tested simultaneously during this study) and a window of stance times. In addition, this methodology could be used in applications of other joint systems such as the hip or wrist by substituting the target AP and ML COP with some other type of reaction force.

Integration of the algorithm with the UMS provided the capability of testing the optimization algorithm using cadaver feet. Test results with three cadaver feet demonstrated that this algorithm is able to optimize muscle forces to simultaneously

improve AP and ML COP. Improvements to COP was greatest in the mid stance portion of gate especially in the range of 41-50% stance where a reduction in the mean error in the range of 83.0% to 93.4% for AP COP and from 81.6% to 98.6% for medial COP after three iterations. The derivation [24] of the optimization algorithm constraints (Equations 2 and 3 above) assumes a flat foot contacting the ground which offers some insight as to why in terminal stance, when the heel is off the ground and weight is shifted under the head of the metatarsals, the optimization is not as successful as mid stance where the foot is flat. Additionally, the derivation assumes that ankle joint angle only influences dorsiflexion and that the subtalar joint angle only influences inversion. These constraints are only a rough approximation, as there is some cross-talk due to the fact that the subtalar joint axis is not in-line with the AP axis and the ankle joint is not in-line with the ML axis of the foot. Figure 17 is instructive for understanding this phenomenon. Furthermore, the forefoot joint (metatarsophalangeal joint) is also absent from the derivation of the constraints and hence adjustments of COP due to moments about this axis have been ignored. Shift in the COP, due to forces acting about this joint, may be substantial.

Optimization of muscle forces generally had an adverse outcome on the target GRFs, although for specimen 63529-L, there was an improved superior GRF after optimization of the muscle forces. The derivation [24] of the optimization algorithm constraints does incorporate the superior (vertical) GRF, but the AP and ML direction GRFs are ignored. In addition, there is no active control for the tibia position (foot distance from simulated ground). This may provide insight as to why the optimization algorithm performed better against the static foot/ankle model, since the model ensures that the sum of forces

generated by the contact points equals the target superior GRF (Equation 22), in addition to satisfying the constraint of the sum of moments about the joints due to muscle forces and contact points is zero (Equations 20 and 21). Furthermore, adjustment of extensor muscles by the optimization algorithm, beyond the loading response appears to cause a substantial shift from the desired ground reaction forces. For instance, extensor digitorum was active between 80 and 90% stance for specimen 63496-L (Figure 36) and appears to have adversely affected all ground reaction forces in that region (Figure 37).

7.4 Individual Muscles Effect on the Center of Pressure during Gait

Table XV summarizes the resulting shift in ML and AP COP due to individual muscles. The body of this table contains the direction of the shift, the stance range that applies to the shift and the peak COP shift in normalized units for that direction.

The observed behavior of the triceps surae acting as both an everter and inverter, depending on stance time, indicates that modeling this muscle with a fixed moment arm may not be sufficient to dramatically improve the ML COP through optimization. Furthermore, this may explain why the optimization algorithm had difficulty improving the ML COP above 65% stance. The medial COP was found to shift substantially depending on what muscle set is simulated (Muscle Set 1 with peroneus longus/flexor hallucis longus or Muscle Set 2 with peroneus brevis/flexor digitorum longus) during triceps surae group COP testing. This change is assumed to be attributed to a change in foot posture due to differing levels of eversion for these two muscles.

Tibialis posterior causes only a small anterior shift in COP, but it is effective even at terminal stance, unlike the triceps surae muscle group. The tibialis posterior muscle demonstrated a weak lateral shift below 65% stance and then transitions to a more

Table XV Summary of Effect of Individual Muscles on COP

Muscle	COP Shift Results (Stance Range, Mean Peak)		Comments
	AP Direction	ML Direction	
Triceps Surae	Anterior (<70%, 24%FL)	Medial (< 65%, 5%FW) Lateral (>65%, 21%FW)	When used in conjunction with peroneus longus provides higher lateral shift than when used with peroneus brevis
Tibialis Posterior	Posterior (>35%, 3%FL)	Lateral (50-65%, 1%FW) Medial (>65%, 12%FW)	No medial shift in COP below 85% stance when used in conjunction with peroneus brevis
Peroneus Longus	Anterior (38-76%, 4%FL) Anterior (>85%, 4%FL)	Medial (38-92%, 12%FW) Lateral (>92%, 5%FW)	
Peroneus Brevis	Anterior (> 38, 6%FL)	Medial (38-86%, 4%FW) Lateral (>86%, 10%FW)	
Flexor Hallucis Longus	Posterior (<50%, 0.5%FL) Anterior (> 50, 0.9%FL)	Medial (> 50%, 6%FW)	
Flexor Digitorum Longus	Anterior (> 20, 0.8%FL)	Lateral (<91%, 0.4%FW) Medial (>91%, 0.3%FW)	

substantial medial shift in COP above 65% stance that increases as the foot proceeds into terminal stance.

Peroneus longus muscle was shown to be a weak plantar flexor as it provides only a small shift the COP in the anterior direction and is ineffective in the range of 76 to 86 % stance. Peroneus longus is a strong everter, causing a substantial medial increase to the COP below 92% stance and shifting to a weaker lateral COP shift above 92% stance.

Peroneus brevis exhibits similar COP change patterns as peroneus longus, except it result in a slightly higher anterior COP shift, approximately one-third of the medial COP shift as peroneus longus and twice the lateral shift in COP in terminal stance.

Flexor hallucis longus activity showed a slight shift in anterior COP above 60% stance, a gradual medial shift between 50% and 90% stance and larger shift above 90% stance.

Flexor digitorum longus revealed slight anterior COP shift above 50% stance and a slight lateral shift in COP from 50 to 90% stance and above 90% stance a medial shift in COP was observed as terminal stance progresses.

CHAPTER VIII

RECOMMENDATIONS FOR FUTURE WORK

The subsequent sections below provide recommendations based on the results of this work.

8.1 Assumption of Constant Moment Arms for Extrinsic Muscles

A constant value for muscle moment arms was used in the derivation of the objective function constraints (Equations 1 and 2) used in the muscle optimization algorithm. This assumption does not appear to hold true since triceps surae, peroneus longus and peroneus brevis muscles have shown a clear sign change in the COP shift in the ML-direction during the latter half of stance. In all cases, there was a shift in the COP from the medial direction early in stance to a lateral direction at a later stance time.

Based on this finding, the constant moment arms should be replaced with a linear expression that vary with percent stance. It may be possible to derive the individual moment arm expressions from testing. For instance, one could applying a fixed force to the triceps surae muscle group through the rotary tendon actuator and observing the

superior force measured during each region of gait to estimate the moment arm length as a function of percent stance

8.2 Incorporate Muscle Phasing Limitations

Testing of the individual muscle effect on COP has revealed that certain muscles, even when simulated at reasonably high forces, do not affect the COP in certain regions of stance. A good example is the triceps surae muscle group simulated force (Figure 44) that had a peak at around 78% stance and has significant force that continues even beyond 90% stance and yet the AP COP (Figure 42) is unaffected above 70% stance. For this particular case, it could be argued that adjustments to triceps surae force attempting to adjust AP COP above 70% stance should be prevented by the muscle force algorithm. Another situation where the muscle phasing should be limited is the used of the extensor muscles by the optimization algorithm above 50% stance since EMG measurements [27] would indicate that these muscles are not active after heel loading response and hence are antagonists to plantar flexor muscles during mid and terminal stance. As discussed previously, preventing the optimization algorithm from adjusting of extensor muscles beyond loading response after heel strike may substantially improve the ground reaction forces.

8.3 Enhance the Static Ankle/Foot Model to include the Metatarsalphalangeal Joint

It may be extremely beneficial to add the metatarsophalangeal joints to the static ankle/foot model to allow more physiologically accurate evaluation of the optimization algorithm during terminal stance where the heel is significantly lifted from the ground.

An additional balance equation would be added to include and muscle moments and contact point moments due to this joint as were included for the ankle and subtalar joints (Equations 20 and 21). Testing the muscle force optimization algorithm against the revised static ankle/foot model would most likely reveal necessary enhancement to the algorithm necessary to provide improvements to the COP adjustments during terminal stance. For instance, an additional constraint to the algorithm might be required that parallels Equations 11 and 12 for dorsiflexion/plantar flexion and inversion/eversion, respectively.

8.4 Tibia Position Constraint to Maintain Proper Ground Reaction Forces during Muscle Adjustments to Correct COP

An additional constraint may be necessary for the muscle force optimization algorithm to ensure that the tibia position (relates to the 3D orientation of foot with respect to the simulated ground) is being corrected to ensure that the proper ground reactions forces are maintained during COP corrections. This change should only be considered if the ground reaction forces are not sufficiently corrected by implementation of the other recommendations, as it will add significant complexity to the algorithm and static model. It should be noted that, in order to evaluate the muscle force optimization algorithm enhancements in this area, it will also be necessary to modify the static ankle/foot model, as it is currently constrained (Equation 22) to adjust the tibia position to maintain the superior (vertical) ground reaction force equal to the sum of the contact point forces. Therefore, the tibia position in the static ankle/foot model will need to be

changed from an output to be an input. New outputs of the model will be the resulting ground reaction forces in the AP, ML and superior/inferior (vertical) directions.

CHAPTER IX

REFERENCES

[1] Lanyon, L.E., Hampson, G.J., Goodship, A.E., Shan, J.S., 1975. "Bone Deformation Recorded In Vivo from Strain Gages Attached to the Human Tibial Shaft", Acta Orthopaedica Scandinavia, **46**, pp. 256–268.

[2] Burr, D.B., Milgrom, C., Fyhrie, D., Forwood, M., Nyska, M., Finestone, A., Hoshaw, S. and Saiag, E., Simkin, A., 1996, "In Vivo Measurement of Human Tibial Strains during Vigorous Activity", Bone, **18**, pp. 405–410.

[3] Beynnon, B.D. and Fleming, B.C., 1998, "Anterior Cruciate Ligament Strain In-Vivo: A Review of Previous Work", Journal of Biomechanics, **31**, pp.519-525.

[4] Woo, S.L-Y., Debski, R.E., Wong, E.K, Yagi, M. and Tarinelli, D., 1999, "Use of Robotic Technology for Diathrodial Joint Research", Journal of Science and Medicine in Sport, 2 (4), pp. 283-297.

[5] Weiss J.A., Gardiner J.C., Ellis B.J., Lujan T.J. and Phatak N.S., 2005, "Three-dimensional Finite Element Modeling of Ligaments: Technical Aspects", Med. Eng. Phys., **27**(10), pp. 845-61.

[6] Hamel, A. J. and Sharkey, N. A., 1998, "A Dynamic Cadaver Model of the Stance Phase of Gait: Performance Characteristics and Kinetic Validation", Clinical Biomechanics, **13**, pp. 420-433.

[7] Sinacore, D. R., "Acute Charcot Arthropathy in Patients with Diabetes Mellitus: Healing Times by Foot Location", Journal of Diabetes and Its Complications, 1998, **12**, pp. 287–293.

[8] Milgrom, C., Finestone, A., Hamel, A., Mandes, V., Burr, D. and Sharkey, N., 2004, "A Comparison of Bone Strain Measurements at Anatomically Relevant Sites using Surface Gauges Versus Strain Gauged Bone Staples", Journal of Biomechanics, **37** pp. 947–952.

[9] Hurchler, C., Emmerich, J. and Wülker, N., 2003, "In Vitro Simulation of Stance Phase of Gait – Part 1: Model Verification", Foot and Ankle International, **24**(8), pp. 614-622.

[10] Kim, K-J, Kitaoka, H. B., Luo, Z-P, Ozeki, S., Berglund, L. J., Kaufman, K. R. and An, K-N, 2001, "In Vitro Simulation of the Stance Phase in Human Gait", Journal of Musculoskeletal Research, **5**(2), pp. 113–121.

[11] Kim, K-J., Uchiyama, E., Kitaoka, H. B. and An, K-N, 2003, "An in Vitro Study of Individual Ankle Muscle Actions on the Center of Pressure", Gait and Posture, **17**, pp. 125-131.

[12] Ward, E.D., Smith, K. M., Cocheba, J. R., Patterson, P. E. and Phillips, R. D., 2003, "In Vivo Forces in the Plantar Fascia During the Stance Phase of Gait - Sequential Release of the Plantar Fascia", Journal of the American Podiatric Medical Association, **93** (6), pp. 429-442.

[13] Erdemir A., McLean S., Herzog W. and van den Bogert A.J., 2007, "A Model-based Estimation of Muscle Forces Exerted During Movements, Clinical Biomechanics, **22**, pp. 131–154.

[14] R. D. Crownshield and R. A. Brand, A Physiologically Based Criterion of Muscle Force Prediction in Locomotion, J. Biomechanics, 1991, 14(11):793-801.

[15] Belegundu A.D and Chandrupatla T.R, 1999. "Optimization Concepts and Application in Engineering", Prentice Hall, pp. 182-188.

[16] May B, Saha S and Saltzman M, 2001. "A Three-Dimensional Mathematical Model of Temporomandibular Joint Loading", Clinical Biomechanics, **16**, pp. 489-495.

[17] Neptune, R. R., 1999. "Optimization Algorithm Performance in Determining Optimal Controls in Human Movement Analyses," J. Biomech. Eng., **121**, pp. 249–252.

[18] Schutte J.F, Koh B-I, Reinbolt J.A, Haftka R.T., George A.D. and Fregly B.J, 2005. "Evaluation of a Particle Swarm Algorithm For Biomechanical Optimization", Journal of Biomechanical Engineering, **127**, pp. 465-474.

[19] L. D. Noble, R. W Colbrunn, D-G. Lee, A. J. van den Bogert, B. L. Davis, Design and Validation of a General Purpose Robotic Testing System For Musculoskeletal Applications, J. Biomech. Eng., 132:025001 (2010).

[20] Coughlin, M. J. and Mann, R. A., Surgery of the Foot and Ankle, Volume 1, 7th ed., St. Louis Missouri: Mosby; 1999.

[21] Lee, D. G., and Davis, B. L., 2009, "Assessment of the Effects of Diabetes on Midfoot Joint Pressure Using a Robotic Gait Simulator", Foot and Ankle Int., 30, pp. 767-772.

[22] F. H Netter, The Ciba Collection of Medical Illustrations, Musculoskeletal System: Part 1, Anatomy, Physiology, and Metabolic Disorders.-(book reviews), Volume 8, Ciba Pharmaceutical Company, 1989.

[24] K-J. Kim, E. Uchiyama, H. B. Kitaoka and K-N. An, An in vitro Study of Individual Ankle Muscle Actions on the Center of Pressure, Gait and Posture, 2003, 17:125-131.

[25] http://www.mathworks.com/access/helpdesk/help/toolbox/optim/ug/fmincon.html

[26] R. E Isman and V. T Inman, Anthropometric Studies of the Human Foot and Ankle, Bull. Prosthet. Res., 1969, 11: 97–129.

[27] J. Perry, Gait Analysis: Normal and Pathological Function, Slack Incorporated, 1992, 57-59.

[28] J. A. Friederich and R. A. Brand, Muscle Fiber Architecture in the Human Lower Limb, J. Biomech, 1990, 23(1):91-95.

APPENDIX A

PUBLICATION RESULTING FROM THIS WORK:

DESIGN AND VALIDATION OF A GENERAL PURPOSE ROBOTIC TESTING SYSTEM FOR MUSCULOSKELETAL APPLICATIONS

Lawrence D. Noble[a], Robb W. Colbrunn[a], Dong-Gil Lee[a,b], Antonie J. van den Bogert[a], and Brian L. Davis[a]

[a]Department of Biomedical Engineering, Lerner Research Institute, and Orthopaedic and Rheumatologic Research Center, Cleveland Clinic, Cleveland, OH 44195

[b]Now of Department of Orthopaedics & Sports Medicine, University of Washington, Seattle, WA 98195

Contact Information:

Brian L. Davis, Ph.D.

Department of Biomedical Engineering/ND20

Cleveland Clinic

9500 Euclid Avenue

Cleveland, OH 44195

Tel: (216) 444-1055, Fax: (216) 444-9198, Email: davisb3@ccf.org

Abstract

Orthopaedic research on *in vitro* forces applied to bones, tendons and ligaments during joint loading has been difficult to perform because of limitations with existing robotic simulators in applying full-physiological loading to the joint under investigation in real time. The objectives of the current work are to 1) describe the design of a Musculoskeletal Simulator developed to support *in vitro* testing of cadaveric joint systems, 2) provide component and system-level validation results, and 3) demonstrate the simulator's usefulness for specific applications of the foot-ankle complex and knee.

The Musculoskeletal Simulator allows researchers to simulate a variety of loading conditions on cadaver joints via motorized actuators that simulate muscle forces while simultaneously contacting the joint with an external load applied by a specialized robot. Multiple foot and knee studies have been completed at the Cleveland Clinic to demonstrate the simulator's capabilities. Using a variety of general-use components, experiments can be designed to test other musculoskeletal joints as well (e.g., hip, shoulder, facet joints of the spine). The accuracy of the tendon actuators to generate a target force profile during simulated walking was found to be highly variable and dependent on stance position. Repeatability (the ability of the system to generate the same tendon forces when the same experimental conditions are repeated) results showed that repeat forces were within the measurement accuracy of the system. It was determined that synchronization system accuracy was 6.7 ± 2.0 ms and was based on timing measurements from the robot and tendon actuators. The positioning error of the robot ranged from 10 μm to 359 μm, depending on measurement condition (e.g., loaded or unloaded, quasistatic or dynamic motion, centralized movements or extremes of travel,

maximum value or root-mean-square, and x-, y- or z-axis motion). Algorithms and methods for controlling specimen interactions with the robot (with and without muscle forces) to duplicate physiological loading of the joints through iterative pseudo-fuzzy logic and real-time hybrid control are described. Results from the tests of the Musculoskeletal Simulator have demonstrated that the speed and accuracy of the components, the synchronization timing, the force and position control methods, and the system software can adequately replicate the biomechanics of human motion required to conduct meaningful cadaveric joint investigations.

Keywords

Orthopaedic biomechanics, foot and ankle, knee, robotics, instrumentation, simulation, actuators.

1 Introduction

The fundamental understanding of strain and stress within bone and soft tissue during various loading conditions is of great importance to researchers of degenerative diseases, injury prevention and rehabilitation. *In vivo* and *in vitro* studies as well as computational modeling have helped investigators gain valuable insights into the strains and stresses developed within the joint in response to loading, but each technique has some inherent limitation. Human *in vivo* studies of load-induced bone strains, as might be experienced during exercise, are difficult to conduct because of the nature of the invasive surgery required to implant strain gauges and the failure of bonding techniques between strain gauges and bone during exercise [1, 2]. *In vivo* studies designed to measure tissue breakdown using strain gauges could provide significant insight to progressive diseases

such as diabetes. However, for ethical and scientific reasons, this is not practical. Furthermore, from a scientific standpoint, obtaining accurate, repeatable *in vivo* results during long-term joint loading sessions would be difficult because of variability of responses from one trial to another, even within the same subject. Computational models to predict internal tissue loads based on external motion and applied loads require accurate data on tissue geometry and material properties. Reliability of these models is still problematic for mechanically complex systems such as the knee or foot, wherein soft tissue plays an important role [3, 4]. In contrast, *in vitro* testing with cadavers under simulated loading conditions can complement these other techniques and offers additional advantages. Musculoskeletal simulators and loading devices have been developed [5-10] to study the lower extremities. By reproducing varying degrees of the target kinematics and kinetics *in vitro*, investigators have acquired meaningful and clinically relevant data. Although these previous simulators have yielded new insight into the biomechanics of those particular joints, our general-purpose Musculoskeletal Simulator can support a wider range of investigations because of the following capabilities:

1. Simulating loading conditions on multiple joints (knee, hip, wrist, shoulder, etc.);
2. Simulating various loading conditions beyond walking (running, jumping, etc.);
3. Scaled velocities that simulate real-time (or near real-time) dynamics;
4. Simulating loading conditions in all 6 degrees of freedom (DOF) as compared to simple planar motion;

5. Simulating full- or near full-physiological loading (internal muscle forces and external forces) of the joint.

The Musculoskeletal Simulator has been developed to simulate a large spectrum of loading conditions for essentially any joint of interest through coordinated control of the external loading device (rotopod) and tendon actuators (servomotors). Knowledge of the specimen location and orientation with respect to the external loading device is provided using a spatial digitizer. The Musculoskeletal Simulator uses this knowledge to form kinetic and/or kinematic inputs to drive the devices based on the target loading conditions. To control these loading conditions, the Musculoskeletal Simulator can be configured to employ either 1) position control, 2) iterative optimization (affecting kinetic and kinematic trajectories), or 3) real-time proportional-integral-derivative (PID) force feedback control.

The objectives of the current work are to 1) describe the design of a Musculoskeletal Simulator developed to support *in vitro* testing of cadaveric joint systems, 2) provide component and system-level validation results, and 3) demonstrate the simulator's usefulness for specific applications of the foot-ankle complex and knee.

2 Materials and Methods

2.1 Component Design

2.1.1 Design Overview. The major components of the Musculoskeletal Simulator (Fig. 1) are the tendon actuators, rotopod, MicroScribe, external sensor data acquisition system, and external loading sensor. The type of external loading sensors used is based on the particular joint under investigation. The foot application used a six-axis force platform to measure forces and moments, whereas a six-axis load cell was used in the

knee studies. Additional components of the Musculoskeletal Simulator include the specimen mounting device, tendon load cells, tendon freeze clamps, knee flexion fixture, and application software.

2.1.2 Tendon Actuators. Three different tendon actuators have been developed to meet the unique demands of different muscle groups in the leg. It was assumed that the most rigorous exercise tested would be running and that the Achilles actuator would be the most demanding. We estimated, using gastrocnemius muscle kinematic data from Cavanagh [11], that the peak tensile force would be 2,300 N, velocity 0.54 m/s, and acceleration 56 m/s^2. Actuators are attached to tendons through pulley/cable systems that terminate at the freeze clamps, which are affixed to the tendons (Fig. 2). The rotary actuator consists of a Baldor (Fort Smith, AR) Model BSM80N-275AE servomotor, a Harmonic Drive Systems (Hauppauge, NY) Model CSG-40-50 harmonic drive and 175 mm diameter pulley (Table 1). This actuator was selected because it can exceed the force of the Achilles tendon during rigorous exercise. The velocity and acceleration capabilities of the actuator suggest that it can perform simulations of near real-time running. Since it incorporates a pulley system, there are practically no limitations regarding tendon stroke, making this actuator suitable for simulating the action of many different musculoskeletal systems. The linear actuators are Parker Hannifin Corp. (Cleveland, OH) ET50-Series electric actuators with SM233A servomotors (Table 2). Two different varieties of linear actuators have been developed. One design provides a 50-mm stroke and the other a 100-mm stroke. The 50-mm stroke design was selected because the muscles used in the foot during walking would not exceed this range. The 100-mm stroke was selected for some future application that might need an extended

stroke. The peak force is sufficient for the other muscles, and the velocity and acceleration parameters indicate that running simulations at half speeds are possible (note: acceleration scales by one fourth when speed is scaled by one half).

Table 1 Rotary tendon actuator characteristics.

Feature	Value
Drive reduction ratio	50:1
Peak static force	6,110 N
Continuous force	1,880 N
Maximum velocity	0.40 m/s
Maximum acceleration	120 m/s^2

Table 2 Linear tendon actuator characteristics.

Feature	Value
Peak static force	1,450 N
Continuous force	560 N
Maximum velocity	1.0 m/s
Maximum acceleration	14 m/s^2

2.1.3 Rotopod. The R2000 rotopod, developed by Parallel Robotic Systems Corp. (Hampton, NH), is a 6 DOF robot (Table 3). The rotopod is similar to a standard hexapod robot, but, due to the unique mounting configuration of the six actuators on a circular path, it is additionally capable of rotating a payload ±720 degrees about the Z-axis of the rotopod base coordinate system (ROB) (Fig. 1). The high load capacity of the rotopod makes it possible to provide full-physiological loading simulations, including running loads [12]. However, the velocity capabilities suggest running simulations must be time scaled. The motion path and corresponding velocities required of the robot for simulating running will exceed the translational and rotational velocity capabilities of the

robot. The repeatability and inherent high stiffness of this configuration are important for superposition testing methods.

Table 3 Rotopod specifications.

Feature	Value	Feature	Value
Platform size (diameter)	780 mm	Repeatability	25 μm
Load capacity	2,000 N	X-Axis range of motion	±110 mm
Torque capacity	1,000 N-m	Y-Axis range of motion	±110 mm
Payload capacity	227 kg	Z-Axis range of motion	±93 mm
Translational velocity	100 mm/s	Roll range of motion	±13°
Angular velocity	120°/s	Pitch range of motion	+12°, -19°
Static accuracy	±50 μm	Yaw range of motion	±720°

2.1.4 MicroScribe. The MicroScribe G2L digitizer, developed by Immersion Corp. (San Jose, CA), provides spatial information on the rotopod, external load sensor, and the cadaver specimen for use by the application software. Once the relative locations of these components are determined, this software performs all three-dimensional transformations necessary to execute motion and calculates loading response in clinically relevant coordinate systems. One limitation of the MicroScribe (Table 4) is that the resolution and accuracy are not on the same order of magnitude as that of the rotopod. However, since the MicroScribe is used to define the relative coordinate systems of the Musculoskeletal Simulator components and the specimen, it must also be considered that the variation and precision in determining anatomical references are much larger than the uncertainty in the MicroScribe. For these reasons, the software contains mitigation

techniques such as optimization in the foot experiments and hybrid (force and position) control in the knee experiments.

Table 4 MicroScribe specifications.

Feature	Value
Workspace	168 cm sphere
Resolution	0.13 mm
Accuracy (100 point ANSI sphere)	0.43 mm

ANSI, American National Standards Institute.

2.1.5 External Sensor Data Acquisition System. The stand-alone data acquisition system is synchronized with the Musculoskeletal Simulator, via the common digital synchronization bus and Ethernet, to provide up to 16 additional channels of analog data. Bone or soft tissue strain, joint pressure, or other analog voltage signals are acquired and conditioned using a National Instruments (Austin, TX) PCI-6229 data acquisition board and SCXI-1000 signal conditioning chassis with a SCXI-1143 Butterworth 200 Hz low-pass, anti-aliasing filter.

2.1.6 Force Platform. A Bertec (Columbus, OH) force plate (Model 4060) and amplifier (Model 6800) were used for the foot experiments in combination with the National Instruments PCI-6034E data acquisition board for analog/digital conversion of the voltage analog outputs of forces (F_x, F_y and F_z) and moments (M_x, M_y and M_z). Characteristics of the force platform are provided in Table 5.

Table 5 Bertec force platform performance characteristics.

Feature	Value
Load rating	F_x, F_y: 5,000 N, F_z: 10,000 N M_x: 1,500 N-m, M_y: 1,000 N-m, M_z: 750 N-m
Sensitivity	F_x, F_y: 0.44 N/mV, F_z: 0.89 N/mV M_x: 0.27 N-m/mV, M_y: 0.18 N-m/mV, M_z: 0.13 N-m/mV
Linearity	±2.0 % Full scale (FS)
Hysteresis	±2.0 % Full scale
Gain, selectable per channel	1, 2, 5 10, 20, 50, 100

2.1.7 Specimen Mounting Device. An aluminum tube that contains the potted specimen (foot, knee, etc.) slides into a receptacle device, where it is clamped into a stationary position during loading.

2.1.8 Tendon Freeze Clamps. Freeze clamps of two different sizes were developed at the Cleveland Clinic to attach the tendons to the tendon actuator cables. The bodies of these clamps allow the attachment of liquid nitrogen feed lines (Fig. 2).

2.1.9 Tendon Load Cells. Three Omega (Stamford, CT) LCFD-100 load cells (range: 0-445 N, accuracy: ±0.15% FS, repeatability: ±0.05% FS) and one LCFD-500 load cell (range: 0-2,224 N, accuracy: ±0.2% FS, repeatability: ±0.1% FS) were used to measure the force of the individual tendons. Load cells were located in-line between the tendon freeze clamps and tendon actuator cables. In addition, one custom-made load cell incorporated into the pulley of the rotary tendon actuator, manufactured by Strainsert (West Conshohocken, PA) is capable of measuring force in the range of 0-6,720 N (accuracy: ±1% FS, repeatability: ±0.15% FS).

2.1.10 Six-Axis Load Cell. The ATI Industrial Automation (Apex, NC) Theta-series SI-1500-240 six-axis load cell (Table 6) was used during knee experiments to measure the loads observed at the tibia attributable to the rotopod. In this configuration, the tibia is purposely mounted in the inverted stationary position.

2.1.11 Knee Flexion Fixture. Given the range of motion of the rotopod, the Musculoskeletal Simulator is not able to explore the full range of motion of the knee without an additional fixture to provide a seventh DOF. Although relatively small dynamic changes in flexion (about ±10º) are possible with the Musculoskeletal Simulator, the custom fixture illustrated in Fig. 3 allows for flexion of the knee from 0º to 120º.

Table 6 ATI Theta SI-1500-240 load cell performance characteristics.

Feature	Value					
	F_x	F_y	F_z	M_x	M_y	M_z
Load rating (N, N-m)	1,500	1,500	3,750	240	240	240
Resolution (N, N-m)	0.5	0.5	1.1	0.07	0.07	0.07
Accuracy (% FS)	1.50	1.25	0.75	1.25	1.00	1.50

2.1.12 Application Software. A software framework for the Musculoskeletal Simulator has been developed using National Instruments (Austin, TX) LabVIEW™ version 8.2. The framework was tested with both foot and knee applications. The system block diagram (Fig. 4) provides a general organization of application software required for the foot experiment. The external sensor data acquisition system software has been designed to run on a stand-alone workstation to handle the data acquisition processing, independent of the Musculoskeletal Simulator workstation processor that provides the

main application software. This architecture supports operation in master-slave configuration, by which the Musculoskeletal Simulator application software controls timing aspects of the external sensor data acquisition system during the experiment.

A graphical user interface captures key aspects of the configuration and set-up prior to execution of the experiment simulations. The application software provides the ability to interface with the MicroScribe to digitize the unique anatomical features of each specimen prior to testing to ensure that data are collected in a clinically relevant anatomical coordinate system. A flexible text-file-based system facilitates the input of muscle electromyogram data, kinematic data (motion analysis) and externally induced load data, such as would result from exercise. These input data are used to establish motion trajectories and tendon force profiles in the same clinically relevant coordinate systems as those used for the simulated exercises. During the experiment, the Musculoskeletal Simulator software produces real-time graphs of engineering data retrieved through analog data input channels. For instance, displays of real-time force and moment data are provided in the tibial coordinate system during knee experiments.

2.2 Equipment Configuration

2.2.1 Foot Test Configuration. To conduct foot experiments, the Musculoskeletal Simulator uses kinetic trajectories (force profiles) for the tendon actuators and for the target ground reaction forces (GRFs). The kinematic trajectory of the tibia relative to the ground, as measured in a gait lab, drives the rotopod motion. The Musculoskeletal Simulator uses iterative optimization techniques to produce the target loading conditions, GRFs and/or tendon actuators. The anatomical coordinate system is based on a proposed International Society of Biomechanics standard [13]. However, because of the unique

nature of cadaveric simulators, a custom reference frame was defined as the tibial coordinate system (TIB). Since the TIB defines the ankle center and is used to orient GRF and ground tibia position data, one needs to consider the orientation of the tibia as well as the foot. Like the knee joint, variations from the standard coordinate system account for missing anatomical reference points caused by the cutting and mounting of limbs. The tibial intercondylar point is replaced with the centroid of the tibia measured at the most proximal location possible, and to increase repeatability of the specimen coordinate system, the mediolateral axis is redefined as an axis perpendicular to the midline of the foot [14]. For orientation of the tibia relative to the ground, Yeadon's [15] "somersault-tilt-twist" variables are used. The Yeadon rotation sequence twist (which is renamed internal rotation) is measured about the tibial long axis; somersault is measured about the global mediolateral axis. To recreate typical foot-ankle motion, the tibia is fixed horizontally on the surrounding frame, and the force plate is mounted vertically on the top of the rotopod platform to create an inverted ground-tibia motion (Fig. 1). This method provides two major benefits. First, it does not require moving the entire tendon actuator system along with the tibia motion during a simulation. Second, the largest foot-ankle rotation, somersault, can be adequately simulated because of the rotopod's unique ability to provide large rotations in the horizontal plane. One limitation of this configuration is that the inertial loading of the specimen cannot fully be replicated because of the quasi-static nature of the simulations; we compensate for this factor by slight changes in rotopod motion via the optimization process.

2.2.2 Knee Test Configuration. The Musculoskeletal Simulator, configured to conduct knee experiments, can operate in position or force control. Given a kinematic

input file, the Musculoskeletal Simulator can step through the motion sequence and store data at each position. Given a kinetic input file, the Musculoskeletal Simulator can ramp to each loading condition via a real-time hybrid controller (simultaneous position and force control). The knee joint coordinate system translations and rotations follow the system proposed by Pennock and Clark [16], with one difference: the long axes of femur and tibia do not have the proximal femoral head and ankle joint as reference points since the ends of these bones have been removed to mount the specimen. Instead, these points are replaced with the centroids of the remaining bone at the proximal femur and distal tibia. Although the motions are defined in the knee joint coordinate system, the loads are measured in the tibial reference frame [17]. As a result, the tibia is attached to the load cell since this configuration ensures that the coordinate transformation is a static rather than a dynamic matrix. The load cell is attached to the frame rather than the rotopod not only to keep the elements clean but also to remove inertial loads and eliminate concerns about wire pinching. The mounting of the knee and flexion fixture are done so as to maximize the joint range of motion with respect to the rotopod range of motion.

2.3 Data File Organization

2.3.1 Data File Overview. The rotopod trajectory and servomotor actuator force profiles are defined through a set of data files to provide maximum flexibility and ease of configuration. The data file inputs that must be supplied to define the loading conditions include:

1) Kinematic trajectory (single- or multi-axis):

a) Rotopod motion trajectory of joint or external load device (examples: force platform simulating the ground, or superposition testing in knee joint coordinate system);

2) Kinetic trajectories (single- or multi-axis):

a) Target load response (examples: target superior GRF, knee force profile);

b) Individual tendon actuator force profiles.

2.3.2 Kinematic Trajectory Data File. The rotopod motion trajectory file contains the trajectory for the relative motion between the joint under investigation and the external loading device during a specified loading condition. The rotopod trajectory is generated through a series of transformations (see Appendix) based on the motion specified in the trajectory data file. In the foot experiment, this file would be the trajectory of the force platform (ground) with respect to the mounted foot. The motion trajectory terms need to be normalized using foot length (FL) and foot width (FW) since these are the characteristic measurements that provide insight to overall foot size. Time is normalized to a percentage of total motion time. Before any normalization calculations occur, the raw data (i.e., data collected in the actual gait lab) must be transformed to the ground tibia position reference frame, which includes the trajectory variables (a, m, s, r, t, and o) defined below. Additionally, the origin is defined as the point of intersection of the ground plane and the long axis of the tibia at the time when that axis is in the global frontal plane. For physiological normalization, researchers would typically normalize using equations such as these:

$$a = [\,Forward\ translation\ position / FL\,] \times 100\% \quad (1)$$

$$m = [\,Medial\ translation\ position / FW\,] \times 100\% \quad (2)$$

$$s = \{Upward\ translation\ position/[½ \times (FW + FL)]\} \times 100\% \quad (3)$$

$$Time = [Elapsed\ time/Total\ motion time] \times 100\% \quad (4)$$

The angles r, t, and o do not require scaling:

r = *Twist angle (positive for internal rotation of the tibia*)

t = *Tilt angle (positive for lateral tilt)*

o = *Somersault angle (positive for forward rotation)*

2.3.3 Target Load Response Data File. This file contains the expected reaction forces and parameters derived from the moments that result from the specific loading condition performed. In the foot experiment, the data would be the expected GRF profiles (F_a, F_m, and F_s) as measured in the gait lab, along with the calculated center of pressure (COP) in the anterior (COP_a) and medial (COP_m) directions and the internal rotation couple moment (T_r) at the COP. Ultimately, these parameter values should be observed between the foot and the force platform during the simulated walking conditions. As in the case of the external load device motion trajectory, the profile values at any time need to be normalized to physiological parameters and placed into the external loading device coordinate system reference using a standard transformation matrix.

For the foot, this normalization would typically adjust for body weight (BW), FL and FW. For the COP parameters (COP_a and COP_m), the method used for the averaging and normalization is similar to the method developed by Motriuk and Nigg [18]. Normalization of the forces (F_a, F_m, and F_s) makes use of the commonly accepted practice of using percentage of BW (%BW). The last parameter, T_r, is scaled by percentage of BW and the average of FL and FW. The target force platform response

data file would include the following normalized parameters at each normalized time profile point:

$$F_a = [\,Measured\ force\ in\ anterior\ axis / BW\,] \times 100\% \quad (5)$$

$$F_m = [\,Measured\ force\ in\ medial\ axis / BW\,] \times 100\% \quad (6)$$

$$F_s = [\,Measured\ force\ in\ superior\ axis / BW\,] \times 100\% \quad (7)$$

$$COP_a = [\,COP\ in\ anterior\ axis / FL\,] \times 100\% \quad (8)$$

$$COP_m = [\,COP\ in\ medial\ axis / FW\,] \times 100\% \quad (9)$$

$$T_r = \{\,Couple\ moment\ in\ internal\ rotation\ axis / [BW \times ½ \times (FW + FL)]\,\} \times 100\% \quad (10)$$

2.3.4 Tendon Actuator Force Profile Data Files. The application expects that the tendon force profile during the simulated loading will be provided in terms of normalized force at each normalized time as defined below:

$$Force = [\,Actuator\ force / BW\,] \times 100\% \quad (11)$$

2.4 Force Control Techniques

2.4.1 Iterative Optimization. After any experiment simulation, optimization can be used to adjust the input data file for the external load environment/joint motion trajectory (i.e., results in an adjusted rotopod trajectory) and individual tendon actuator force profiles to eliminate offset between the actual and target load response. The optimization algorithm used in the foot experiment can calculate optimized rotopod trajectories and tendon actuator force profiles based on actual data recorded from a previous experiment and the target GRF. For example, an experiment would be conducted to simulate the stance phase of walking, and then the experimenters would look at the results to

determine what optimization modes are necessary. The optimization feature is used to iteratively make the necessary adjustments until convergence criteria are achieved.

The optimization algorithm is a combination of individual configurable pseudo-fuzzy logic controllers. Each controller uses one input and one output. The input signal is the error in one of the six GRF channels, and the output signal is then added to the chosen simulator channel (e.g., superior motion, tibialis anterior force, etc.). The controller processes the input by selective windowing (% stance range within which data are to be analyzed), applying the chosen algorithm (i.e., use mean, absolute value, or point-by-point), low-pass filtering, multiplying by a gain parameter, and finally adding to the output channel data from the previous run to produce the optimized output signal for that same channel. Multiple controllers acting on the same simulator channel are collectively summed to produce the optimized trajectories used for the subsequent test.

Optimization of muscle forces is considered to be adaptive such that the viscoelastic response of the tendon from the previous experiment is taken into consideration when making adjustments for the subsequent experiment. For instance, if the superior GRF (F_s) did not achieve the target peak value at toe-off (e.g., the triceps surae muscle group did not reach the target tension at that time), then optimization can increase the force to this muscle group at that same time by an amount equal to the following:

$$F_{triceps\,surae}(new) = F_{triceps\,surae}(previous) + Gain \times (F_s\ Target - F_s\ Actual) \quad (12)$$

Similarly, optimization provides the flexibility necessary to adjust for positional misalignment between the joint coordinate system and device contacting the joint to provide loading. To illustrate this possibility, consider the origin of the tibia coordinate system X, Y, and Z in the ankle (identified as TIB in Fig. 1). If the actual origin were 1

mm in the Z-direction from what was recorded with the MicroScribe during set-up of the experiment, then it would manifest itself as low F_s during the experiment, and optimization can be invoked to adjust for this discrepancy. The result would be to shift the force platform trajectory by a constant amount in the Z-direction for all time increments during simulated stance, such that the Z-position (new) is now computed as shown:

$$Z\text{-}position(new) = Z\text{-}position(previous) + Gain \times Mean(F_s\ Target - F_s\ Actual) \quad (13)$$

In this case, the mean value is computed for the difference in F_s across all time increments. This mean is then multiplied by a constant gain value to achieve the Z-value offset for the force platform trajectory.

2.4.2 Real-Time Hybrid Control. In the knee experiments, the aim is to provide simultaneous position and force control. The flexion axis of the knee has very little stiffness, and controlling moment about that axis would be unlikely to provide a unique solution. For this reason, the joint is controlled in three axes of force control (anterior, medial, superior), two axes of torque control (varus, internal rotation), and one axis of angle control (flexion). This PID hybrid control scheme operates in a variation of the knee joint coordinate system to maximize decoupling. The controller transforms the data from the load cell coordinate system to the tibial coordinate system [19]. Then superior force and varus torque are decoupled into two superior forces, each located at the center of each femoral condyle. Following the PID algorithm, the resulting command signals are integrated with respect to time, recoupled to the knee joint coordinate system, and transformed to the rotopod coordinate system. In addition, the hybrid controller employs

other tools, such as gain scheduling and feed forward, to further enhance speed and stability.

2.5 Validation Methods

Validation of this complex system included evaluating the general capabilities of the major components (subsystems) as well as demonstrating the performance of the full system when configured to conduct foot and knee experiments.

2.5.1 Tendon Actuator Accuracy and Repeatability Validation Tests. A foot study designed to simulate gait was used to test the mean absolute accuracy and repeatability of the tendon actuators at achieving the target tendon force levels. Six experiments conducted on two specimens provided data from multiple experiments at the same loading conditions. Absolute errors were computed between actual and target force at each time interval during stance for each experiment and reported as a mean ± 1 standard deviation. Repeatability was visualized by plotting the target force against the actual force for the various experiments for periods of simulated muscle contractions. Simulated relaxation was not included in the plots because hysteresis that results between contraction and relaxation further complicates the plots (i.e., two points per experiment at each stance point).

2.5.2 Component Synchronization Validation Tests. To synchronize the entire system, the low-level programs of the rotopod and tendon actuators and the internal and external data acquisition systems were coded to start their respective processes at the moment when the rotopod's controller generates a digital falling trigger signal. Since the external data acquisition system was coded to poll the digital trigger signal every 1 ms, the timing delay between the digital trigger signal and the external data was a maximum

of 1 ms. The internal data acquisition system pre-acquires data and is post-processed to align to the trigger resulting in a delay, which is also ≤1 ms. The timing delay of the mechanical components' motion from the digital trigger signal was evaluated by performing a step function-like motion profile. Ten tests each were conducted on the rotopod, rotary tendon actuator, and linear tendon actuators to measure the motion delay from the start of the synchronization trigger signal. System synchronization accuracy can be estimated by the following equation:

$$Synchronization\ System\ Accuracy = \frac{Max.\ delay + Min.\ delay}{2} \pm \frac{Max.\ delay - Min.\ delay}{2} \qquad (14)$$

2.5.3 Rotopod Position Accuracy Validation Test. The rotopod provides motion, force input, or both to the joint of interest. The control of force is done through real-time feedback control, as in the knee experiments, or iterative force control, as in the foot experiments. Fundamentally, position is iterated to reach the target force. Therefore, a series of tests were run to determine the quasi-static and dynamic translational accuracy of the rotopod when loaded (with a payload of 98.2 kg) and unloaded. The quasi-static test motion path was a stepped triangle wave (10 mm per step) over the full range of motion (± 100 mm in each axis), quantifying uniaxial position error. The dynamic test path was a 0.167 Hz sinusoidal waveform corresponding to a peak speed of 100 mm/s (maximum capability of the rotopod) for the same range of motion. A Heidenhain Corp. Model LS679 linear encoder (Shaumburg, IL), having an accuracy of 10 μm and a resolution of 0.5 μm, was used to measure the movement of the robot. Accuracy was assessed by maximum (max.) and root-mean-square (rms) positional errors for the full range of motion (similar to the foot experiment) and for the center range of motion (± 30 mm, as in the knee experiment).

2.5.4 Optimization Validation Test. Experiment optimization was invoked to target the heel strike and the latter half of stance during foot experiments to achieve reasonable simulated walking. This capability was tested through a series of seven experiments: Experiments 1-4 focused on adjusting offsets during heel strike, whereas experiments 5-7 focused on adjusting the muscle forces from mid stance through toe-off.

2.5.5 Foot Test Demonstration. The foot experiment configuration of the Musculoskeletal Simulator has been used to measure various biomechanical parameters in studies of normal and pathological gait. In a recent study [20], it was used to investigate the effects of diabetes on the midfoot joint pressures. A foot study designed to acquire tibial and calcaneal bone strain data during simulating gait is used to demonstrate the Musculoskeletal Simulator capabilities in a foot experiment configuration. Tibial and calcaneal strain data were collected using Vishay Micro-Measurements rosette C2A-06-031WW-120 (Raleigh, NC). Testing was performed to verify that analog data (in this case, strain data) could be synchronized through the digital synchronization bus and collected during the entire stance phase of simulated walking in a reliable and repeatable manner. Two 2100 System signal conditioning amplifiers (Vishay Micro-Measurements) were used to provide quarter-bridge circuit conditioning and amplification required for these strain gauge rosettes. The locations of these rosettes were anterior tibia (lateral and medial sides), posterior tibia, and lateral calcaneus for a total of 12 channels of raw strain data. The foot study simulated walking at one-fourth speed and varying BW percentages (16.5%, 38.4%, 66.7%, and 100% BW). Graphs of the target and actual GRF data, along with the tendon force data, for a representative experiment are presented.

2.5.6 Knee Test Demonstration. The Musculoskeletal Simulator has been used to study native kinematics, arthroplasty, and surgical techniques in the knee joint. In one study, the knee test system was programmed to apply 108 combinations of the following loading conditions at three flexion angles (0º, 30º, and 60º): internal/external rotation (0, ±5 N-m), varus/valgus (0, ±10 N-m), compression (100, 700 N), posterior drawer (0, 100 N). The combined loading condition was ramped, held, and released in 2 s, 3 s, and 1 s, respectively. The error between the target and actual force, or torque, is analyzed continuously as well as during the plateau (at which point auxiliary data is typically collected).

3 Results

3.1 Tendon Actuator Accuracy and Repeatability Results.

Tests conducted to measure the error between target and actual tendon actuator forces revealed a large variability in absolute error (which was dependent on the stance time; Fig. 5), but these tests demonstrated that within multiple runs of the same experiment there was excellent repeatability (Fig. 6).

3.2 Component Synchronization Results.

Test results of synchronization revealed that the rotopod contributes the largest delay at 10.8 ± 1.0 ms, followed by the linear actuator at 5.2 ± 1.4 ms, then the rotary actuator at 4.1 ± 1.0 ms. Using Eq. (14), the total synchronization system accuracy was 6.7 ± 2.0 ms.

3.3 Rotopod Positioning Results.

The rotopod positioning test results (Table 7) ranged from 10 μm to 359 μm, depending on measurement condition. The Z-axis position error is roughly 2 times the error for the X- and Y-axes. In general, loaded errors were higher than unloaded errors by 1.2, 1.3 and 1.6 times, for the X, Y and Z-axis, respectively.

3.4 Optimization Results.

A typical optimization scenario is depicted in Fig. 7. Experiments 1-4 were used to adjust the superior GRF to achieve the target level at the initial heel strike contact by changing the anterior and superior coordinates of the tibial coordinate system. Table 8 summarizes what changes were made for the first four experiments to simulate heel strike. Experiments 5-7 used time-based adjustments to the plantarflexors (triceps surae, flexor hallucis, tibialis posterior and peroneus longus) to bring the superior GRF to within ±10% of the target force during loading response, mid stance, terminal stance and toe-off contact phases.

Table 7 Rotopod positioning results.

Position error (μm)	X-axis		Y-axis		Z-axis	
	Unload.	Loaded	Unload.	Loaded	Unload.	Loaded
Quasi-static full (max)	56	99	37	50	74	234
Quasi-static full (rms)	24	28	18	29	36	84
Quasi-static center (max)	55	27	32	44	58	61
Quasi-static center (rms)	26	16	19	24	33	30
Dynamic full (max)	89	108	79	127	206	359
Dynamic full (rms)	31	38	30	31	63	110
Dynamic center (max)	27	39	62	58	95	85
Dynamic center (rms)	10	15	26	19	52	49

Max, maximum; rms, root mean square.

3.5 Foot Test Demonstration.

The optimization target of ±10% was achieved at heel strike and toe-off in the superior axis during simulated gait using the Musculoskeletal Simulator (Fig. 8). In the anterior and COP channels, the goal was to optimize the kinetic and kinematic trajectories to the point where the target and actual curves had a similar form. For this experiment, further optimization to better achieve the target profiles was not necessary to obtain the desired bone strain results.

3.6 Knee Test Demonstration.

The hybrid controller demonstrated that low errors can be achieved on the superior compression channel during the course of the 108 combined loading conditions (see Fig. 9 for a representative graph). The highest errors (rms and max.) were found to be in the continuous comparison analysis (Table 9).

Table 8 Optimization during heel strike.

Experiment no.	Anterior offset (mm)	Superior offset (mm)	Summary of results
1	0	-13	Starting point; no heel contact with force platform.
2	4	-11	Force platform contacted the heel 4 mm forward (anterior direction) of the initial run and moved 2 mm closer (superior direction) to the bottom of the foot. This achieved 36% BW (target 44% BW).
3	5	-10.5	Force platform trajectory was adjusted another 1 mm and closer to the mounted foot by 0.5 mm. This achieved 43% BW.
4	9.5	-10.5	Force platform trajectory was adjusted 4.5 mm forward (anteriorly) from previous run with no change in the proximity to the foot (superior direction) at the start. This had an adverse affect by overshooting to 47% BW. Note: the previous iteration's anterior offset (5 mm) was ultimately used for the final experiment settings.

Table 9 Representative knee force/torque control errors.

Force/Torque control error	Value				
	$F_{lateral}$ (N)	$F_{anterior}$ (N)	$F_{superior}$ (N)	T_{Varus} (N-m)	T_{ER} (N-m)
Plateau (max.)	1	3	10	0.1	0.2
Plateau (rms)	<1	1	4	0.04	0.1
Continuous (max.)	73	69	330	9.4	1.4
Continuous (rms)	11	16	71	1.3	0.3

T_{ER}, torque, external rotation; max., maximum; rms, root mean square.

4 Discussion

4.1 Tendon Actuator Accuracy and Repeatability

Force accuracy results achieved with the tendon actuators during the Musculoskeletal Simulator performance verification process were sufficient to accurately simulate gait for the foot bone strain study. The ability of the tendon actuators to achieve the target muscle force profile is dependent on the resolution of the in-line load cells and controller gains (PID). The load cell resolution was found to correlate ($R^2 = 0.85$) with the tendon actuator accuracy. The load cell used with the actuator simulating the tibialis posterior muscle had a resolution of 0.54 N per count (12 bit analog/digital converter counts), the load cell used with the triceps surae actuator had a resolution of 0.19 N per count, and the remaining load cells had resolutions of 0.10 N per count. Excellent repeatability results were demonstrated for the tendon actuators, with an average error of 0.3% BW. Tendon actuator accuracy posed no limitations to the particular foot study, therefore no further optimization was deemed necessary. A one-time adjustment was made to controller PID gains, velocity parameters and acceleration parameters for the linear tendon actuators. This adjustment resulted in a substantial performance improvement, which was sufficient for the foot study. Future studies that require an even higher level of accuracy may achieve it by optimization of these parameters.

4.2 Component Synchronization

Provided the duration of the activity being simulated is significantly larger than the synchronization error (6.7 ± 2.0 ms), the effect of the error will be insignificant for future researchers. For the foot study presented, the simulated walking motion was 2.8 s.

Therefore, this error represents 0.24% of the total experiment time and is not considered significant.

4.3 Rotopod Positioning Discussion

The highest error values measured were for Z-axis motion, potentially due to considerable changes in the configuration of the robot legs. Loading generally increased error magnitude but was not pronounced for the center range of motion. The error values were less than those found in other studies [10] and therefore are adequate for *in vito* reproduction of certain motions.

4.4 Optimization

A typical optimization procedure was discussed, showing that the system has the necessary flexibility to successfully optimize the trajectory (required for heel strike adjustment) and for muscle force optimization (required for the latter phase of stance). During the foot study, it was found that typically within 3-6 iterations of trajectory optimization, it was possible to obtain a heel strike force within the target limit of ±10% of the target superior GRF. Similarly, within 4-8 iterations of muscle force optimization, the latter half of stance was within this limit. Optimization adjusted the target muscle forces by an amount proportional to the measured parameter (superior force error), therefore subsequent iterations of optimization converged on acceptable muscle forces regardless of whether or not they matched the target force set point. Stability of the optimization algorithm is therefore much more dependent on repeatability of the actuators and the rotopod, which has been shown to be very high. Although the fuzzy logic controllers were effective on this experiment, one limitation is that the algorithms

provided non-unique solutions to the optimization, given that there were 6 inputs (GRF) and 11 outputs (6 DOF kinematics and 5 tendon actuators). Future enhancement of the optimization algorithm may be necessary, depending on the requirements for a given study. To provide for this possibility, the Musculoskeletal Simulator software can be customized within the existing software framework to allow the implementation of fuzzy logic, model predictive, linear optimization, or any other control philosophy.

4.5 Foot and Knee Test Demonstrations

Through the completion of the performance validation process, several key features of the Musculoskeletal Simulator have been demonstrated. Multiple joints have undergone 6-DOF simulations at full-physiological loading conditions. Full-physiological loading of the foot and knee was achieved with the Musculoskeletal Simulator in a stable and highly repeatable manner.

Foot experiments used programmable loading conditions and operated at one-fourth walking speed. Synchronization of system components, accuracy of tendon actuators and of rotopod position, and the results of the foot experiment systematically demonstrate that the Musculoskeletal Simulator is able to simulate an entire gait cycle through coordinated motion of the rotopod and tendon actuators while simultaneously recording 12 channels of bone strain.

In the knee experiment, one limitation to achieving the dynamic motion demonstrated by the foot experiment is the static adjustability of the flexion fixture. As a result of this limitation, tests had to be paused in order to manually adjust the fixture to provide greater changes in knee flexion. Work has recently been completed to remove this constraint by

developing a rotary stage mounted on top of the rotopod. This stage provides dynamic flexion capabilities for knee, shoulder, and hip experiments with a range of ±180º.

The representative errors in the real-time hybrid control are minimal in the plateau measurements and sufficient for testing where quasi-static combinations of loads are applied. Figure 9 suggests that the continuous errors in Table 9 result from the inherent lag in PID control algorithms. In studies for which real-time dynamic loading is desired, improvements would need to be made in the response time of the control system by modifying this algorithm or implementing a new one.

5 Conclusions

The Musculoskeletal Simulator has been shown to simulate the biomechanics of human motion through (i) a set of actuators that, when connected to selected tendons traversing a joint, can imitate muscular contractions, and (ii) a rotopod that can simulate environmentally induced loading of and contact with the cadaver specimen. The benefit of these coupled systems is that they enable fully synchronized joint loading at physiological levels, at or near real-time speeds. The design of the Musculoskeletal Simulator makes it readily adaptable for investigation of many different joint systems. The Musculoskeletal Simulator has been developed to enable fundamental research that is focused on injury prevention, but the applications extend into other areas such as the evaluation of surgical interventions and total joint replacements and the development of rehabilitation regimens.

Acknowledgments

The authors would like to acknowledge support for this research from NASA Grant NNJ05HF55G and from the Cleveland Clinic Musculoskeletal Core Center, funded in part by NIAMS Core Center Grant 1P30 AR-050953. In addition, the efforts of Katherine Muterspaugh in providing LabVIEW routines for sampling and storing bone strain data are appreciated. Special thanks to Ken Kula (Cleveland Clinic Center for Medical Art and Photography) for providing the artist renditions of the Musculoskeletal Simulator. Finally, the support of the Cleveland Clinic is gratefully acknowledged through the contributions of Peter R. Cavanagh, Ph.D., D.Sc. (now of the University of Washington/Seattle) for providing the rotopod and Ahmet Erdemir, Ph.D., Computational Biomodeling Core, for providing rotopod test results.

Appendix: Transformation of Three-Dimensional Kinematic Data to Rotopod Trajectory (Foot and Knee Examples)

This appendix illustrates the kinematic chain equation, as shown in Eq. (15) and (16), for a typical foot or knee experiment, respectively. The expressions include reference frames for the rotopod base (ROB), the rotopod platform (PLA), the force plate (GND), the knee flexion fixture (FIX), the 6-axis load cell (LOD), the MicroScribe (MIC), the tibia (TIB), and the femur (FEM). The static transformation matrices for the foot are $\mathbf{T}_{ROB,MIC}$, $\mathbf{T}_{PLA,GND}$, and $\mathbf{T}_{TIB,MIC}$. The corresponding dynamic matrices are $\mathbf{T}_{ROB,PLA}$, and $\mathbf{T}_{GND,TIB}$. The static transformation matrices for the knee are $\mathbf{T}_{ROB,MIC}$, and $\mathbf{T}_{TIB,MIC}$ and the configurable $\mathbf{T}_{PLA,FIX}$. The corresponding dynamic matrices are $\mathbf{T}_{ROB,PLA}$, and $\mathbf{T}_{FEM,TIB}$. These equations can be used to derive the elements of any one dynamic matrix

given the other dynamic matrix (such as deriving rotopod positions given the motion of the tibia relative to the ground) that may have been collected in a gait lab setting. Refer to Figs. 1 and 3 for the location of each reference frame.

$$T_{ROB,MIC} = T_{ROB,PLA}(q) \cdot T_{PLA,GND} \cdot T_{GND,TBD} \cdot T_{TIB,MIC}(r) \quad (15)$$

$$T_{ROB,MIC} = T_{ROB,PLA}(q) \cdot T_{PLA,FIX}(\theta) \cdot T_{FIX,FEM} \cdot T_{FEM,TIB}(K_{JCS}) \cdot T_{TIB,MIC} \quad (16)$$

Where:

Rotopod Coordinates:

q = (x, y, z, roll, pitch, yaw)

Ground/Tibia Position:

r = (a, m, s, r, t, o)

Flexion Fixture Setting:

θ = Nominal knee flexion angle

Knee Joint Coordinates [16 and 21]:

K_{JCS}= (a, b, c, α, β, γ)

References

[1] Lanyon, L. E., Hampson, W. G., Goodship, A. E., and Shah, J. S., 1975, "Bone Deformation Recorded *In Vivo* from Strain Gauges Attached to the Human Tibial Shaft," Acta Orthop. Scand., **46**, pp. 256–268.

[2] Burr, D. B., Milgrom, C., Fyhrie, D., Forwood, M., Nyska, M., Finestone, A., Hoshaw, S. Saiag, E., and Simkin, A., 1996, "*In Vivo* Measurement of Human Tibial Strains during Vigorous Activity," Bone, **18**, pp. 405–410.

[3] Weiss J. A., Gardiner J. C., Ellis B. J., Lujan T. J., and Phatak N. S., 2005, "Three-Dimensional Finite Element Modeling of Ligaments: Technical Aspects," Med. Eng. Phys., **27**, pp. 845-861. Epub 2005 Aug 8.

[4] Sharkey, N. A., and Hamel, A. J., 1998, "A Dynamic Cadaver Model of the Stance Phase of Gait: Performance Characteristics and Kinetic Validation," Clin. Biomech., **13**, pp. 420-433.

[5] Milgrom, C., Finestone, A., Hamel, A., Mandes, V., Burr, D., and Sharkey, N., 2004, "A Comparison of Bone Strain Measurements at Anatomically Relevant Sites using Surface Gauges Versus Strain Gauged Bone Staples," J. Biomech., **37**, pp. 947–952.

[6] Hurschler, C., Emmerich, J., and Wülker, N., 2003, "In Vitro Simulation of Stance Phase Gait – Part I: Model Verification," Foot Ankle Int. **24**, pp. 614-622.

[7] Kim, K-J, Kitaoka, H. B., Luo, Z-P., Ozeki, S., Berglund, L. J., Kaufman, K. R., and An, K-N., 2001, "In Vitro Simulation of the Stance Phase in Human Gait," Journal of Musculoskeletal Research, **5**, pp. 113–121.

[8] Kim, K. J., Uchiyama, E., Kitaoka, H. B., and An, K. N., 2003, "An in Vitro Study of Individual Ankle Muscle Actions on the Center of Pressure," Gait Posture, **17**, pp. 125-131.

[9] Ward, E. D., Smith, K. M., Cocheba, J. R., Patterson, P. E., and Phillips, R. D., 2003, [2003 William J. Stickel Gold Award] "*In Vivo* Forces in the Plantar Fascia During the Stance Phase of Gait: Sequential Release of the Plantar Fascia," J. Am. Podiatr. Med. Assoc., **93**, pp. 429-442.

[10] Howard, R. A., Rosvold, J. M., Darcy, S. P., Corr, D. T., Shrive, N. G., Tapper, J. E., Ronsky, J. L., Beveridge, J. E., Marchuk, L. L., and Frank, C. B., 2007, "Reproduction of *in Vivo* Motion Using a Parallel Robot," J. Biomech. Eng., **129**, pp. 743-749.

[11] Cavanagh, P.R., ed. 1990. *Biomechanics of Distance Running*, Human Kinetics Publishers, Champaign, IL, pp. 92-93.

[12] Riley, P.O., Dicharry, J., Franz, J., Croce, U.D., Wilder R.P., Kerrigan D.C., 2008, "A kinematics and kinetic comparison of overground and treadmill running." Med. Sci. Sports Exerc., **40**, pp. 1093-1100.

[13] Wu, G., Siegler, S., Allard, P., Kirtley, C., Leardini, A., Rosenbaum, D., Whittle, M., D'Lima, D. D., Cristofolini, L., Witte, H., Schmid, O., Stokes, I., and Standardization and Terminology Committee of the International Society of Biomechanics, 2002, "ISB Recommendation on Definitions of Joint Coordinate System of Various Joints for the Reporting of Human Joint Motion – Part I: Ankle, Hip, and Spine." J. Biomech., **35**, pp. 543-548.

[14] Isman, R. E., Inman, V. T., 1969, “Anthropometric Studies of the Human Foot and Ankle”, Bulletin of Prosthetics Research, **11**, pp. 97-129.

[15] Yeadon, M. R., 1990, “The Simulation of Aerial Movement--I. The Determination of Orientation Angles from Film Data,” J. Biomech., **23**, pp. 59-66.

[16] Pennock, G.R., and Clark, K.J., 1990, “An Anatomy-Based Coordinate System for the Description of the Kinematic Displacements in the Human Knee,” J. Biomech., **23**, pp. 1209-1218.

[17] Woo, S. L., Kanamori, A., Zeminski, J., Yagi, M., Papageorgiou, C., and Fu, F. H., 2002, “The Effectiveness of Reconstruction of the Anterior Cruciate Ligament with Hamstrings and Patellar Tendon. A Cadaveric Study Comparing Anterior Tibial and Rotational Loads”, J. Bone Joint Surg. Am., **84-A**, pp.907-914.

[18] Motriuk, H. U., and Nigg, B. M., 1990, “A Technique for Normalizing Centre of Pressure Paths,” J. Biomech., **23**, pp. 927-932.

[19] Fujie, H., Livesay, G. A., Woo, S. L., Kashiwaguchi, S., and Blomstrom, G., 1995, “The Use of a Universal Force-Moment Sensor to Determine in-Situ Forces in Ligaments: A New Methodology,” J. Biomech. Eng., **117**, pp 1-7.

[20] Lee, D. G., and Davis, B. L., 2009, “Assessment of the Effects of Diabetes on Midfott Joint Pressure Using a Robotic Gait Simulator”, Foot and Ankle Int., **30**, pp. 767-772.

[21] Grood, E. S., and Suntay, W. J., 1983, “A Joint Coordinate System for the Clinical Description of Three-Dimensional Motions: Application to the Knee,” J. Biomech. Eng., **105**, pp. 136-144.

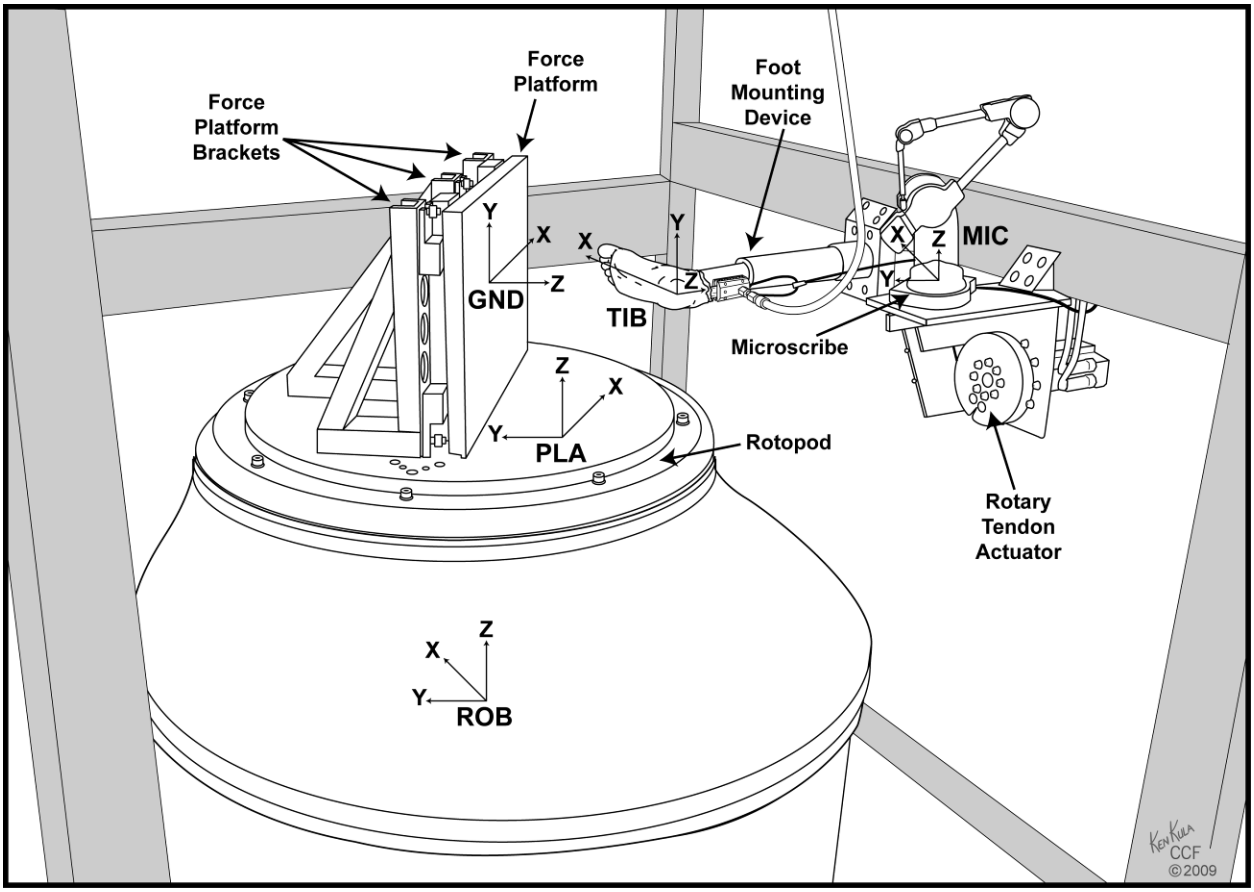

Fig. 1. Simplified illustration of the Musculoskeletal Simulator, as it would be configured for a foot study. The various coordinate systems shown illustrate the necessary mathematical transformations required to achieve motion of the force platform against the foot to simulate gait. GND, force plate; MIC, MicroScribe; PLA, rotopod platform; ROB, rotopod base; TIB, tibia. Reprinted with permission, Cleveland Clinic Center for Medical Art & Photography © 2009. All Rights Reserved.

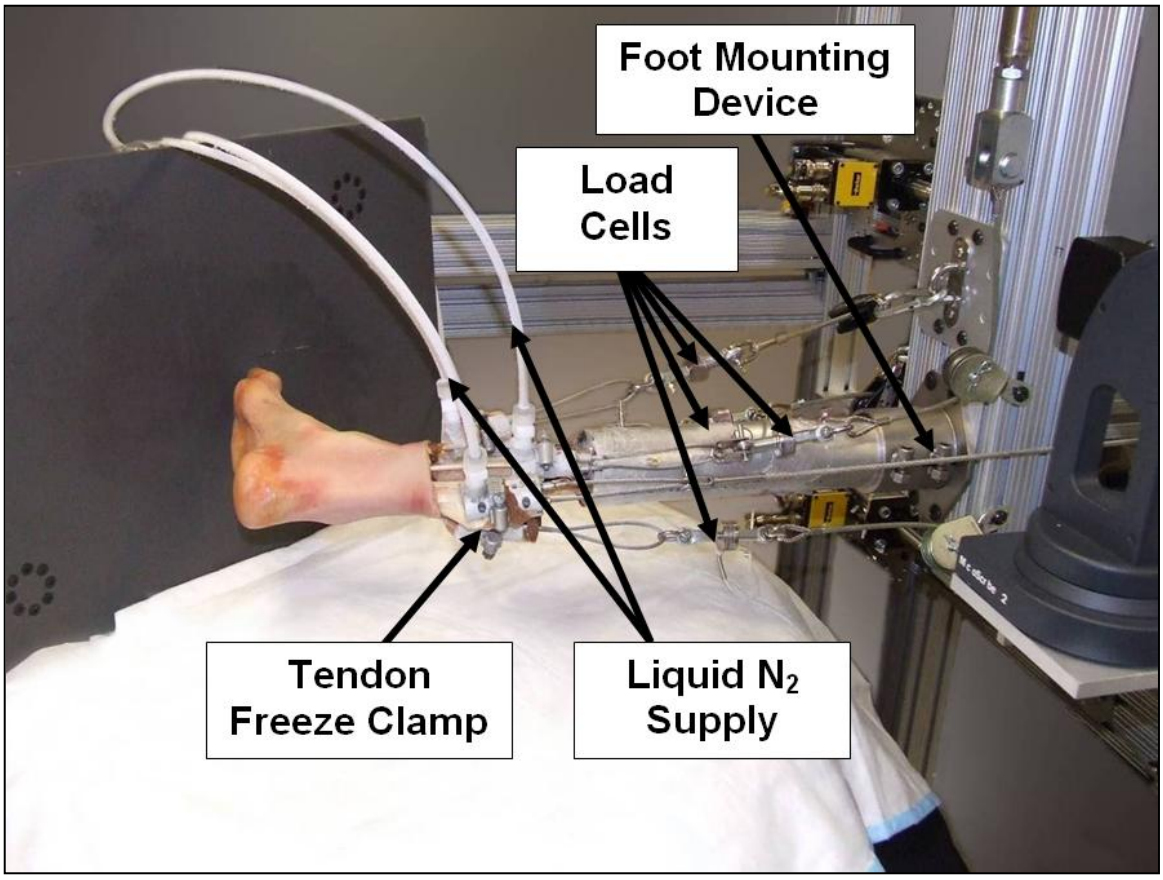

Fig. 2. Musculoskeletal Simulator, demonstrating cadaver foot mounting and attachment of five tendons to the actuators through freeze clamps, cables and pulleys.

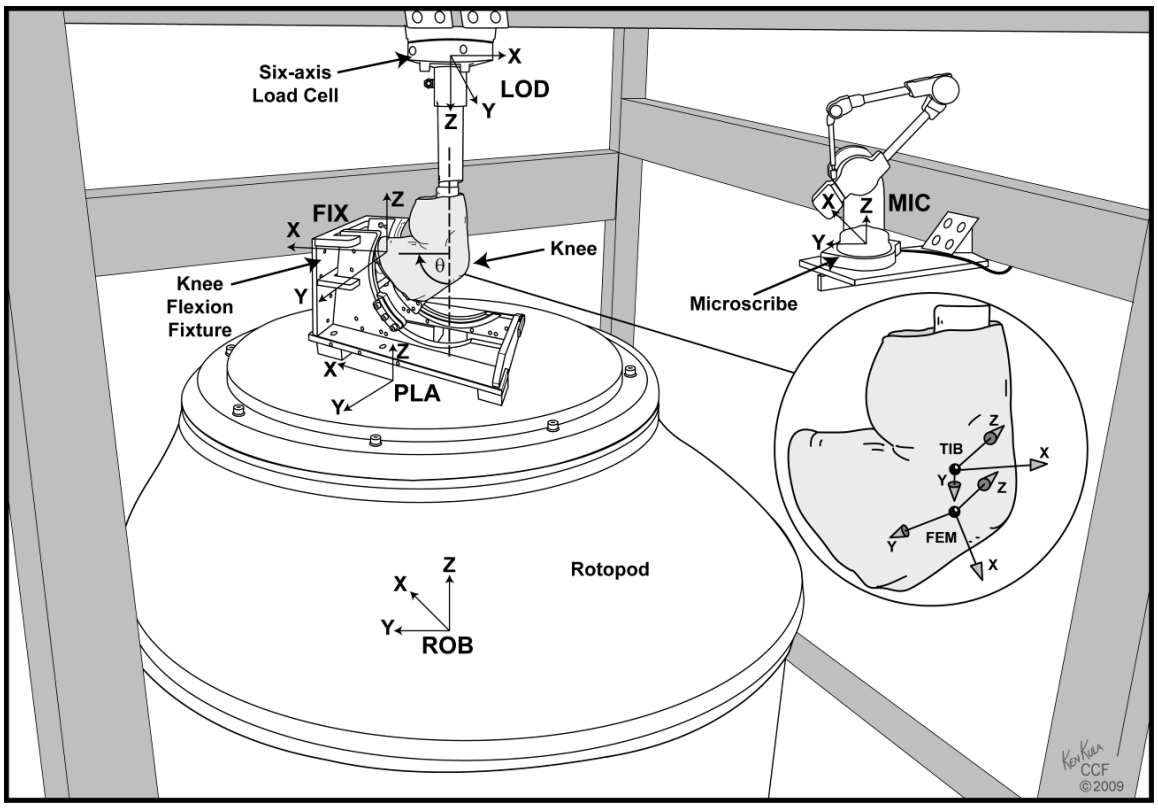

Fig. 3. Simplified illustration of the Musculoskeletal Simulator, as it would be configured for a knee study. The various coordinate systems shown illustrate the necessary mathematical transformations required to achieve motion of the knee fixture to cause knee flexion. FEM, femur; FIX, knee flexion fixture; LOD, six-axis load cell; MIC, MicroScribe; PLA, rotopod platform; ROB, rotopod base. Reprinted with permission, Cleveland Clinic Center for Medical Art & Photography © 2009. All Rights Reserved.

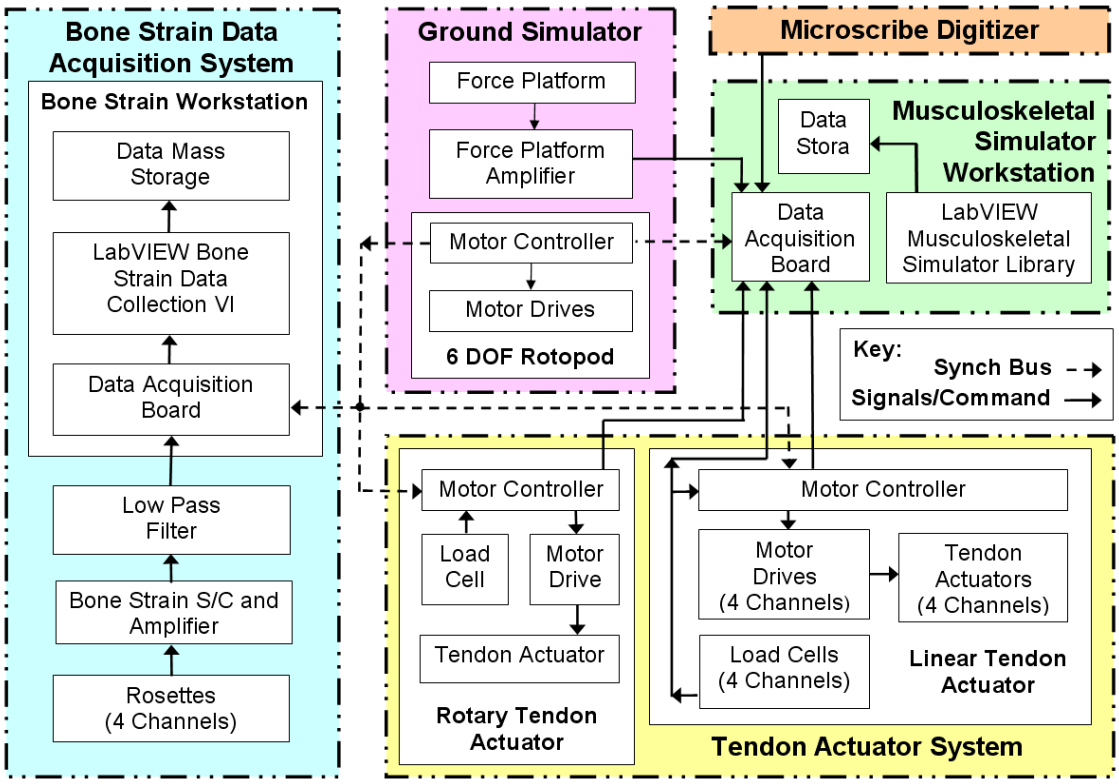

Fig. 4. Musculoskeletal Simulator block diagram showing general components required for foot experiments. The synch bus allows synchronization between the rotopod, strain gauge data acquisition and tendon actuators during simulated gait. DOF, degrees of freedom.

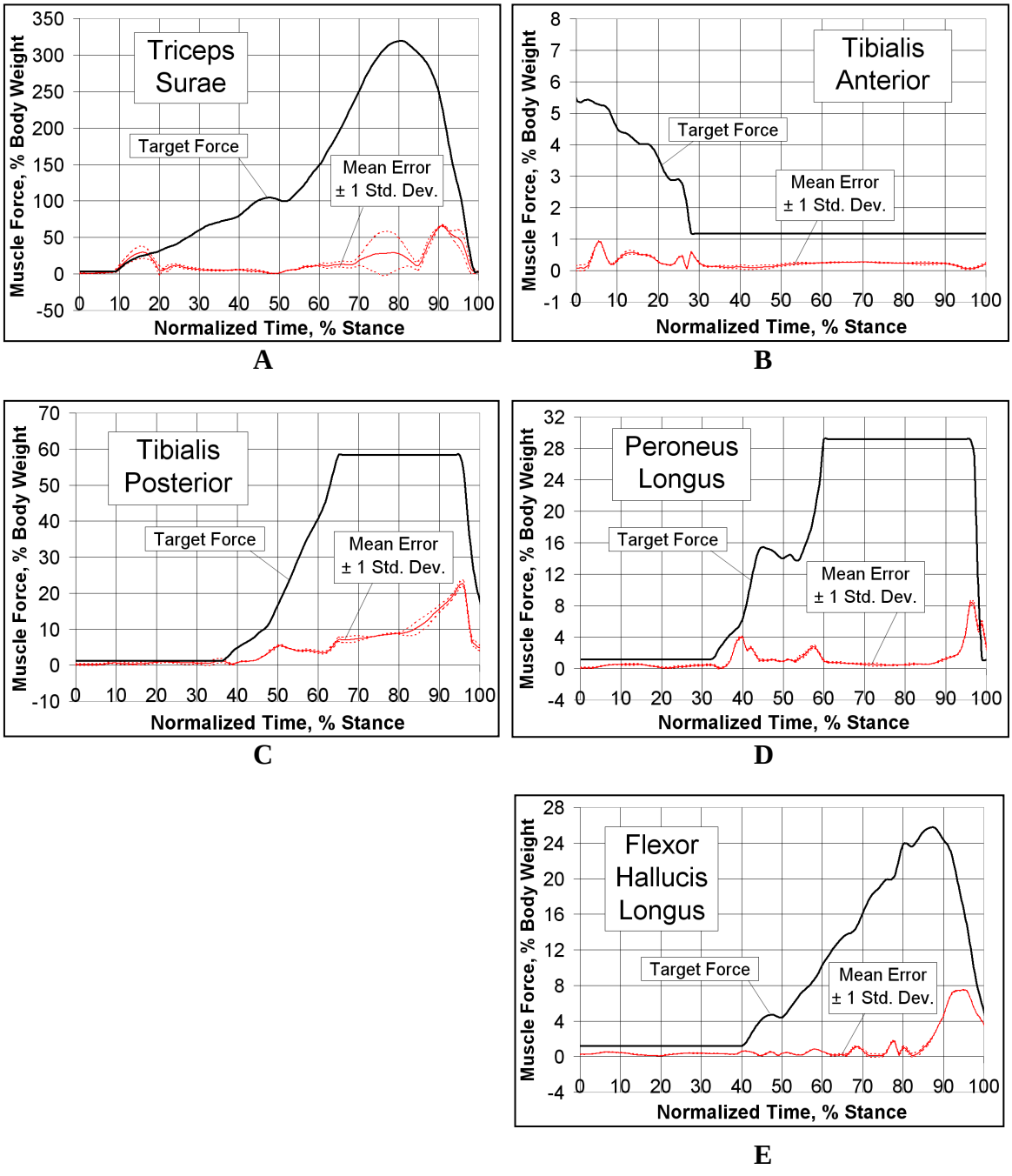

Fig. 5. Tendon actuator accuracy results for two experiments of three runs each, in which under closed-loop feedback, the actuator of the Musculoskeletal Simulator simulates muscle contractions. Muscles included triceps surae (A), tibialis anterior (B), tibialis posterior (C), peroneus longus (D) and flexor hallucis longus (E). Note that absolute error is shown as a mean ± 1 standard deviation. Target force is included as a reference.

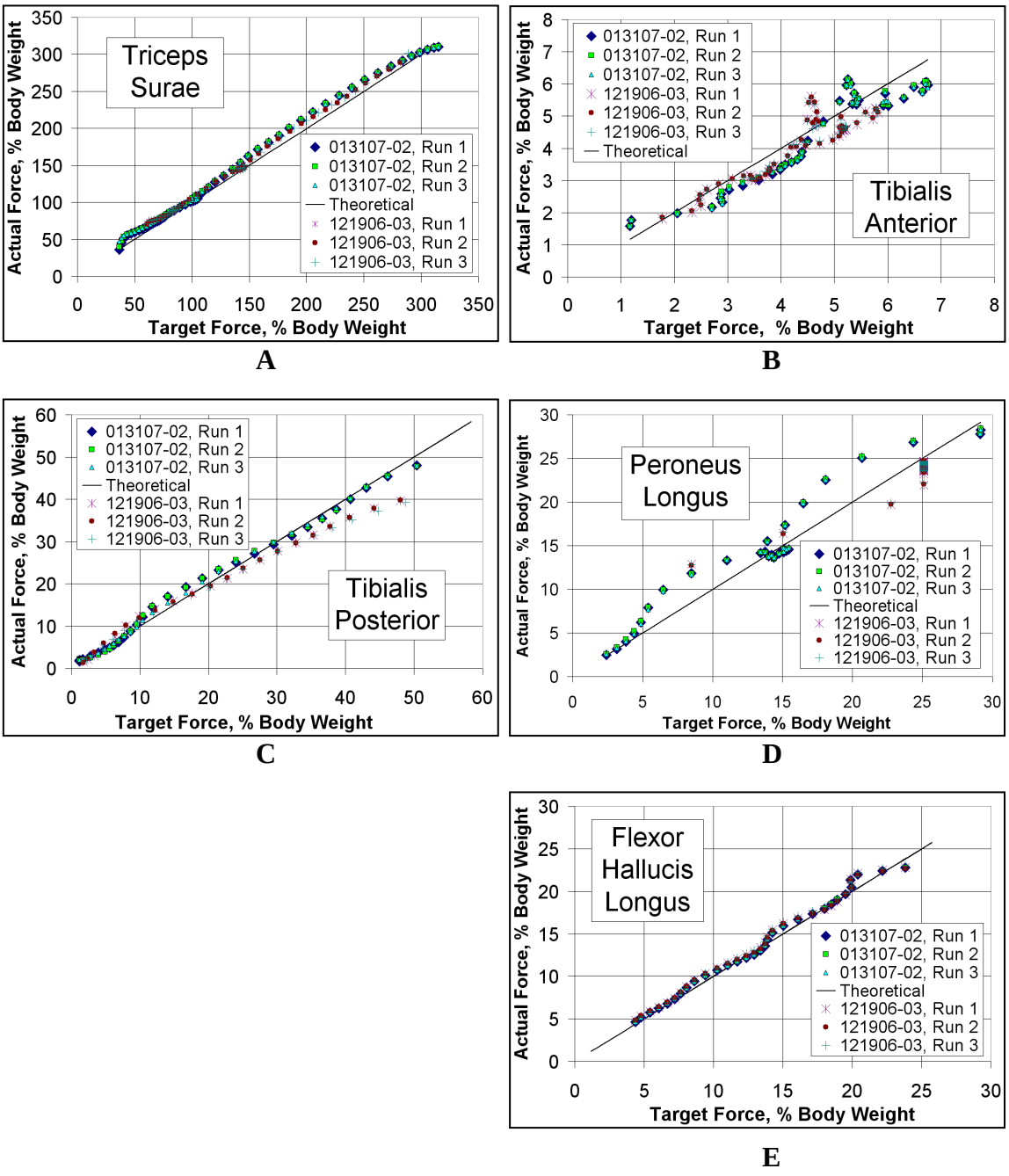

Fig. 6. Tendon actuator repeatability results for two experiments of three runs each, in which under closed-loop feedback, the actuator of the Musculoskeletal Simulator simulates muscle contractions. Muscles included triceps surae (A), tibialis anterior (B), tibialis posterior (C), peroneus longus (D) and flexor hallucis longus (E). Note that relative accuracy can be seen in deviation from the theoretical line.

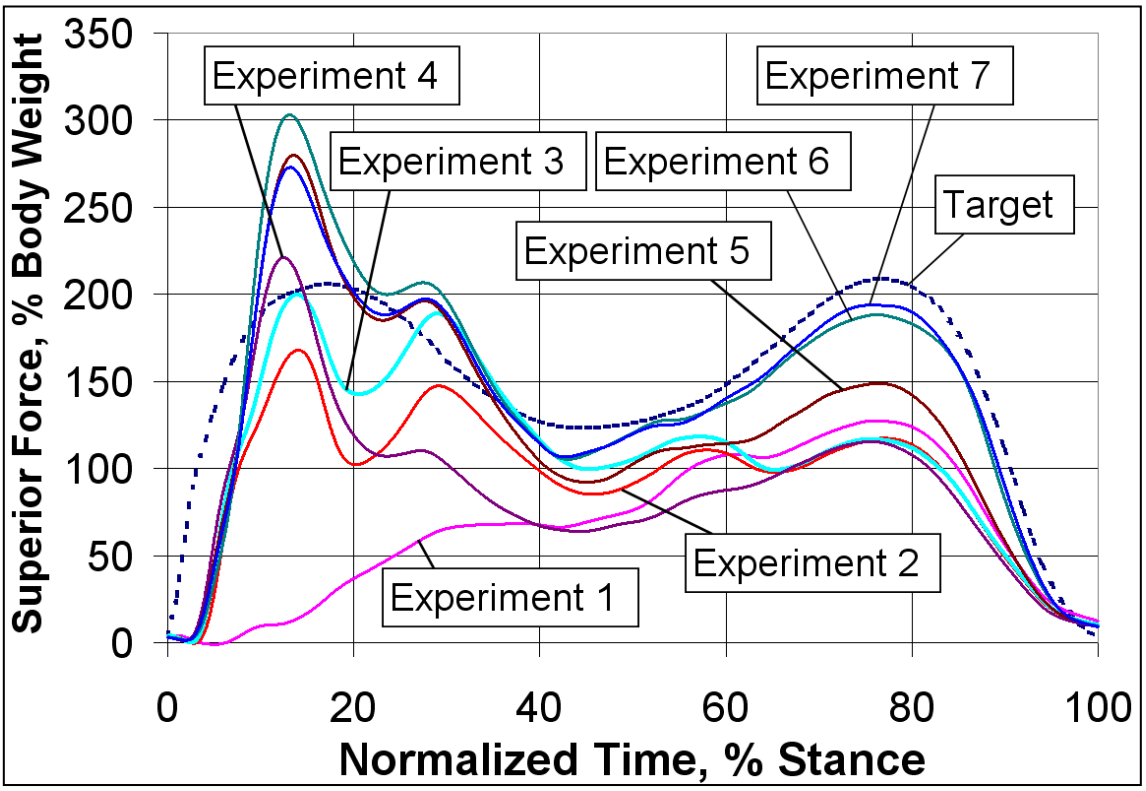

Fig. 7. Optimization results for seven experiments, showing convergence of superior force against the target toe-off region profile during simulated gait using the Musculoskeletal Simulator.

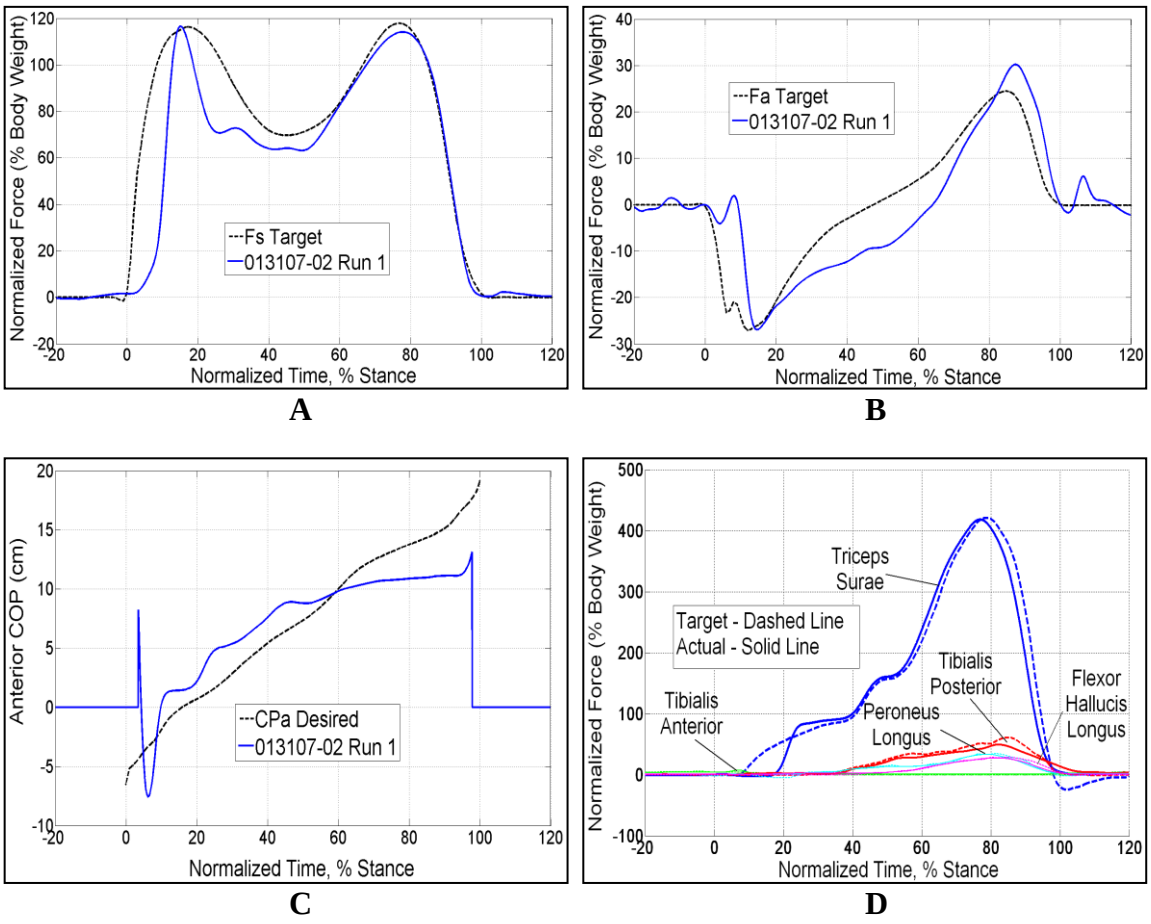

Fig. 8. Selected results from the foot bone strain study using the Musculoskeletal Simulator are shown. Full-physiological loading is demonstrated through the superior (A) and anterior ground reaction force (B), anterior center of pressure (C) and muscle forces (D). Results shown are indicative of a typical experiment run.

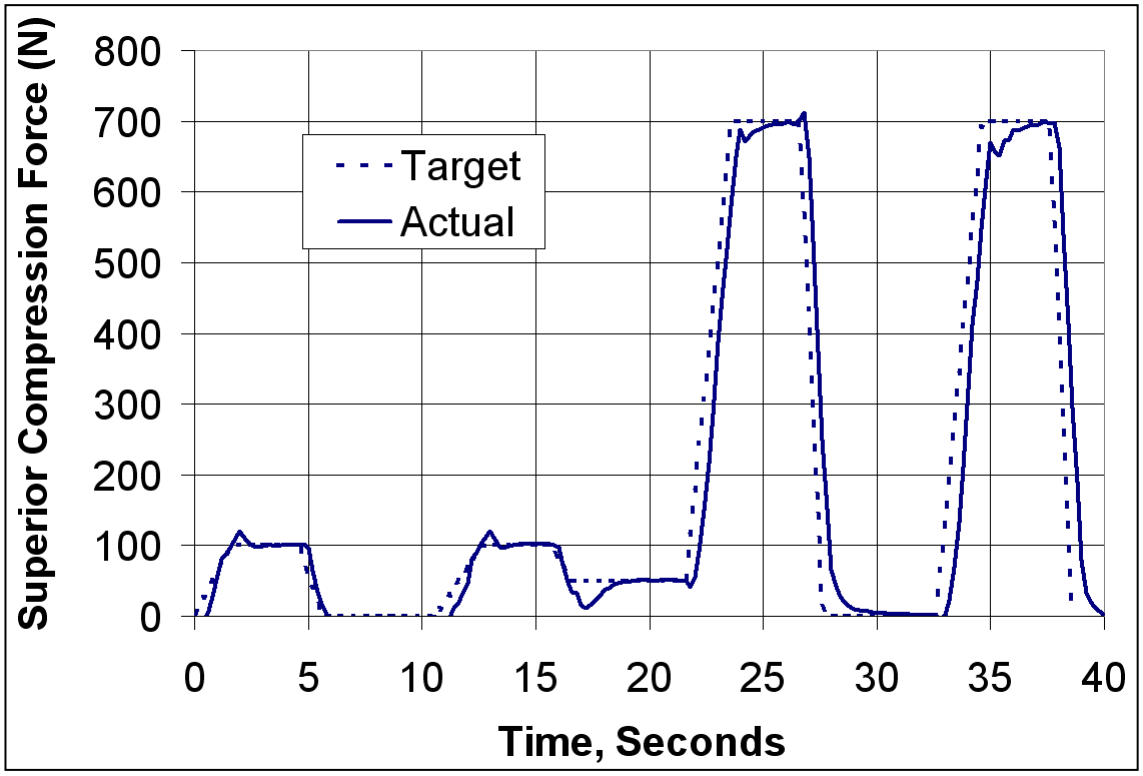

Fig. 9. Representative superior compression force profile of the real-time proportional-integral-derivative (PID) hybrid control for a knee experiment using the Musculoskeletal Simulator.